DOCTORAL DISSERTATION

Assessment and methods to mitigate head injuries in American Football using experimental and numerical approaches

MSc BEng Mateusz Dymek

Supervisor:
Mariusz Ptak, PhD, Associate Professor
Assistant supervisor:
Fábio António Oliveira Fernandes, PhD, Assistant Professor

WROCŁAW 2024

Contents

List of abbreviations	
AC	Agglomerated cork
aHEAD	advanced Head models for safety Enhancement And medical Development
αHEAD	Simplified numerical head model
ALE	arbitrary Lagrangian–Eulerian
ATD	Anthropometric test device
Biocore	Biomechanical Consulting and Research
BPU	Petrochemical polyol and bio-polyol
BrIC	Brain Injury Criteria
BV	Bridging Vein
CAD	Computer-Aided Design
CAE	Computer-Aided Engineering
CDSM	Cumulative Strain Damage Measure
CFC	Channel Filter Class
CoG	Centre of Gravity
CSF	Cerebrospinal Fluid
CT	Computed Tomography
CTE	Chronic Traumatic Encephalophaty
DAMAGE	Diffuse Axonal Multi-Axis General Evaluation
DICOM	Digital Imaging and Communications in Medicine
DoF	Degrees of Freedom
ELF	European League of Football
FE	Finite Element
FEHM	Finite Element Head Model
FEM	Finite Element Method
GCS	Glasgow Coma Scale
GHBMC	The Global Human Body Models Consortium
HARM	Head Acceleration Response Metric
HIC	Head Injury Criteria
HIE	Head Impact Exposure
HIP	Head Impact Power
ICP	Intracranial Pressure
MIPS	Multi-directional Impact Protection System
MPS	Maximum Principal Strain
MRI	Magnetic Resonance Imaging
mTBI	Mild Traumatic Brain Injury
NCAA	National Collegiate Athletic Association
NFL	National Football League
NOCSAE	National Operating Committee on Standards for Athletic Equipment
PFL	Polish Football League
PU	Petrochemical polyol
PUR	Polyurethane
SI	Severity Index
SPH	Smoothed Particle Hydrodynamics
SSS	Superior Saggital Sinus
STAR	The Summation of Tests for the Analysis of Risk
STL	Stereolithography
TBI	Traumatic Brain Injury
THUMS	Total HUman Model for Safety
YEAHM	Yet Another Head Model

List of symbols	
A	Resultant acceleration
t	Time (duration)
a	Linear acceleration
α	Rotational acceleration
L	Impact location
V	velocity
R	Concussion risk
G	Gravity acceleration constant (9.81 m/s^2)
C_i	Mass and appropriate moments of inertia
ω	Angular velocity
φ	Scale factor that relates the maximum resultant displacement of the system
σ	Stress
ε	Strain
ρ	Density
N	Polynomial order
ν	Poisson's ratio
E	Young's modulus
B	Bulk modulus
G_0	Shear modulus
G_1	Long-time (G_∞) shear modulus
G_{First}	First shear modulus
ι	First exponent for Ogden rubber (Hyperelastic) model material in LS-DYNA code
f	Frequency
f_0	Starting frequency
f_1	Frequency at the end of the test
β	Maxwell decay constant
τ	Kelvin relaxation constant
W	Strain energy density
μ	Shear modulus
E	Energy absorbed
C_i	Constants that were determined from fits to head kinematics measured in physical dummy reconstructions

Abstract

In contact sports, such as American Football, the players head trauma remains a significant challenge. This topic is highlighted each year by the players association and media. The literature analysis proved that using Finite Element (FE) models to explore head kinematics and injury mechanisms is an ongoing trend. My career as an American Football player led me to understand that human safety awareness is not enough highlighted. The findings will focus on American Football; however, an accident can occur while riding a bicycle or walking.

The first study describes an attempt to record the behaviour of the athletes during the simulated tackling situation. Due to the limited game recordings and poor video quality at the domestic game level, it was decided to attempt to record the athlete in two separate movements and combine them in prepared simulations. The recordings took place cooperating with the Wrocław University of Science and Technology and Wrocław University of Health and Sport Sciences. To verify, the attempts were recorded for further analysis with TEMA software (IMAGESYSTEMS). Finally, coupling two numerical codes – MADYMO and LS-DYNA enabled the author to progress further and prepare a set of two simulations with different tackling mechanics (so-called *open-field* and *side tackle*). The multibody dummies available in MADYMO served as athletes' models, and the American Football helmet was modelled in LS-DYNA.

The second experiment aimed to develop an additional energy-absorbing layer for the developed American Football helmets. There was an established cooperation between the Cracow University of Technology, the University of Aveiro (Portugal) and the Wrocław University of Science and Technology to develop state-of-the-art cork porous composites from sustainable materials. Twelve different samples were tested under dynamic loading to assess the ability to absorb energy, and finally, the tests were recreated numerically to obtain a validated material model. With the analysed and chosen material the thesis leads to physical experiments carried out during my stay at the University of Virginia in the Center for Applied Biomechanics (United States of America). The aim of the dissertation was to develop an additional absorbing layer that would minimize the probability of injury. The tests with two different design approaches proved that cork could serve as an additional energy-absorbing layer.

The final study focused on the verification of linear accelerations as a predictor for head injury. Analysing the trend visible in car or urban accidents, I adopted a similar strategy in sports accidents. Analysing the available simplified numerical head model αHEAD I proved that hydrostatic pressure values do not correlate with HIC under selected impact conditions. After considering that the available numerical head models on the market offer a broad but simplified geometry choice. According to the state of the art presented, the geometry of the human brain might greatly influence the results.

The first examined objective of the study was partially fulfilled due to the multi-body models limitations. The lack of literature studies about the active human body models is not sufficient to use the models with success. The dynamic testing of biocomposites were successful, however the tests proved that agglomerated cork would perform better under dynamic impact conditions. The scientific target was partially proven as the additional energy-absorbing layer, designed as an add-on, has successfully mitigated head acceleration for lower energy impacts. Lastly, no linear correlation was found between the head's centre of gravity accelerations and intracranial pressure. This information showed that the standards should be refreshed and updated to provide sufficient safety to users.

Streszczenie

W sportach kontaktowych, takich jak Futbol Amerykański, urazy głowy są istotnym wyzwaniem dla zachowania zdrowia zawodników. Temat ten jest na przestrzeni lat coraz częściej podkreślany zarówno przez stowarzyszenia zawodników jak i przez media. Przeprowadzona przeze mnie analiza literatury wykazała, że wykorzystanie modeli numerycznych głowy może z powodzeniem służyć za narzędzie do badań mechanizmów urazów. Natomiast moje doświadczenie jako gracza Futbolu Amerykańskiego, naświetliły brak świadomości dotyczącej bezpieczeństwa sportowców. Zaprezentowane wyniki badań będą się skupiać na Futbolu Amerykańskim, jednak wypadki mogą się wydarzyć się choćby podczas jazdy rowerem czy spaceru, co daje możliwość ekstrapolacji rezultatów na wiele różnych dyscyplin.

Pierwszy rozdział rozprawy doktorskiej skupia się na próbie zarejestrowania kinematyki sportowców, którzy symulują powalenie przeciwnika. Ze względu na ograniczoną liczbę oraz niewystraczającą jakość nagrań z krajowej ligi Futbolu Amerykańskiego, zdecydowałem się zarejestrować kinematykę zawodników w odrębnych sytuacjach i połączyć je za pomocą symulacji *multibody*. Badania te odbyły się we współpracy Politechniki Wrocławskiej z Uniwersytetem Wychowania Fizycznego we Wrocławiu. Nagrania zostały przeanalizowane przy pomocy oprogramowania TEMA (IMAGESYSTEM), co pozwoliło na wyznaczenie warunków brzegowych do symulacji. Połączenie dwóch kodów numerycznych, MADYMO i LS-DYNA, umożliwiło przygotowanie symulacji z rozróżnieniem na sposoby powalenia przeciwnika (tak zwane *open-field* i *side tackle*, z ang. powalenie). Modele *multibody* w oprogramowaniu MADYMO służyły jako modele zawodników, a kask do Futbolu Amerykańskiego był zamodelowany w kodzie LS-DYNA.

Drugi rozdział opisuje badania mające na celu użycie materiałów odnawialnych, uwzględniając ich właściwości do absorpcji energii impaktora i ich zastosowanie jako dodatkowa warstwa energochłonna do kasków. Dzięki współpracy z Uniwersytetem w Aveiro i Politechniką Krakowską opracowano kompozyty z korka naturalnego oraz oleju spożywczego, użytego wcześniej do smażenia. Dwanaście próbek, o różniących się proporcjach korka naturalnego, zostało zbadanych przy użyciu obciążeń dynamicznych, w celu oceny absorbcji energii. Po przeanalizowaniu wyników i wyborze materiałów, nawiązałem współprace z Uniwersytetem w Wirginii, *Center for Applied Biomechanics,* gdzie odbyłem staż i przeprowadziłem eksperymenty z kaskiem do Futbolu Amerykańskiego. Celem stażu było opracowanie dodatkowej warstwy absorbującej energię, która miałaby zredukować prawdopodobieństwo urazów. Testy z dwoma konfiguracjami dodatkowego materiału wykazały, że aglomerat korkowy może z powodzeniem służyć za dodatkową warstwę do kasków futbolowych.

Finalnie, badanie skupiło się na weryfikacji przyspieszeń liniowych jako kryterium urazów głowy. Analizując trendy w wypadkach samochodowych, przyjąłem podobną strategię i zdecydowałem się na przeprowadzenie badań przy użyciu symulacji numerycznych. Dzięki wykorzystaniu uproszczonego modelu głowy człowieka αHEAD wykazałem, że wartości ciśnienia śródczaszkowego, nie korelują się liniowo z wartościami HIC. Wspierając się przeglądem literatury, wywnioskowałem, że zbyt uproszczona geometria modelu numerycznego mózgu może znacząco wpływać na wyniki badań.

Pierwszy cel badań został wykazany częściowo z uwagi na ograniczenia modeli *multibody*. Ograniczony stan wiedzy na temat modeli aktywnych może wskazywać na ich wątpliwą wiarygodność. Testy z obciążeniem mechanicznym dla próbek pozyskanych z materiałów odnawialnych powiodły się. Wykazały, że zdolności próbek do pochłaniania energii uderzenia są zbyt małe w porównaniu do aglomeratu korkowego. Wykorzystanie materiału korkowego okazało się być dobrym rozwiązaniem dla uderzeń z mniejszą energią uderzenia, podobnie jak w literaturze dla *guardian caps*. Nie wykazano liniowej korelacji pomiędzy wartościami kryterium HIC, a ciśnieniem śródczaszkowym dla modelu αHEAD. Jednoznacznym wnioskiem z badań jest stwierdzenie, że kryteria urazów powinny być zaktualizowane, aby zapewnić maksymalne bezpieczeństwo zawodnikom Futbolu Amerykańskiego.

1. Introduction

In contact sports, such as American Football, managing brain trauma remains a challenge [1]. The occurrence of concussions, particularly in American Football, is frequent, providing extensive research using Finite Element (FE) models to explore brain kinematics and injury mechanisms (Table 1) [2]. These models have evaluated injury probabilities by assessing brain strain, stress, and intracranial pressure, even though the theoretical nature of this approach lacks direct validation, such as cadaver studies, which could significantly boost their credibility [3]–[7].

Lincoln et al. [8] analysed over 2 600 concussions from more than 10 000 000 exposures in high school sports, with American Football accounting for over half of these incidents and showing the highest incidence rate. Similarly, sports such as Rugby Union and Australian Football report a considerable number of head injuries despite the absence of protective gear [9]–[11].

American Football, played at various levels globally, influences athlete safety. Despite mandatory protective gear, such as helmets and shoulder pads, injuries often occur from direct player-to-player impacts and collisions with the ground [5], [12], [13]. Studies by Crisco et al. [14] and Brolinson et al. [15] observed a wide distribution of impacts across football teams and sessions, revealing substantial head impacts during practices and games. Additional research by Rowson et al. [16] incorporated acceleration-measuring devices in football helmets, reporting peak linear head accelerations reaching significant magnitudes. Studies analysing head impacts through systems such as helmet impact telemetry and 6 degrees of freedom devices underline the need for further investigations into head kinematics post-impact, emphasizing the potential for even slight reductions in velocity to minimise concussion probabilities [17].

Table 1. Summary of studies investigating head injury statistics in American Football, adapted from [7].

Reference	Objective of the study
Beckwith et al. 2012 [5]	Correlation of the measures of head impact biomechanics recorded when tested on the linear impactor,
Ji et al. 2014 [6]	Investigation of the sensitivities of regional strain-related responses to kinematic variables of accelerations,
Lincoln et al. 2011 [8]	Examination of the incidence and relative risk of concussion in 12 high school boys' and girls' sports,
Kucera et al. 2017 [12]	Identification of traumatic brain and spinal cord injury deaths during 2005-2014 among high school and college football players,
Crisco et al. 2010 [14]	Quantification of the frequency and location of head impacts,
Brolinson et al. 2006 [18]	Utilisation of an in-helmet system that measures and records linear head accelerations,
Rowson et al. 2012 [16]	Characterisation of the tolerance to the rotational kinematics resulting from helmeted head impacts,
Viano et al. 2003 [17]	Simulation in laboratory tests of impacts causing concussions.

The study by Choi et al. [19] described the relationship between head impacts and subsequent brain injuries in American Football players, focusing on youth and collegiate levels. Head Impact Exposure (HIE) metrics were evaluated among these players. Across multiple seasons, 639 athletes were enrolled (354 collegiate; 285 youth aged 9–14), with a total recording of 476 209 head impacts (367 337 collegiate; 108 872 youth) over 971 sessions (480 collegiate; 491 youth). Notably, youth players experienced significantly fewer impacts per competition and practice, around 43% and 65% less than collegiate players. Moreover, the impact magnitudes were lower among youth players. For instance, in the 95th percentile measurements, peak linear acceleration during the competition was 45.6 G (youth) versus 61.9 G (collegiate), and peak rotational acceleration was 2 262 $rad \cdot s^{-2}$ (youth) versus 4 422 $rad \cdot s^{-2}$ (collegiate). These trends were consistent for both competition and practice settings, where impacts during competitions were more frequent and of greater magnitude than practice sessions at both levels [19].

A retrospective analysis published by Rowson et al. [20] investigated head impact data from 1 833 collegiate football players equipped with helmet-mounted accelerometers during games and practices between 2005 and 2010. The study included eight collegiate football teams: Virginia Tech, the University of North Carolina, the University of Oklahoma, Dartmouth College, Brown University, the University of Minnesota, Indiana University, and the University of Illinois from the United States of America. Among 1 281 444 recorded head impacts, 64 concussions were diagnosed. The comparison between players using Riddell VSR4 and Riddell Revolution helmets was presented. The study revealed that the relative risk of sustaining a concussion in a Revolution helmet compared to a VSR4 helmet was 46.1% smaller. Even when considering individual players' head impact exposure, a significant difference in concussion rates occurred between those wearing VSR4 and Revolution helmets (to VS4 disadvantage). This research emphasized that distinctions in helmet models within football correlate with varied abilities to lower the risk of concussions.

Beyond highlighting traumatic brain injury (TBI) rates among players, attention is drawn to the diagnosis of chronic traumatic encephalopathy (CTE) in former players [3], [17], [21]–[26]. These findings underscore the importance of ongoing research into protective measures and the long-term consequences of head injuries in sports [7].

2. State of the art

The state of the art chapter will present the basic information about American Football helmets, head anatomy, Finite Element Head Models (FEHM), Head Injury Criteria (HIC), energy absorption and cork material based on the literature review. In order to introduce the reader to the topic, the design of helmets, a brief anatomy description and energy-absorbing materials are described.

2.1. American Football helmets[1]

This chapter will include detailed information about American Football helmets. Firstly, the design and function are described, then the history of helmets is presented, and finally, the regulations on helmet performance are described.

2.1.1. Design and Function

Each helmet is designed from at least two primary components. The first one is the hard exterior shell, which plays a crucial role in spreading the force of impact across the surface of the liner. Due to the energy distribution, the probability of head injuries decreases. This stiff outer layer also serves as a barrier against penetration and as an initial buffer for shocks. The second key element is the energy-absorbing material, typically polyurethane foam. Its primary role is to absorb the energy from impacts and decrease the head's acceleration through viscoelastic compression [27].

The features mentioned above are fundamental to helmets, regardless of their specific type or use. They dictate the design in terms of materials used, shape, and other factors. With varying requirements, innovations or new designs created for one kind of helmet can be adapted for other uses. For example, technologies have been developed to reduce head injuries from rotational forces in motorcyclists or bikers (i.e., Multi-directional Impact Protection System – MIPS) [27].

It is crucial that the helmet is not too heavy, as this could reduce comfort and potentially raise the risk of spinal injuries. Achieving the right balance between the stiffness and thickness of the inner layer is essential to maximize energy absorption. If the liner is too soft, it might compress entirely upon impact, leaving no capacity to absorb more energy. In such cases, since the outer layer is rigid, the head would suddenly stop, causing high accelerations on the brain [27].

During an impact, the head experiences various levels of acceleration, causing the brain to move slightly within the skull due to brain inertia. Depending on the force, this movement can lead to severe injuries. Due to limited space inside the skull, there is no separate brain movement *per se*. The brain's outer layers move quickly with the head, but the inner layers remain relatively stationary. These movement differences induce neuron strain and even shear. The inside layers will eventually move and, in some cases, overshoot the outer motion. In frontal collisions, the initial impact is in front, compressing the tissue and stretching on the opposite side. Then, the brain moves in the reverse direction, stretching the tissue at the impact site and compressing it on the other side. This phenomenon, known as coup and contrecoup, occurs because the brain is suspended in cerebrospinal fluid (CSF) within the skull.

---

[1] The chapter was adapted from one of the co-authored publications, Design and virtual testing of American football helmets - a review. Archives of Computational Methods in Engineering. 2022, vol. 29, s. 1277-1289, https://doi.org/10.1007/s11831-021-09621-7

However, CSF often fails to provide sufficient cushioning during high-energy impacts. The forces involved in a head impact can cause considerable damage to brain tissue and the structure of bridging veins, leading to brain swelling and bleeding. It has to be underlined that the brain remains in motion even when the head has stopped [27].

2.1.2. History

The evolution of the American Football helmet dates to the late 19th century, with the inaugural deployment of a helmet in an Army-Navy Universities game in 1893. Initially, these helmets, robust in design and crafted from leather, featured distinctive styles such as beehive, flat-top, or dog-ear (Figure 1). It is remarkable to witness the substantial transformation in helmet design, a change propelled by an enhanced understanding of cranial biomechanics and injury mechanisms [27].

Figure 1. A chronology of American Football helmets, upper left – the oldest design [27].

In American Football, helmets are critical for protecting players' heads during tackling and falling. However, it underlined that these helmets do not prevent head and neck injuries. According to regulations, the helmet reduces the probability of an injury. The National Collegiate Athletic Association (NCAA) mandated helmets in 1939, a mandate that the NFL adopted in the subsequent year. The technological evolution of these helmets has been significant, considering advanced materials such as metal alloys and polymers for better protection. The introduction of facemasks to helmets in the 1950s marked a pivotal development in the history of helmet safety [27].

The establishment of the National Operating Committee on Standards for Athletic Equipment (NOCSAE) in 1969, in response to a series of head and spinal injuries, led to the formulation of the first safety standards for helmets in 1973. Continual enhancements in helmet safety have characterized this period. Authorities in the field introduced helmet designs based on a thorough understanding of skull and brain anatomy, aiming to mitigate head injuries effectively. These designs are intended to protect the most susceptible regions of the cranial and cerebral structures.

Figure 2. Current models for leading helmet brands: a) Riddell SpeedFlex Diamond, b) Schutt F7 LTD, c) Xenith Shadow XR, adapted from [7].

Focusing on the leading manufacturers in the helmet industry – Riddell, Schutt, and Xenith – these entities are consistently engaged in developing innovative designs to enhance player safety (Figure 2). The current market contains diverse helmet models, each engineered to address the impact forces encountered during gameplay uniquely. For instance, Schutt's F7 model incorporates innovative tectonic plates on its outer shell, designed to counteract rotational forces independently. Riddell's design features a frontal cut-out on the shell, engineered to flex and dissipate impact energy. In the newest design, the upper facemask bar is removed to reduce the overall stiffness of the front of the helmet. Beyond technological advancements, the emphasis is put on a precise fit. Xenith has directed its focus towards the helmet's internal padding, integrating dual-stage shock absorbers. These respond to both linear and rotational forces. The absorbers are designed to compress or shift laterally during impacts, offering tailored cushioning. Additionally, most companies offer a precise fitting procedure and manufacture helmets based on the head 3D scan [27].

2.1.3. Regulations

The NOCSAE standards, set in place in 1973, require using a head model that accurately simulates the human head's response to impact. To these standards, the controlled drop test for helmets is presented. Each helmet is tested on a head form and a special rig (Figure 3). The head is encompassed with an accelerometer to record the data. The aim of this standard is to assess the resilience of football helmets against repeated impacts of varying strengths across diverse playing conditions while ensuring they retain their protective qualities. The drop impact test involves testing the helmet at six different points of impact and at four varying speeds (3.46, 4.23, 4.88, 5.46 m/s) [27].
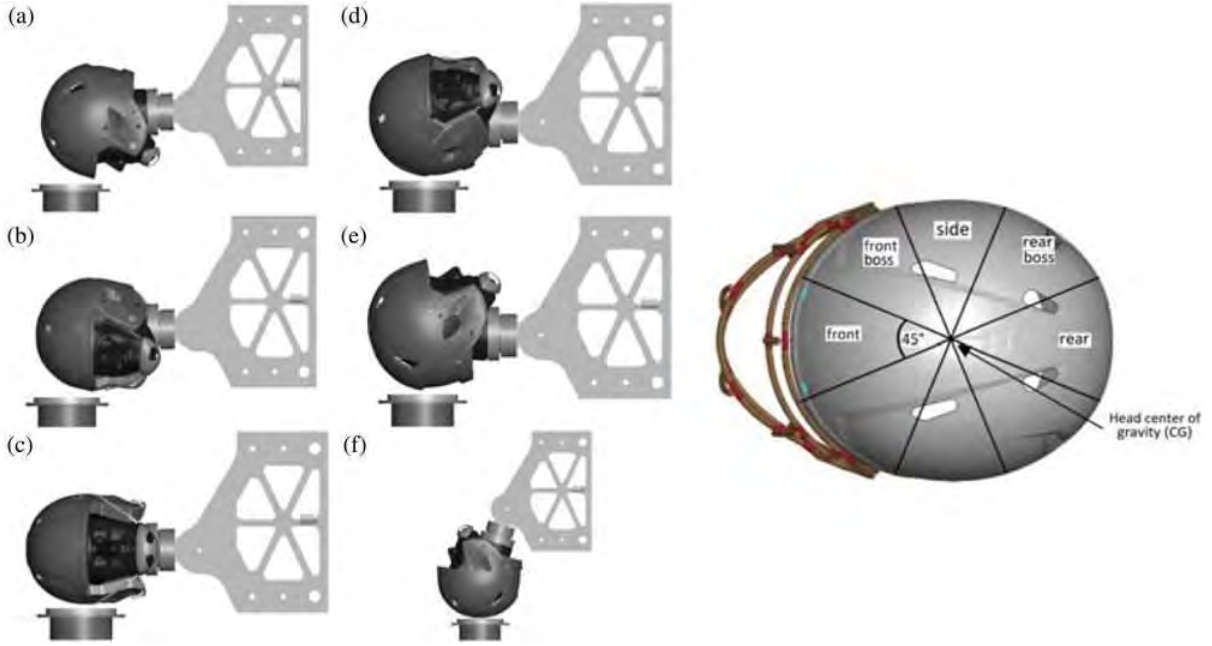
Figure 3. NOCSAE linear drop setup on the left: a) Front, b) Front Boss, c) Side, d) Rear Boss, e) Rear,
f) Top; Impact location bins on the right, based on [28].

The Summation of Tests for the Analysis of Risk (STAR) evaluation system, devised by Virginia Tech University, grades a helmet's performance by its capacity to reduce linear and rotational head acceleration after a series of impacts. This method uses a pendulum impactor that hits the helmet at four locations and three speeds: 3.1, 4.9, and 6.4 m/s. A critical difference between NOCSAE and STAR tests is that STAR fits the helmet onto a medium-sized NOCSAE head attached to a Hybrid III neck. This assembly is then mounted onto a Biokinetics slide table with a 16 kg sliding mass and five degrees of freedom [27].

The drop impact test employs an anthropomorphic test device (ATD), which resembles human features and is fitted with accelerometers at the headform's centre of gravity (CoG). The recorded data includes longitudinal and rotational accelerations measured by the accelerometer. The Severity Index (SI) is calculated using a formula (equation 1), where 'A' denotes the instantaneous resultant acceleration (as a multiple of G, the acceleration due to gravity), and 'dt' is the time increment in seconds. The integration covers the critical duration (t) of the acceleration pulse.

$$SI = \int_0^t A^{2.5} dt \qquad (1)$$

The SI is designed not to exceed 1 200. The peak rotational acceleration aims to replicate linear and rotational movements, representing the head, neck, and torso of an average 50th percentile male. The STAR rating, calculated using Equation 2, predicts the likelihood of a player sustaining a concussion over a season, as indicated in studies [29]–[31].

$$STAR = \sum_{L=1}^{4} \sum_{V=1}^{3} E(L,V) \cdot R(a,\alpha) \qquad (2)$$

The equation is based on lab tests that simulate the range of impacts seen in college American Football, linking each impact to its seasonal frequency (exposure) and associated concussion risk. The STAR value is determined by multiplying the predicted on-field exposure at each impact location (L) and velocity (V) by the concussion risk (R) for that impact, using the peak resultant linear (a) and rotational accelerations (α) from lab impacts [31]. All helmets discussed achieved a 5-star rating, the highest possible. However, their performance varies, with the Schutt F7 LTD scoring 0.75, the Riddell SpeedFlex Diamond 1.69, and the Xenith Shadow XR 1.91, where a lower score indicates better performance.

Currently, there are two most frequent studies used to recreate the American Football impacts physically and numerically. The first study was published by Viano et al. [32], where the authors chose eight points of impact based on 182 NFL game impacts of helmet-to-helmet, helmet-to-ground, and helmet-to-shoulder pad type. The impact scenarios evaluated were recreated by a linear impactor described in the literature [33]–[35] and used by the study's author. The second approach is analysed by Lessley et al. [36], [37]. The study aimed to verify position-specific relations concerning concussions sustained by NFL players by exploring game footage (both broadcast and non-broadcast) across four seasons. Analysing 647 concussions with identifiable primary exposures, the study catalogued position-specific features such as impact source, helmet impact location, activity during impact, and the involved player from the opposing team. The analysis highlighted trends, including the dominance of helmet-to-ground impacts toward the rear of quarterbacks' helmets—frequent impacts on the upper side location for both concussed players and their counterparts, irrespective of position.

2.1.4. Guardian Caps

Recent trends in American Football helmet design showed that the capability of energy absorption of the structure might be limited. Bailey et al. [38] and Cecchi et al. [39] evaluated the capabilities of energy absorption for Guardian Cap NXT (Guardian Sports, Peachtree Corners, GA, USA) and ProTech (Defend Your Head, Chester Springs, PA, USA) helmet covers. The purpose of this concept is to add padding on the outside of the helmet's hard shell to increase the overall thickness of soft padding. These products have become commercially available for athletes and are rapidly gaining popularity, with some even becoming mandated under certain conditions at the elite level of American Football competition [39], [40].

While the increased thickness of the helmet and add-on should theoretically reduce average decelerations, the add-on devices are often required to work with multiple helmets and may not be optimized for use such as the helmet shell and liner were designed [41]. The purpose of the mentioned study [38] was to assess the ability of two contemporary helmet add-on products to mitigate impact severity in helmet-to-helmet collisions typically experienced by American Football linemen, who typically experience more frequent helmet impacts per game.

Helmets demonstrating superior baseline performance, assessed by HARM, generally exhibited reduced mitigation of head injury criteria. The Riddell SpeedFlex Precision Diamond is shown as the top-performing helmet model in its original condition. The addition of Guardian cap NXT marginally improved its performance, the inclusion of ProTech decreased it. The authors hypothesize that the additional padding may have restricted the outer shell's flexion, thus changing the way the helmet manages energy [38]. The biggest improvements in helmet performance were noted in the Schutt Vengeance Z10 LTD and Riddell Speed Classic Icon.

According to HARM scores, these models ranked lowest among the helmets tested in their stock helmet condition. This pattern suggests that the potential of add-on products to improve head protection might be restricted in higher-performing helmet models, which are already finely tuned for these specific loading conditions. Interestingly, the add-ons also boosted the performance of the VICIS Zero1, known for its inherently flexible outer shell [38].

The second study was prepared with the on-field data collection system, including the in-house developed MiG2.0 instrumented mouthguards (Stanford University, USA). To best compare the bare and padded helmet impacts, only helmet-to-helmet impacts were retained for analyses, rather than impacts caused by body-to-body, body-to-head, or head-to-ground contact. A helmet-to-helmet impact for the padded condition was classified as any impact where the helmet of one player equipped with a padded helmet shell cover hit the helmet of another player equipped with a padded helmet shell cover. If only one player wore a padded helmet shell cover, the impact was discarded and not included in any analyses [39].

Both studies concluded that the add-ons perform better for lower velocity impacts (~4 m/s) than high velocity impacts. The effectiveness can significantly vary for the helmet type and the impact location. The American Football helmets are designed to absorb the impact energy maximally, and the additional padding can influence the flexion of the original shell under loading and worsen its energy-absorption capabilities [38]. The in vivo evaluation showed that in the majority of lineman impacts, the facemask is the primary contact in collisions. The proposed designs do not cover the facemask and thus do not provide any additional absorbing-energy material [39]. There are raised concerns about the additional mass, which may influence the risk of neck fatigue and injuries or can affect the helmet's stability leading to uncontrolled movement during the impact.

In summary, the proposed add-ons to the helmets show promising results in terms of mitigating head accelerations in impacts and improving the player's safety. Nevertheless, there is a significant need to continue the research that will include a variety of weather and impact conditions, and more importantly, collect more on-field data on the performance of guardian caps.

2.2. Head anatomy

The human brain is the most complicated and mysterious organ known to humankind. It is responsible for controlling all living functions, memory, emotions and intelligence. As a part of the central nervous system, the brain works simultaneously with the spinal cord. It is baffling that, having approximately 1227±135 cm^3, the brain is responsible for all autonomous functions, such as the cardiovascular system, voluntary and involuntary functions and movement of all limbs [42], [43]. In order to protect such a vital organ, the human body surrounds the brain with a CSF and a skull. In addition, there are three meninges: the dura, 0.3-0.8 mm thick, firm membrane made primarily from collagen fibres; the arachnoid, 0.035-0.040 mm thick membrane containing blood vessels; and the pia, 0.015 mm thick membrane that follows the folds of the brain and contains a large number of blood vessels. A dura folds into two halves of the cerebrum, referred to as falx, and folds into the inferior regions covering the cerebellum and brainstem, referred to as tentorium [44]–[47]. The middle layer – the arachnoid covers most of the brain and contains blood vessels, some of which span the subdural space between the dura and arachnoid to reach the brain [48]. The pia follows the brain's folds and contains many blood vessels [49]. All spaces in the cranial cavity, such as hollow channels within the brain – ventricles and areas between meninges, are filled with CSF. The fluid is a clear, watery substance that is constantly being absorbed and replenished [44], [50].

The cranium is composed of cortical and trabecular bone. Bones' structure and mechanical properties can differ depending on various parameters, such as age, sex and health conditions, for example the thickness changes with age. Due to changes in chemical composition, thickness and proportions, child's skull cannot be compared to an adult's skull [50]. The bone structure is nonhomogeneous, which leads to mechanical properties depending on the share of hard tissue – the bigger the share, the stronger the bones. From the mechanical point of view, it is important to underline the direction in which the properties were determined (Figure 4), as it turns out that the energy absorption is higher for longitudinal than for transverse compression [51]–[54].
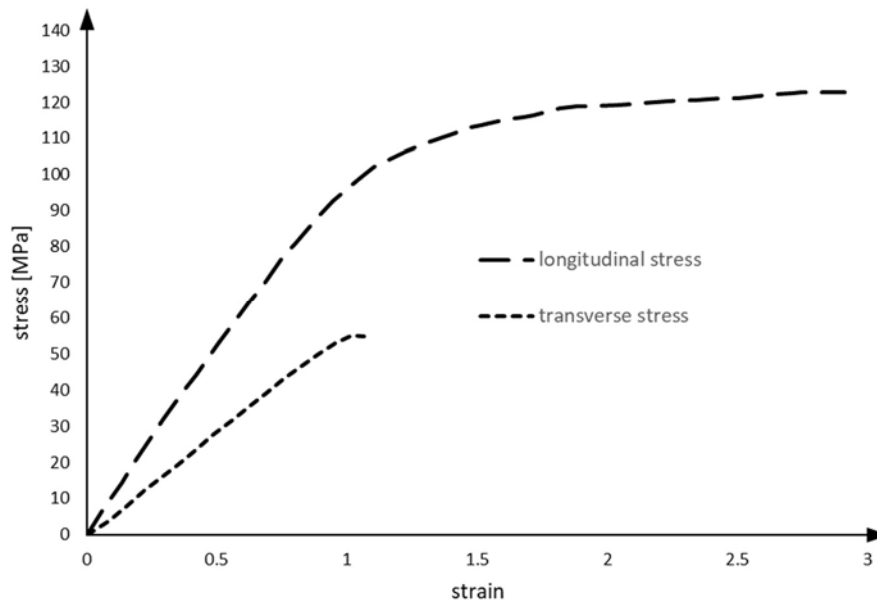
Figure 4. Stress-strain curve for cranium bones, adapted from [51].

The human brain consists of two major parts, which are called cerebral hemispheres, which are connected with the corpus callosum. Each hemisphere is divided into four lobes: frontal, parietal, occipital and temporal. Additionally, there are brainstem and cerebellum distinguished. The outer surface of the cerebrum – grey matter, is wrinkled in appearance (Figure 5) and are called sulci and gyri. Beneath the cortex is the white matter, composed of connecting fibres between the brain's neurons [50].
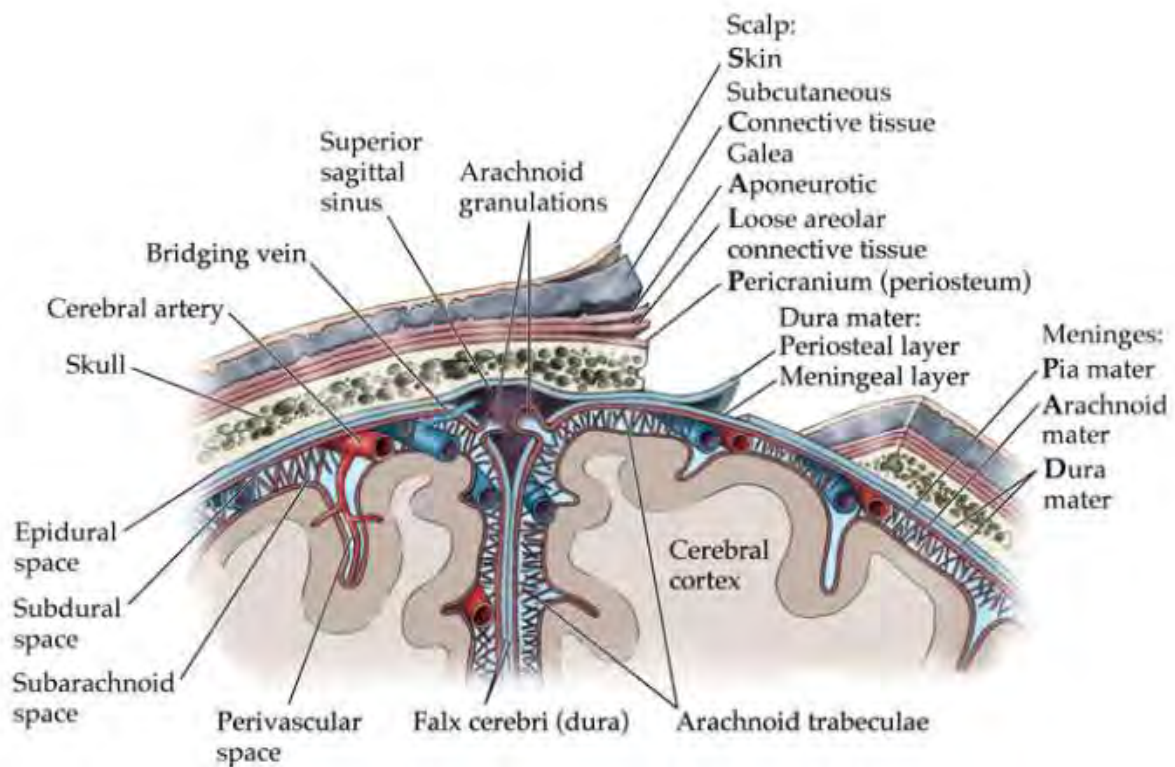
Figure 5. Human head anatomy, coronal section, adapted from [55].

Since each lobe is responsible for different actions, the brain damage can result in various symptoms, depending on which lobe was affected. The summary of each lobe responsibility is presented in Table 2 [56], [57].

Table 2. Human brain lobes with their responsibilities, adapted from [50], [57].

	Healthy brain	Damaged brain
Frontal lobe	Personality (behaviour, emotions); Judgment, problem-solving; Speaking, writing; Motor system; Intelligence, concentration, self-awareness;	Changes in behaviour and emotions; Impaired judgment, motivation; Memory loss; Impaired smell sense, vision loss; One body side paralysis;
Parietal lobe	Language interpretation; Sense of touch, pain; Vision, hearing interpretation; Memory; Spatial and visual perception;	Difficulty in distinguishing right or left; Lack of awareness of certain body parts; Difficulties in eye-hand coordination; Reading, writing, drawing, naming problems;
Occipital lobe	Vision interpretation;	Defects in vision (black spots, blurred vision, illusions); Difficulties with reading and writing;
Temporal lobe	Language understanding; Memory; Hearing; Organization;	Short-term and log-term memory problems; Changes in sexual behaviour; Increased aggression; Difficulties recognizing faces, identifying objects; Difficulties understanding language, speaking;
Cerebellum	Balance, coordination; Posture;	Difficulties with coordination; Slurred speech;
Brainstem	Autonomous functions (i.e. breathing, heart rate, body temperature, swallowing, etc.);	Difficulties in breathing; Difficulties in swallowing; Problems with balance; Dizziness;

2.3. Finite Element Head Models[2]

Over the past decades, Finite Element Head Models (FEHM) have been developed to help understand and predict the head response to various impact conditions. With anatomical knowledge based on Computed Tomography (CT) and Magnetic Resonance Imaging (MRI) scans, as well as medical experience, it is possible to model an accurate representation of human structures with its material models. The biomechanical community across the world has been working tirelessly to verify human anatomical structure under several loading conditions and to recreate the response using computational methods [58].

There are three major conclusions from the review of numerical head models. The majority of FEHM are modelled on a similar level, and it is difficult to distinguish major differences between them. There is a visible trend of simplifying anatomical structures in modelling and material models to only linear elastic models. The third conclusion is that all the mentioned models represent CSF with solid finite elements. This solution is understandable in terms of computational power and time. However, the downside of this solution is that the behaviour is artificially stiffened due to the limitations of solid finite elements. Even a simplified brain model remains a complicated geometry. In order to keep the element deformation without the hourglass phenomenon at a reasonable level, it is necessary to adjust the material model, reduce the element size or increase the integration points. Common sense suggests it is difficult to mitigate fluid behaviour with solid elements. In addition, all the presented models have different components with shared or rigidly connected nodes that directly influence the brain's intracranial movement [58].

At the time of writing this dissertation, there are three most frequently used models in literature: Total HUman Model for Safety (THUMS), The Global Human Body Models Consortium (GHBMC) and KTH Finite Element Head Model. Nevertheless, each model represents a simplified geometry. According to Cloots et al. [59], the gyri and sulci significantly affect the maximum Huber-Mises-Hencky stress value. There is a missing contribution to the detailed geometry and local tissue deformation. The abovementioned models contain nonlinear, validated material models. The summary of FEHM models with a brief description is available in Table 3 [58].

---

[2] The chapter was adapted from one of the co-authored publications, *Symmetry of the human head - are symmetrical models more applicable in numerical analysis?* Symmetry-Basel. 2021, vol. 13, nr 7, art. 1252, s. 1-15, https://doi.org/10.3390/sym13071252

Table 3. Summary of Finite Element Head Models available in the literature, adapted from [60].

Author(s)	Numerical Head Model Description
L Zhang et al. 2001 [61]	Head geometry of a 50-centile adult man; Anatomical drawings. Mass: 4.5 kg, number of elements: 314 500 Linear viscoelastic brain material, elasto-plastic skull material, elastic material for dura matter and skin.
Liying Zhang et al. 2002 [62]	Model I and II. Number of elements: 4 501 Anatomical drawings. Mass: 4.107 kg. Linear viscoelastic brain material, elastic behaviour for cerebrovascular elements.
Kleiven and Hardy 2002 [63]	Finite Element Head Model (KTH FEHM) developed in Kungliga Tekniska Högskolan (Royal Institute of Technology), number of elements: 18 400 Model consisting of skin, skull, cerebrovascular, cerebrospinal fluid (CSF), 11 bridging vein pairs and simplified neck. Sliding connection between skull and brain.
Horgan and Gilchrist 2003 [64]	University College Dublin Brain Trauma Model (UCDBTM) model. Consisting of: three-layered skull, dura matter, cerebrospinal fluid, falx, tentorium, separate hemispheres, cerebellum and brain stem. Linear viscoelastic brain material, elastic material for skull and skin, mixed elements for cerebrospinal fluid.
Belingardi, Chiandussi, and Gaviglio 2005 [65]	Numerical model generated from CT scans of 31-year-old patient, composed of scalp, 3-layered-skull, facial bones, dura matter, CSF, brain tissues, ventricles, falx and tentorium membrane
Zong, Lee, and Lu 2006 [66]	Simplified model consisting of three-layered non-uniform skull, incompressible cerebrospinal fluid and homogenous brain.
Kleiven 2007 [67]	11 454 hexahedral elements, 6 940 four-node elements, 22 two-node elements truss type Hyperelastic and viscoelastic materials for brain tissue, linear-elastic for skull, skin and dura matter.
Takhounts et al. 2008 [68]	Number of elements: 45 875; brain model consisting of: skull, dura matter, cerebrospinal fluid based on outer brain layers and brain.

Yang et al. 2011 [69]	The newest WSUBIM model including viscoelastic brain and elastic-plastic skull behaviour, number of elements: 314 500.
Zhao et al. 2012 [70]	Worcester head injury model (WHIM) – the model consists of the scalp, skull, cerebrum, cerebellum, brain stem, corpus callosum, cerebrospinal fluid, ventricles, sinus, falx cerebri, tentorium cerebelli, pia mater, dura mater, facial bone, mandible, facial muscle, masseter, temporalis, submandibular soft tissue, detailed ocular structures and teeth. The total mass is 3.569 kg.
Mao et al. 2013 [71]	Global Human Body Consortium (GHBMC) is based on MRI scans collected form an average adult male. The model consists of facial tissue, scalp and separate brain structures such as Cerebrum grey, Cerebellum, Thalamus, Brainstem, Basal ganglia, CSF, 3rd Ventricle, Later ventricle, Corpus callosum, Cerebrum white dura, falx and pia.
Sahoo, Deck, and Willinger 2014 [72]	Strasbourg University Finite Element Head Model (SUFEHM) is composed of scalp, brain, brainstem, cerebrospinal fluid (CSF), skull, face and two membranes (the falx and the tentorium).
Atsumi, Nakahira, and Iwamoto 2016 [73]	The Fe head model is an advanced model from the head model of THUMS Ver. 3. The brain consists of separate parts such as cerebrum, cerebellum, stem, dura, arachnoid, pia, falx, CSF, superior sagittal sinus. The mesh size and fineness are almost the same as THUMS Ver. 3, contact conditions and material properties are updated to improve computational stability and accuracy to physical model.
Ghajari, Hellyer, and Sharp 2017 [74]	Imperial College London head model based on a 34-year-old male subject, consisting of skin, skull, cerebrospinal fluid and brain. Falx, tentorium and pia matter was modelled as shell elements.
Fernandes et al. 2018 [75]	Yet Another Head Model (YEAHM) consists of skull, CSF and brain. The brain model has all important sections: frontal, parietal, temporal and occipital lobes, cerebrum, cerebellum, corpus callosum, thalamus, midbrain and brain stem. Nonlinear, viscoelastic model for brain material, hyperelastic model for cerebrospinal fluid and isotropic linear elastic material for skull material.
Ratajczak et al. 2019 [76]	αHEAD brain model consisting of skull, dura matter, falx cerebri, tentorium cerebelli, superior sagittal sinus, bridging veins, hemispheres and cerebellum. Number of elements: solid: 55 117, shell: 3 784, beam: 133

Li, Zhou, and Kleiven 2021 [77]	Detailed and Personalizable Head Model with Axons for Injury Prediction (ADAPT) is based on ICBM152 template generated from 152 healthy subjects. The head model includes the brain, skull (compact and diploe porous bone), meninges (pia, dura, falx, and tentorium), CSF, and superior sagittal sinus. Hyper-viscoelastic material is prescribed for brain structure.
Ptak et al. 2023 [78]	aHEAD (advanced Head models for safety Enhancement And medical Development) is distinguished by high geometrical accuracy (sulci and gyri representation), cardiovascular system including the specific bridging veins connections to sinuses and pia, the CSF represented by the mesh free method (Smoothed Particle Hydrodynamics). The models consists of only hexahedral FE.

FE head models have become a tool to investigate and verify injuries sustained in sports, car, and work accidents. There is a knowledge gap on how the human brain is behaving during the impact. For example, if an athlete suffered a concussion in an American Football game, the athlete is being examined after the collision. The necessary procedures are being conducted. However, these do not shed light on the injury's mechanism. With the help of FEHM, it is possible to observe the tissue behaviour with known boundary conditions. There is a highlighted finding from the Camarillo's research group, which revealed high tensile strains in the corpus callosum during a simulated head impact from an American Football game, correlating with a concussion incident [79]. Such insights demonstrate how FEHM can be instrumental in refining helmet designs to better protect against severe injuries. Furthermore, significant growth is observed in the field of computational biomechanics. With deeper insights into injury mechanisms through the use of sophisticated numerical models, the contribution to the design of sports protective gear, such as helmets, has been substantial and continues to show promising potential.

2.4. Head injury criteria

Traumatic Brain Injuries is caused by a jolt or a blow to the head from a collision or penetrating trauma. There is a division between primary injury that happens at the moment of impact and secondary injury that occurs as the brain crashes back and forth inside the skull (Figure 6). The primary impact is related to the selected lobe or entire brain and sometimes even to skull fracture. The second injury is related to bruising, bleeding and tearing of nerve fibres. In some cases, the observed person may seem fine right after the impact. Confusion, memory loss, blurry vision, dizziness or sometimes even loss of consciousness may occur. Secondary injury is characterised by occurrence after the impact as the brain undergoes delayed trauma – swelling, pushing against the skull and reducing blood flow [57].
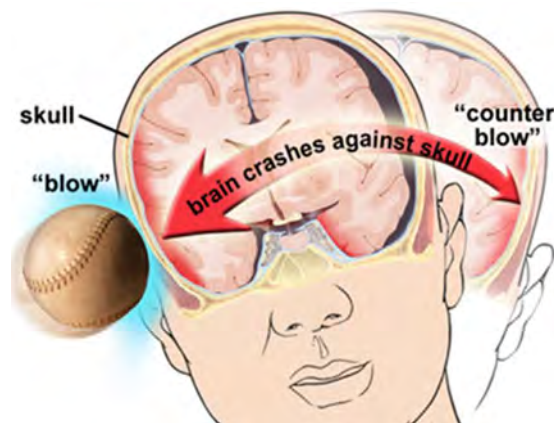
Figure 6. Primary and secondary impact adapted from [57].

TBIs are classified into three categories:

- Mild: confusion, disorientation, memory loss, headache and brief loss of consciousness;
- Moderate: loss of consciousness for 20 minutes to 6 hours, reaction (eyes opening) to stimulation, small brain swelling or bleeding causing sleepiness, arousable;
- Severe: loss of consciousness for more than 6 hours, no reaction (eyes opening) to stimulation.

There are five different types of TBI:

- Concussion: mild head injury, brief loss of consciousness, usually does not lead to permanent brain injury;
- Contusion: bruise to a specific area of the brain caused by an impact, also called coup (brain injured under the area of impact) or contrecoup injuries (brain injured on the opposite side of an impact) ;
- Diffuse axonal injury: shearing and stretching nerve cells at the cellular level (tearing and damaging nerve axons), commonly observed between grey and white matter [80];
- Traumatic Subarachnoid Haemorrhage: bleeding into the space around the brain (occurs when arteries tear during the initial injury);
- Hematoma: blood clot formed when a blood vessel ruptures; examples of epidural and subdural hematoma are presented in Figure 7 [57].
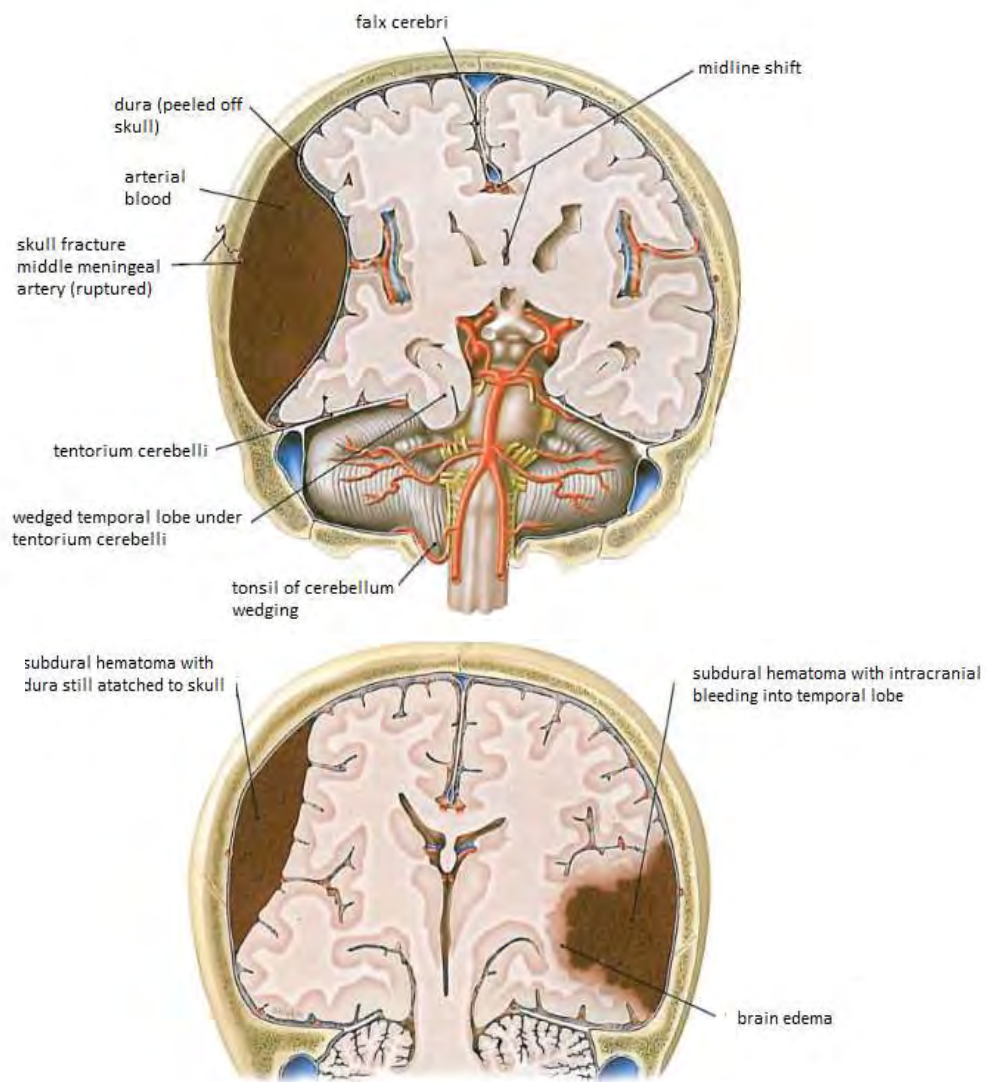
Figure 7. Example of epidural hematoma (top), example of subdural hematoma and intracranial bleeding (bottom) adapted from [81].

In neurotraumatology Glasgow Coma Scale (GCS) is frequently used to determine the type of injury. Points are assigned based on reaction after a skull-brain accident (Table 4) [82].

Table 4. Revised trauma score based on the reaction of Glasgow Coma Scale [82].

Revised trauma score	Points scored	Symptoms according to GCS
Minimal	15	No loss of consciousness or memory
Minor	14-15	Short-lasting unconsciousness, brief memory loss
Moderate	9-13	Unconscious for longer than 5 minutes, slight decremental focal symptoms
Severe	5-8	Unconsciousness, stem reflexes visible
Critical	3-4	Unconsciousness, stem reflexes not visible

In order to have a reference, various criteria were calculated and developed to have the possibility to assess brain injury criterion. The Head Injury Criteria (HIC) is a most frequently used criterium for describing accidents and injuries (Figure 8). However, HIC (equation 3) is based only on longitudinal accelerations and does not include rotational accelerations. The rotational acceleration is associated with strain response, while longitudinal with transient intracranial pressure gradient [50]. Rotational acceleration has as significant influence on the brain as longitudinal acceleration [83]. This parameter is calculated as an integral of acceleration and time. The final value is the maximum result from the equation below:

$$HIC = sup_{t_1 t_2}\left\{\left(\frac{1}{t_2 - t_1}\int_{t_1}^{t_2} a\, dt\right)^{2.5} (t_2 - t_1)\right\}$$

$$a = \sqrt{a_x^2 + a_y^2 + a_z^2}$$

(3)

Where:

a_x, a_y, a_z– linear accelerations components acting on the centre of gravity of the head, expressed in G
t_1, t_2 – time period

In order to define the injury criteria, the following graph was developed:
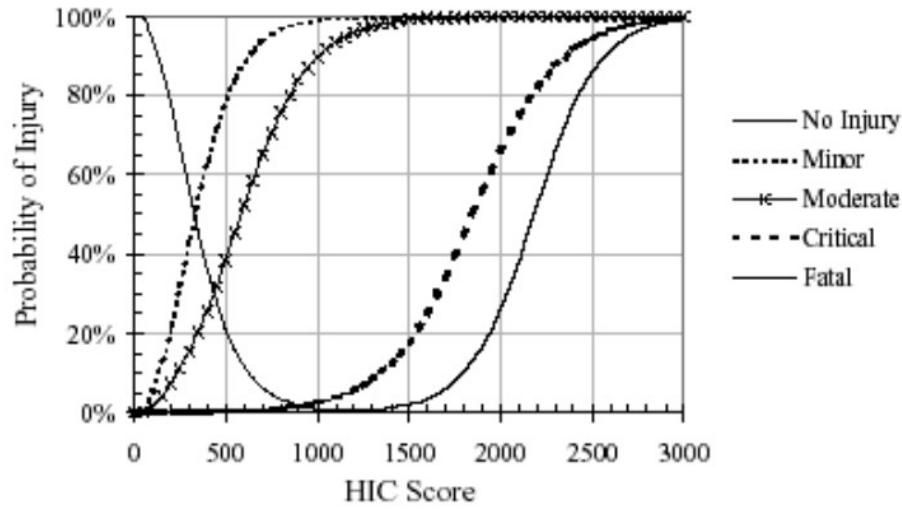
Figure 8. Probability of specific head injury level for a given HIC score [84].

The probability of fatal injury starts with a HIC score equal to 1 000. The HIC is frequently lower than expected because of a very small percentage of direct impacts [50]. Most impacts in sports, racing or urban are oblique, thus the parameter is lower and, on the other hand, values of rotational acceleration are increased.

The Head Impact Power (HIP) criterion was developed to compute linear and rotational accelerations acting on a head that is seen as a one-mass structure. The criterion can be expressed as (equation 4):

$$HIP = \underbrace{C_1 a_x \int a_x dt + C_2 a_y \int a_y dt + C_3 a_z \int a_z dt}_{\text{Linear contribution}} + \underbrace{C_4 \alpha_x \int \alpha_x dt + C_5 \alpha_y \int \alpha_y dt + C_6 \alpha_z \int \alpha_z dt}_{\text{Angular contribution}} \qquad (4)$$

Where:

$C_1 = C_2 = C_3 = 4.5$ kg, $C_4 = 0.0016$ Nm·s^{-2}, $C_5 = 0.0024$ Nm·s^{-2}, $C_6 = 0.022$Nm·s^{-2} for the Hybrid III dummy (50th percentile head), C_i are set as the mass and appropriate moments of inertia,
a_x, a_y, a_z are linear acceleration components (m/s^2)
$\alpha_x, \alpha_y, \alpha_z$ are rotational acceleration components (rad/s^2)

As can be seen, HIP is a time-dependent function. Unfortunately, the criterion does not consider skull fraction [85].

Another widely used brain injury criterion is called Brain Injury Criteria (BrIC). This criterion takes into account not accelerations but rotational velocities. The criterion is expressed as (equation 5):

$$BrIC = \sqrt{\left(\frac{\omega_x}{\omega_{xC}}\right)^2 + \left(\frac{\omega_y}{\omega_{yC}}\right)^2 + \left(\frac{\omega_z}{\omega_{zC}}\right)^2} \tag{5}$$

Where:

ω_x, ω_y, ω_z are maximum angular velocities about the *X*, *Y* and *Z* axis, respectively
ω_{xC}, ω_{yC}, ω_{zC} are critical angular velocities in their directions

The BrIC resultant is expressed as (equation 6):

$$BrIC\_R = \frac{\omega_{max}}{\omega_{cr}} \tag{6}$$

Critical maximal values of angular velocities, based on cumulative strain damage measure (CDSM), Maximum principal strain (MPS) and their average, are depicted in Table 5 [86].

Table 5. Critical maximal angular velocities [86].

Critical Max Angular Velocity	Rad/s (CSDM Based)	Rad/s (MPS Based)	Rad/s (Average of CSDM and MPS)
ω_x	66.20	66.30	66.25
ω_y	59.10	53.80	56.45
ω_z	44.25	41.50	42.87

One of the newest injury criteria introduced is Diffuse Axonal Multi-Axis General Evaluation (DAMAGE) by the University of Virginia, USA [87]. A model representing the maximum brain strain resulting from rotational motion around each head axis was developed using a second-order system. This system was designed as a physical analogue of a mass-spring-damper. It comprises three separate mass-spring-damper units, each corresponding to an independent orthogonal loading direction. Three sets of spring-damper elements were also utilized to interconnect these orthogonal components. The behaviour of this complex system, characterized by damping and encompassing three degrees of freedom (DOF), is governed by equations of motion. The equations describe the system's response to forced excitation applied at the mass points, and they are concisely represented in a matrix format.

Finally, the solution to a matrix representation is a vector containing the displacement time (t) histories of the three coupled masses. These displacements were assumed to be analogous to some measure of brain deformation under rotational motion about each head axis. The maximum magnitude of the system displacement was then fit to maximum brain strain and is referred to as a DAMAGE metric (equation 7):

$$DAMAGE = \wp max_t \left\{ \left| \vec{\delta}(t) \right| \right\}$$

<div align="right">(7)</div>
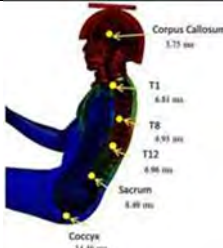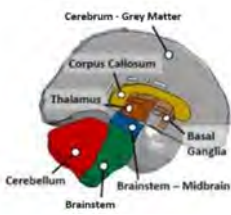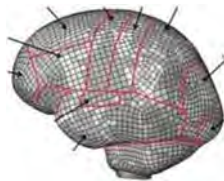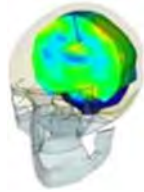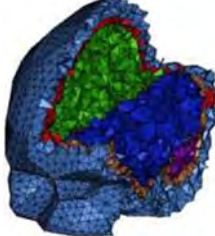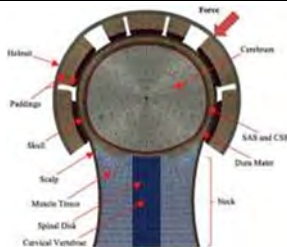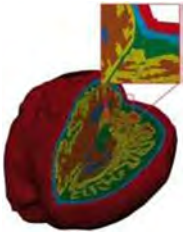
Where $\wp$ is a scale factor that relates the maximum resultant displacement of the system to the maximum brain strain value from the FEHM [87].

2.5.   Finite Element Head Model studies in literature[3]

The use of full numerical human models for head injury verification is uncommon in literature due to the computational effort involved (Table 6). Nevertheless, Darling et al. [88] introduced a study utilizing the GHBMC full-body model with the Riddell Attack Revolution Youth helmet (size Large) model. It is important to note, as per NOCSAE standards, that this model does not include the facemask and retention system. The helmet model underwent validation through convergence analysis [89] and evaluating critical energy-related parameters crucial in explicit finite element analysis [90]–[92], along with validation via experimental methods. The impactor drop test, utilizing vertical acceleration of the impactor, confirmed the model's ability to replicate key features of experimental acceleration profiles [7].

Table 6. Discrete brain models used in the literature adapted from [7].

THUMS [88]	FEHM [93]	UCDBTM [94]	WHIM [95]
KTH Royal Institute of Technology [96]	αHEAD [97]	2D model [98]	Imperial College London [74], [99]

---

[3] The chapter was adapted from one of the co-authored publications, Design and virtual testing of American football helmets - a review. Archives of Computational Methods in Engineering. 2022, vol. 29, s. 1277-1289, https://doi.org/10.1007/s11831-021-09621-7

Different methodologies have been explored by researchers such as Bruneau and Cronin [93], Post et al. [94], and Kuo et al. [95], who focused on helmeted head motion relative to prescribed skull kinematics. These studies utilized linear impactors or drop impacts, conducting a series of impact tests with recorded kinematics (Table 7). Kuo et al. [95] used an instrumented mouthguard to record the data. By applying rigid-body kinematics to the head's centre of gravity and treating the skull as rigid, the authors could apply measured angular and linear head kinematics to their models [100]–[103]. Bruneau and Cronin [57] also explored two neck muscle activation schemes in their model, representing maximally and minimally tensed neck states. The brain models in these studies incorporated regions such as grey matter, white matter, and the corpus callosum [7].

Alizadeh et al. [96] proposed an approach using a damping element consisting of liquid in a linear impactor test. This study first identified the optimal damping force to absorb impact energy from a ballistic mass, then introduced a new energy absorption technology using liquid shock absorbers in helmets. Finite element analysis was employed to integrate an optimal energy absorber into a helmet, and its performance was benchmarked against four other helmets with different energy absorption technologies using kinematic metrics and brain FE criteria [7].

These numerical analyses indicate that loading conditions mimicking NOCSAE standards can be dangerous according to literature injury criteria [88], [93]–[96]. However, numerical brain models have shown that these threshold conditions do not guarantee protection from potential brain injury despite acceptable SI scores. Zhang [104] analysed mild traumatic brain injury (mTBI) occurrences using a finite element model and predicted a 50% injury probability at certain stress and strain levels. In contrast, Willinger and Baumgartner [105] used a similar approach for brain tissue analysis in car accidents. Pfister [106] found that certain levels of strain and strain rates can lead to axonal injury and neural brain cell death.

Bruneau et al. [93] observed minimal peak maximal principal strain increases with balanced muscle activation in helmet-impactor tests. The whole-brain cumulative strain damage measure exhibited more significant increases due to muscle activation than maximal principal strain. However, these were still small, with a maximum rise of 0.07 observed in cumulative strain damage measures. There was no notable change in the magnitude or timing of angular velocity with muscle activation. The study by Alizadeh et al. [96] had multiple limitations in evaluating the performance of a liquid shock absorber in a football helmet. Despite these limitations, the study found a significant reduction in peak kinematics and maximal principal strain with the liquid helmet, corresponding to a substantial decrease in expected concussion numbers from the NFL test [7].

Dymek et al. [97] presented a different approach by investigating Intracranial Pressure (ICP) in setups proposed by Viano et al. [32], comparing it with the HIC calculated with the Hybrid III Head-Neck model. The study highlighted the limitations of criteria based on longitudinal acceleration, noting that most impacts in sports and urban situations are oblique. The study showed that even with permissible HIC values, parameters such as ICP exceed threshold values in every tested configuration, indicating a significant likelihood of head injury. The study emphasizes the need for ongoing research with more advanced models, given that the αHEAD is primarily based on a tetrahedral mesh approach [7].

Table 7. Summary of reviewed research, adapted from [7].

Authors	Impact conditions	FEHM	Investigated parameters
Post et al. 2014 [94]	5 different points of contact	UCDBTM	Maximal principal strain, von Mises stress
Honarmandi, Sadegh, and Cavallaro 2015 [98]	24 different points of contact	2D model	Stress, Strain
Darling, Muthuswamy, and Rajan 2016 [88]	Crown and oblique front	THUMS	Strain, Huber-Mises-Hencky stress
Ghajari, Hellyer, and Sharp 2017 [74]	1 impact	Imperial College London	Strain rate
Kuo et al. 2018 [95]	6 different points of contact	WHIM	Strain
Alizadeh et al. 2019 [96]	8 different points of contact	KTH Royal Institute of Technology	Maximal principal strain
Dymek et al. 2021 [97]	8 different points of contact	αHEAD	ICP
Bruneau and Cronin 2021 [93]	Lateral, Frontal and Rear	Composed of 8 elements	Maximal principal strain, neck activation influence
Zimmerman et al. 2021[99]	148 impacts	Imperial College London	Strain rate

2.6.   Energy absorption

Energy absorption is a critical property in various materials and structures, especially in crashworthiness, impact resistance, or energy dissipation applications. Energy absorption is a material or system's ability to take in energy from impacts and dissipate it rather than transferring it to the object or person. The fundamental principle of energy absorption is the dissipation of kinetic energy. Materials or systems designed for this purpose convert the kinetic energy from an impact into other forms of energy, such as heat or deformation. These are less likely to cause harm. Another key aspect is force distribution, where the impact force is spread over a larger area or longer to reduce the force experienced at any point.

Several studies have investigated the energy absorption characteristics of different materials and structures. Farley in 1983 presented a study comparing the energy absorption characteristics of composite materials with aluminium, highlighting the importance of material selection in energy absorption [107]. Shan et al. in 2015 discussed the role of structural geometry in energy absorption, emphasizing its independence from material properties and loading rates [108]. Moreover, Pham et al. in 2020 investigated the dynamic compressive properties of lightweight rubberized concrete, emphasizing the correlation between failure patterns, compressive strength, and energy absorption capacity [109]. Mei et al. in 2023 highlighted the influence of rubber and cement parameters on predicting the strength and energy absorption properties of aseismic rubber-concrete materials [110]. The mentioned studies underscore the multifaceted nature of energy absorption, which is influenced by material composition, structural design, and dynamic properties.

Various mechanisms are used to absorb energy. Elastic deformation allows materials to absorb energy and return to their original shape. Plastic deformation involves permanent changes in shape and is a principle used in automotive crumple zones. Viscoelastic behaviour, where materials exhibit properties of both viscous and elastic materials, is also critical in efficient energy absorption and dissipation.

Energy absorption is essential in various applications. In automotive safety, crumple zones in vehicles are engineered to absorb impact energy, protecting passengers in collisions. Protective gear such as helmets, body armour, and sports padding rely on energy-absorbing materials to reduce the risk of injury. In the packaging industry, these materials prevent damage to goods during shipping. Design considerations for energy-absorbing materials and systems include their efficiency in absorbing maximum energy while maintaining the weight and size in a reasonable range.

In general, the research on energy absorption spans various materials, including composites, rubberized concrete, aluminium alloys, and metamaterials, as well as diverse structures such as tubes, honeycombs, and cellular materials. The findings underline the dependency between material properties, structural design, and dynamic behaviour in achieving high energy absorption capacity. In conclusion, the thesis will focus on energy-absorbing materials used in American Football helmet technology and the possibility of incorporating different materials and designs.

2.7.   Cork based materials

Cork, a natural cellular material, has garnered significant attention for its energy absorption capabilities and diverse applications. Studies have highlighted the unique properties of cork, emphasizing its potential as an effective energy-absorbing material. Additionally, cork is the main product of the unique forest ecosystem in the world of cork oak trees. It is a material with unique properties that can be reused in any form; it is non-toxic, durable, and wear-resistant. Cork effectively binds atmospheric carbon dioxide, which is essential, especially concerning global warming. With the increased popularity of cork products, there was a significant amount of residual cork pellets that could be reused. With the different approaches of binder type, quantity, grain size and agglomerate density the product agglomerated cork (AC) was developed. Interestingly, AC show remarkable energy-absorbing and isotropic properties.

Cork stands out as an exceptionally versatile sustainable material, with high variety of uses that range from commonplace bottle stoppers to advanced heat shields in aviation. The versatility is thanks to its unique set of properties: lightweight, highly compressible, elastic, and durable. It exhibits resistance to chemicals and biological agents, is flame-retardant, non-toxic, and almost entirely impermeable to both liquids and gases [111], [112]. In addition, it is an excellent vibration, acoustic and thermal insulator [113]–[115].

The honeycomb-like cellular structure is the reason for several cork qualities. This structure, composed of cells and interspersed lenticular tubules, results in relatively low density [116]. The density varies slightly, influenced by the age of the cork oak bark and the harvest timing. Typically, the density of cork falls between 120–240 kg/m^3, with the average density of dry cork estimated to be around 150–160 kg/m^3 [117]. The low density is significant advantage, especially in the context of weight reduction for structures or as an additional layer [118]–[121]. Furthermore, the cork's cellular architecture affects stress distribution. The structure helps distribute stresses under loading in such a way that it prevents cracking and maintains the integrity of the material. Remarkably, cork preserves its characteristics irrespective of environmental conditions such as humidity and temperature. It remains consistently soft yet elastic, pleasant to the touch, and demonstrates impressive wear resistance [122].
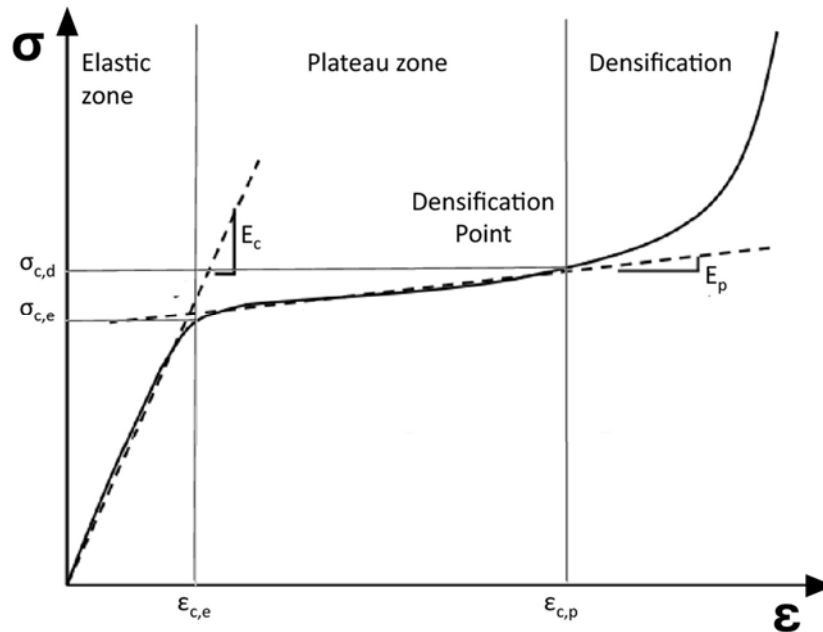
Figure 9. Typical uniaxial stress-strain curve of cork in compression, adapted from [123].

The compression behaviour of cork is characterized by a stress-strain curve that initially shows linearity, followed by an extensive plateau (Figure 9). This plateau phase continues until the cork's cellular structure is completely compressed and densified. The elasticity modulus of the cork, which usually varies between 6–20 MPa, is determined by the slope of this plateau region. Notably, this modulus value depends on the applied load's direction. The modulus values are higher for loads applied in the radial direction than those in the axial and tangential directions [111], [112].

Subjecting cork to temperatures between 100–150°C for 24 hours significantly increases its compressive strength, primarily due to moisture loss. However, extending the heating duration beyond 24 hours reduces strength, as prolonged exposure to heat causes thermal degradation of the cork's structure.

The remarkable flexibility of cork is further demonstrated in compression tests. For example, when a cork sample (with a density of 135 kg/m^3) is compressed to 80% of its original thickness, it quickly recovers to about 80% of its initial size within just 30 s after unloading, showing no signs of buckling. It is important to note that the mechanical properties of cork vary significantly and cannot be represented by a singular value of Poisson's ratio or Young's modulus. This variation is due to differences in cork grades, particularly in density, cell dimensions, and porosity [124]–[127]. Table 8 represents available studies in the literature at the moment of writing the thesis and a brief description of each.

Table 8. Summary of cork and agglomerated cork researched studies under dynamic loading.

Author(s)	Cork research study with dynamic loading
Gameiro, Cirne, and Gary 2007 [128]	The quasi-static (at 0.001 s^{-1}) and the dynamic behaviour of cork (strain rates from 200 s^{-1} to 600 s^{-1}) were compared with the influence of the cork type, the density, the humidity, the cellular structure and the strain rate; static Young's modulus of radial and non-radial cork is higher than the one of agglomerate and micro-agglomerate cork in quasi-static tests; strain rate for the dynamic range considered (200 s^{-1} and 600 s^{-1}), does not have an influence on the mechanical behaviour of the agglomerates but dynamic plateau stress is larger than for statics.
Sanchez-Saez, Barbero, and Cirne 2011 [129]	Analysis of the ballistic behaviour of agglomerate-cork-cored structures in sandwich-panel structures with aluminium; the ballistic limit of the agglomerated cork is low, being approximately half of the ballistic limit of the thin aluminium plates; the additions of a core cork to a structure made from two thin aluminium plates did not alter the failure mechanisms of the plates.
Coelho et al. 2013 [127]	Evaluating the suitability of micro-agglomerated cork combined with expanded polystyrene; difficult to clearly state which arrangement would provide the best compromise on thickness reduction, deceleration and weight.
Fernandes et al. 2014[130]	Simulation of the agglomerated cork's dynamic compressive behaviour (using Finite Element Analysis), including the material's relaxation during the unloading with physical testing; concluded that agglomerated cork has a great capability of returning elastically, mainly at dynamic strain rates, where the permanent deformation was almost none; a numerical model was developed for cork.
Sanchez-Saez et al. 2015 [125]	Analysis of the agglomerated cork's behaviour subjected to several consecutive impacts with different sample thicknesses (35, 50, 70 mm); mixture of cork particles and a polymeric binder, with a density of 140 kg/m^3; a high percentage (70–80%) of the impact energy was absorbed for both impact energies studied (17.5, 35 J); the absorbed-energy percentage increased slightly at higher impact-energy levels.

Jardin et al. 2015 [124]	Uniaxial quasi-static compressive and impact tests performed for a range of distinct agglomerated corks (agglomerated cork and expanded cork) – different grain sizes and binders; less dense agglomerates have lower Young's modulus and a lower stress plateau during deformation stages, the densification stages are reached later than more dense samples, specimens with larger grain size are much more prone to damage mechanisms.
Sanchez-Saez et al. 2015 [131]	Analysis of the dynamic crushing behaviour of the agglomerate cork and the influence of the material thickness in the energy-absorption capacity of a structure; the relationship between the absorbed energy and the impact-energy/thickness ratio is linear for each specimen thickness studied; the energy-absorption capability of the agglomerated cork does not depend on the thickness of specimen in the range of energies 6-46.7 J.
F. A.O. Fernandes et al. 2015 [132]	Comparison of the mechanical response of EPS ($90 \, \text{kg/m}^3$), EPP (60 and $90 \, \text{kg/m}^3$), agglomerated cork ($199 \, \text{kg/m}^3$ and $216 \, \text{kg/m}^3$) and expanded cork ($159 \, \text{kg/m}^3$) under multiple dynamic compressive loading; a larger Young's modulus and higher plateau stresses for synthetic materials (more energy absorbed per unit volume under low stresses and quasi-static conditions), natural materials show a much better compromise between performance and endurance under several impacts.
Santos et al. 2017 [133]	Determination of the influence of the binder type, its quantity, grain size and agglomerate density on the mechanical properties of the agglomerated cork; densification stages can be delayed by using more flexible binders, reducing material density, increasing binder weight percentage or employing smaller cork grains.
Ptak et al. 2017 [134]	Analysis of the dynamic crushing behaviour of the different agglomerated cork (two white agglomerates, with different grain sizes, one black agglomerate) when subjected to impacts (120-850 J); in lower energy levels (120 and 250 J), both white agglomerates kept their integrity, in highest energy levels (500 and 850 J) the samples did not recover the initial shape and formation of cracks was observed.
Kaczyński et. al. 2019 [135]	The assessment of agglomerated cork crashworthiness properties for impact energy of 500 J for temperature range of -30°C to +100°C; material model so-called CAMEA was formulated; cork agglomerates performance is significantly affected by the temperature and grain size.

3. Objectives of the thesis

My career as an American Football player led me to understand that human health awareness is not highlighted enough. The pivotal point was when I suffered a concussion, and I realized how misinformed or uninformed an average person is. With my research, I aim to spread verified literature information about brain health and brain trauma as well as insight into how helmets are regulated and how they are designed. The increased awareness will hopefully result in people taking care of themselves more seriously. The findings will focus on American Football; however, an accident can occur while riding a bicycle or walking. The literature review proved that the number of concussions across all play levels is enormous and that continuous research about minimizing the probability of injury is necessary.

3.1. Main objectives

The main objective of the thesis is to investigate the head injury mechanism related to American Football and minimize the probability of injury. The approach undertaken by the author is first to analyse the tackling mechanism in American Football, mechanical tests and implementation of additional energy-absorbing layer to helmets, verification of applicability of different head injury criteria and finally, validation of the brain tissue material model based on the dynamic response. The primary work tool was numerical analysis, which enabled me to work with multiple simulations, physical measurements and experiments. The thesis is divided into the hypothesis:

In American Football there is, among used, a safer and recommended tackling position in terms of head injury.

and additional scientific targets:

- *Analysis of sustainable energy-absorbing materials for the American Football helmets add-on design.*
- *Verification of HIC for Hybrid III dummy and intracranial pressure for αHEAD numerical models.*
- *Analysis of brain tissue numerical material models under dynamic loading.*

3.2. Author's personal experience as a player

During author's college and doctorate studies, I combined university duties with an amateur and later semi-amateur career as an American Football player on my hometown team. With almost ten years of playing experience, I have linked my interests in sports with a Bachelor's, Master and, finally, PhD thesis. I would like to share my reflections and opinion about the differences in head injury awareness across the Polish Football league (PFL), European League of Football (ELF) and National Football League (NFL) in the United States of America.

Starting with the highest level of American Football, the athletes beginning their sports journey in high school are informed about the probability of head injury and the mechanics of avoiding head-to-head collisions in practices and games. Later, at the college level, seminars are presented with deeper insight into the injury mechanism. With the helmet technological advancement, it is emphasized to use the newest models and recondition them after each season or even throughout the season. Recently, there has been an introduction to college offseason preparation about the guardian caps – the padded soft shells worn over football helmets. According to NFL executive vice president Jeff Miller, there has been a 52% decrease in concussions suffered by players at positions wearing Guardian Caps, compared to the concussion rate of players at the same positions over the last three years of training camps when Guardian Caps were not worn [136]. The caps are mandatory during preseason camps and practices during college-level seasons. Finally, on the highest level, there will be a regulation that caps will now be mandated at every preseason practice and every regular-season and postseason practice with contact. Players in position groups where head contact is most seen are required to wear the Guardian Cap, with running backs and fullbacks joining the previously included linemen and linebackers. The only positions not required to wear the caps are kickers, punters, quarterbacks, wide receivers, and defensive backs.

Looking back at European and Polish field, no seminars are conducted for players on the league or team level addressing the head injury mechanisms, probabilities of injury and the importance of helmets and their technology. It is observed that the highest-rated league – ELF, is providing players with a discount to manufacturers such as Riddell/Xenith so that players can buy new equipment. This is unfortunately not observed in the Polish league. I have faced multiple teams where players had helmets developed in the 2000s. It is noticeable that the awareness about helmet technology and its role in protecting from injuries is minor. It must be highlighted that compared to US standards, each player in Europe is responsible for his equipment, and it is not verified whether the helmet was reconditioned after a regulated by manufacturer time.

4.   Methodology

In order to simplify the reading of the thesis, this description will serve as a reading guide and a brief comment on each subchapter. The idea of all experiments prepared and executed during the preparation of the dissertation aimed to develop an additional energy-absorbing layer for the developed American Football helmets that could be used at the beginning in practices and in the future incorporate them in regular games. Another dissertation concept was to broaden the biomechanical insight regarding the injury mechanisms and ultimately minimize the probability of head injury in American Football. The summary is presented in Figure 10.

	Measurements	Experiments	Results
Field accelerometer tests and multibody simulations			
Cork porous biocomposites with modified polyurethane matrix and polyol based on used cooking oil			
Physical experiments with cork and helmets			
Injury criteria to head biomechanics			
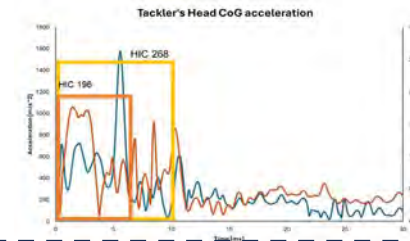
Figure 10. Methodology undertaken in the dissertation.

The author would like to highlight the terminology used in this work related to head and brain injuries. The public tends to associate the negative symptoms with "brain injury" (judged as more serious) rather than with "head injury" (less severe, in their view), despite the fact the description may be related to the same injury event [137]. Thus, the author will use the terms head/brain injury interchangeably regarding brain injury.

At the beginning of the methodology development chapter *Finite element American Football helmet models*, I decided to describe the available numerical helmet models for research purposes. Each helmet was developed as a part of the NFL's "Play Smart, Play Safe" program [138]. This program aims to distribute various helmet models through Biomechanical Consulting and Research, LLC (Biocore), facilitating a collaborative environment. The next chapter 5 (Field accelerometer tests and multibody simulations) describes an attempt to record the behaviour of the athletes during the simulated tackling situation. Due to the limited game recordings and poor quality at the domestic game level, it was decided to attempt to record the athlete in two separate movements and combine them in prepared simulations. The recordings took place cooperating with the Wrocław University of Science and Technology and Wrocław University of Health and Sport Sciences. NORAXON myoMOTION sensors were attached to the athlete's body, and acceleration data was collected. To verify, the attempts were recorded for further analysis with TEMA software (IMAGESYSTEMS). Finally, coupling two numerical codes – MADYMO and LS-DYNA enabled to progress further and prepare a set of two simulations with different tackling mechanics (so-called *Open-field* and *Side tackle*). The multibody dummies available in MADYMO served as athletes, and the American Football helmet was modelled in LS-DYNA. The biggest limitation in this research is that the simulation was possible only under the criteria that a short time window would be considered. Unfortunately, the multi-body system does not include the muscles' mechanisms or tissue stiffness.

The next part of the conducted experiments, chapter 6 (Cork porous biocomposites with modified polyurethane matrix and polyol based on used cooking oil) aimed to develop an additional energy-absorbing layer for the developed American Football helmets. There was an established cooperation between the Cracow University of Technology, the University of Aveiro (Portugal) and the Wrocław University of Science and Technology to develop state-of-the-art cork porous composites from renewable materials. Since the researchers from Cracow mainly prepared the development process, I decided to focus on mechanical testing under dynamic loading. The boundary conditions were set according to the previously studied cork samples. Twelve different samples were tested under dynamic loading to assess the ability to absorb energy, and finally, the tests were recreated numerically to obtain a validated material model. After the results comparison, it was decided that agglomerated cork will suit the intended purpose best. This leads us to physical experiments carried out during my stay at the University of Virginia in the Center for Applied Biomechanics (United States of America) in chapter 7 (Physical experiments with cork and helmets). As mentioned previously, the idea behind the dissertation was to develop an additional absorbing layer that would minimize the probability of injury. The tests with two different approaches proved that cork could serve as an additional energy-absorbing layer.

Finally, with my experience as a player, I decided to verify whether linear accelerations could be a severe predictor for head injury in chapter 8 (Injury criteria to head biomechanics). Analysing the trend visible in car or urban accidents, I adopted a similar strategy in sports accidents. Analysing the available simplified numerical head model αHEAD I proved that hydrostatic pressure values do not correlate with HIC under selected impact conditions.

Finite element American Football helmet models[4]

Numerous academic institutions are at the forefront of developing numerical models for American Football helmets. These include the University of Waterloo, Arizona State University, University of Alabama, University of Virginia, Wayne State University, Mississippi State University, and the KTH Royal Institute of Technology. Many of these researchers utilize finite element helmet models provided by the NFL's "Play Smart, Play Safe" program. This program aims to distribute various helmet models through Biocore, facilitating a collaborative environment. The aim is to enhance the understanding of head trauma in NFL players and partner with helmet manufacturers, other businesses, entrepreneurs, and universities to create highly safe protective gear [139].

a)   b)   c)
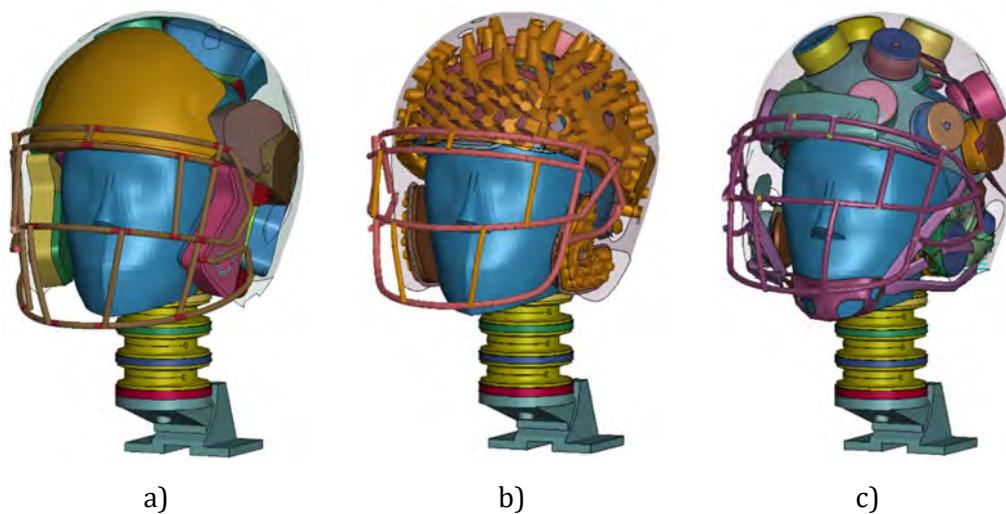
Figure 11. Finite element models with different energy-absorbing technologies: a) foam, b) buckling cone, c) air damper; based on [140].

An example of these models is the Riddell Revolution Speed Classic helmet (Figure 11), which comprises 53 components and 147 384 finite elements (Table 9). The validation process for each material model involved a series of compression, shear, and tension tests. The nonlinear paddings (front, top, sides and rear) have assigned material models based on multiple compression strain rate curves. To ensure the reliability of the helmet model, a total of 62 simulations were carried out, employing either a Hybrid III (HIII) or NOCSAE headform, thereby confirming the accuracy and effectiveness of the helmet in a comprehensive manner [140].

---

[4] The chapter was adapted from one of the co-authored publications, Design and virtual testing of American football helmets - a review. Archives of Computational Methods in Engineering. 2022, vol. 29, s. 1277-1289, https://doi.org/10.1007/s11831-021-09621-7

Table 9. Exemplary material model data for Riddell Revolution Speed Classic.

Part	Density [kg/m³]	Young's Modulus [MPa]	Poisson's Ratio	Material Model in LS-DYNA
Helmet				
FACEMASK	8 546.0	210 000	0.3	ELASTIC
SHELL	1 095.0	1 565	0.3	ELASTIC
PADDING (FRONT)	170.5	3	–	FU_CHANG_FOAM_LOG_INTERPOLATION
PADDING (TOP, SIDES)	70.0 95.0	20	–	FU_CHANG_FOAM_LOG_INTERPOLATION
PADDING (REAR)	100.0	200	–	FU_CHANG_FOAM_LOG_INTERPOLATION
Impactor				
NYLON END CAP	1 140.0	2 410	0.4	ELASTIC
VINYL NITRILE	122.6	1 000	–	FU_CHANG_FOAM_LOG_INTERPOLATION
BACKING PLATE	6 899.0	200 000	0.3	RIGID
RAM	140 700	200 000	0.3	RIGID

5.   Field accelerometer tests and multibody simulations[5]

A new approach is proposed in this research, involving recording an American Football player during three characteristic behaviours: sprinting with the ball, tackling a training dummy in a position with the head in front and in a position with the head behind. The simplified research approach is based on nearly ten years of experience as a player of the author.

The author concluded that only open-field situations should be considered when considering tackling techniques in game and practice recordings. Tackles in the area indicated by the base of the numbers on both sides of the field and ending with the goal areas are very demanding technically: the positioning of the head and the entire body are crucial for effective and safe tackling. Tackles near the sideline are often less technical, as they are sufficient to push a player out of bounds to stop the play (Figure 12).
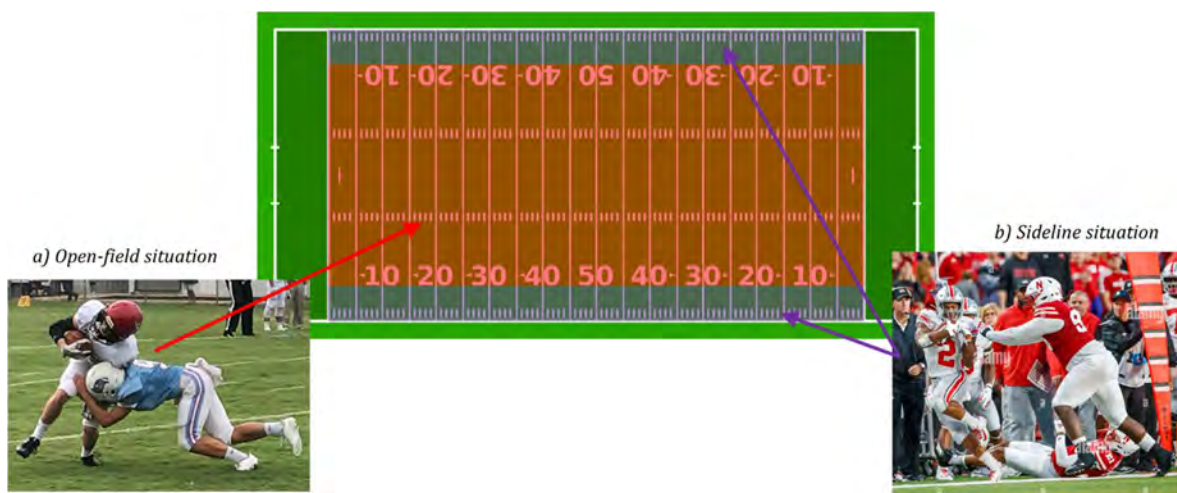
Figure 12. a) Open-field and b) Sideline tackle visualization.

The recordings of an American Football player were conducted using the NORAXON myoMOTION sensors. The camera recordings allowed for the speed analysis of the characteristic points on the helmet and the player's body. With TEMA software (IMAGESYSTEMS), it was possible to track a point with a known reference and read the speed profiles. Five tests were conducted for each situation, and the player's average speed before impact and during a 7 m/s sprint was recorded (Figure 13).

Figure 13. Athlete's recordings with characteristic points to video analysis in TEMA software.

13 NORAXON sensors were attached to the player's body: on the head (firmly placed in the helmet), arms, forearms, chest height, lower back, thighs, calves, and feet (Figure 14). The data were recorded at a sampling rate of 100 Hz.
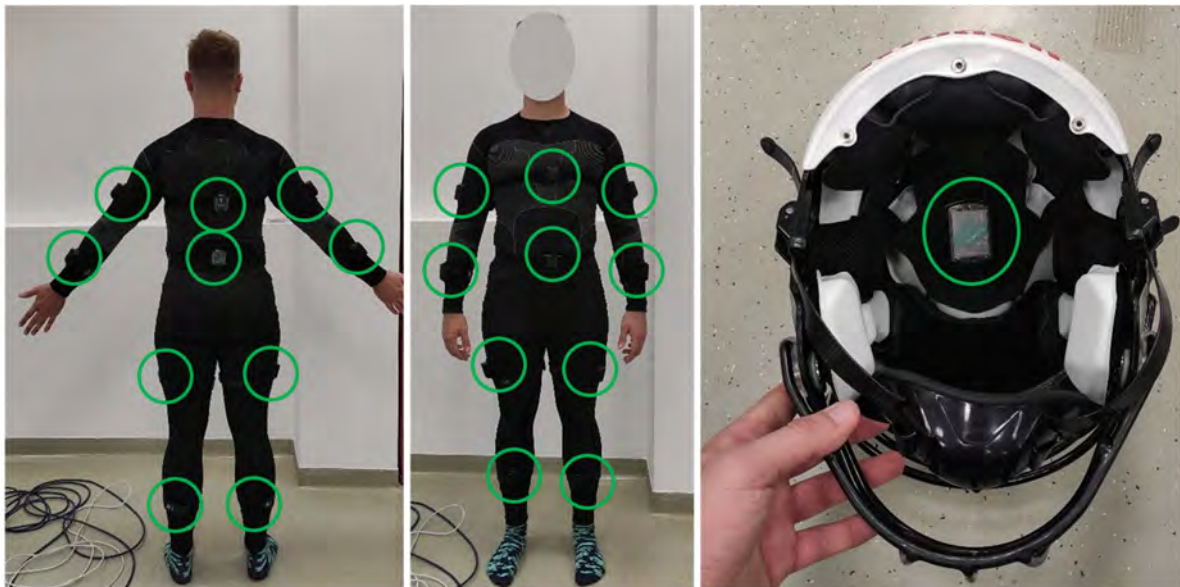
Figure 14. Sensor placement on the athlete's body and helmet.

The next stage of the study was to establish the athletes' position based on the recordings and prepare a numerical simulation. The recorded data (velocity at the time of impact and sprint) was used as boundary conditions for the simulations. The undertaken approach included the Multibody MADYMO 95th percentile pedestrian dummies and a numerical helmet model available in LS-DYNA. The primary assumption was verifying which tackling position is safer regarding head injury. The first simulation exhibits the characteristic position of a tackler in the *open-field* situation. The specific position includes the head placement on the ball carrier's chest or, in the field jargon – on the numbers. The second simulation was designed to recreate the *sideline* simulation. The tackler's head is positioned on the nearest shoulder. In both cases, the tackler is situated under an angle of 30° towards the ball carrier (Figure 15). The initial velocity of both dummies is 7 m/s towards each other. From the game efficiency point of view, the first case is better and was thought of by coaches worldwide.

The proper head position is crucial for the safety of the players. Both players striking with their helmet crowns result in high compressive forces on the neck and, due to the helmet shape, could result in major slips and high bending moments on the neck. The assumed head position, which is head up, is ideal. Putting the head on the chest of the opposing player and maintaining proper technique increases the difficulty for the carrier to battle through the tackler's body. The major assumption in this experiment is that the athletes are under high muscle tension (braced for impact), and the time window is limited. The collected data is focused only on head accelerations.
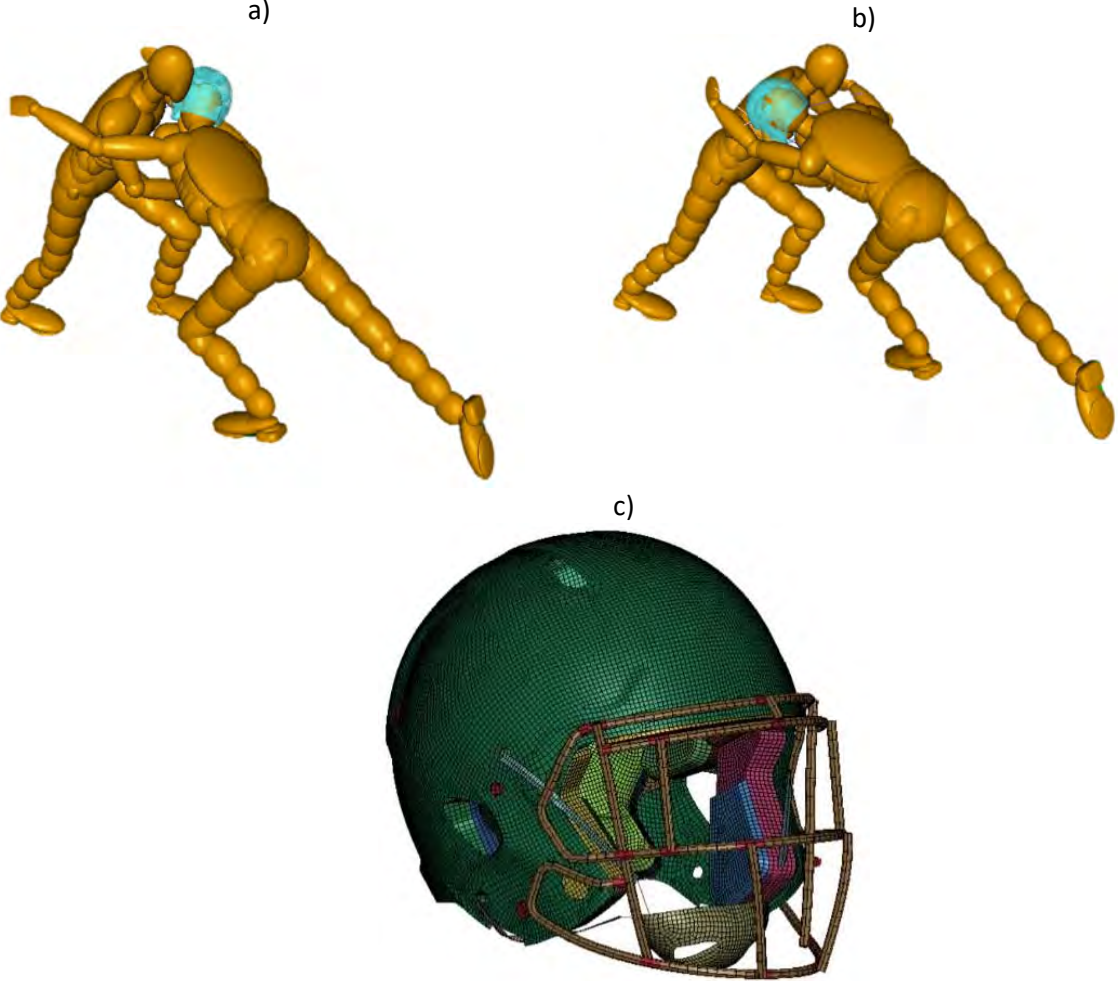
Figure 15. a-b) MADYMO Multibody Human Body Model coupling and c) with helmet composed of finite elements.

5.1.   Results

The field measurements allowed us to define the boundary conditions for the simulation, including the position of the dummies and the initial velocity. The studies are reinforced by the author's experience as an American Football player and include field experience. The MADYMO software enabled the measurement of the linear accelerations for the centre of the head. The tackler, engaged in head impact, was equipped with a numerical helmet. The study included the coupling of two numerical codes, MADYMO and LS-DYNA. The gathered data was analysed with a CFC 180 filter to eliminate noise. It is observed that the lower HIC value is observed for the first position (*open-field*): 196 than for the second position (*sideline*): 268. It is observed that the first contact between the dummies is later for the first position. The specific dummy position can explain this. In the second case, the tackler has contact with the shoulder of the ball carrier. It can be observed that there is a significantly higher magnitude peak for the first position (Figure 16). Analysing the simulation course and the very small time boundary, I believe that it may be due to some instabilities between the numerical codes. It is observed that even after filtering, the noise in recorded data is visible. The simulation aimed to mimic the first contact between the players, obtain the head acceleration data and did not aim to recreate the full kinematics of the tackle. Overall, the results suggest that the first tackling position is safer regarding head injuries.
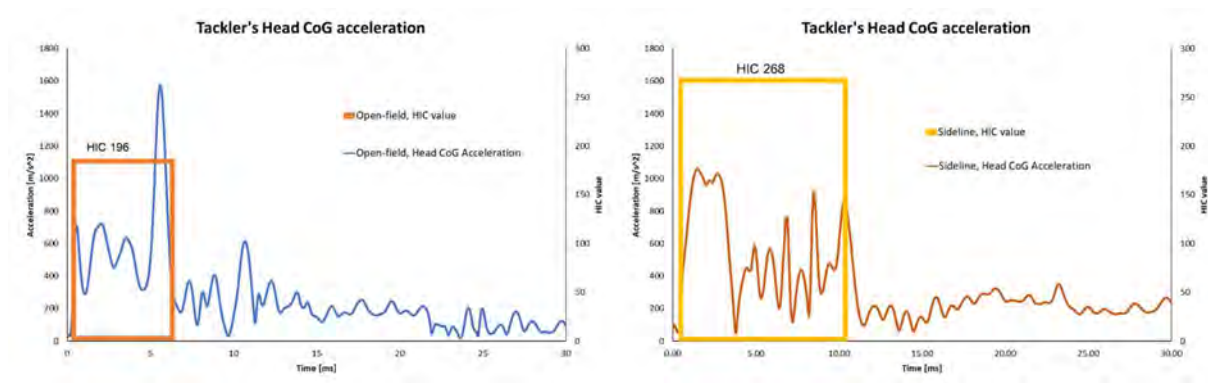
Figure 16. Linear acceleration graphs with HIC36.

5.2.   Chapter conclusions

The field measurements aimed to establish the reference body position for the tackler and ball carrier and the limbs' global and local accelerations. Unfortunately, the frequency of collected data was too small to obtain reliable data sets. During the research, it was decided to use the global velocity and prescribe it to the dummies. Several limitations have to be underlined. The simulations aimed to mimic the first contact between the players and measure the accelerations of the head's centre of gravity. Due to the multibody model characteristics (lack of muscle tensions, general body material models), it was impossible to recreate the full tackle. Considering the limitations, the study proved that tackling the ball carrier with the head positioned in the ball carrier's chest is safer regarding HIC value. The study showed that there were possibly high forces and bending moments acting on the neck of the players. A study examining the neck injury criteria would be highly beneficial for the literature and reference as there is a missing research gap.

6. Cork porous biocomposites with modified polyurethane matrix and polyol based on used cooking oil[6]

The state-of-the-art cork porous biocomposites with modified polyurethane matrix and polyol based on used cooking oil were prepared and tested in cooperation with the University of Aveiro and Cracow University of Technology. The development process was carried out mainly by Maria Kurańska's group at the Cracow University of Technology, and the mechanical testing was carried out at Wrocław University of Science and Technology. This is why I decided to briefly describe the development and focus on mechanical testing and numerical representation. The complete development process is available in one co-authored publication [141].

6.1. Development process

Polyurethane materials from renewable raw materials have gained significant interest across multiple industries. They fit the growing focus on producing eco-friendly materials capable of i.e. enhancing buildings' energy efficiency. The research presented illustrates the potential to substitute certain petrochemical raw materials with renewable alternatives. This was accomplished by replacing a petrochemical component in the synthesis of the polyurethane structure with waste vegetable oil [141].

Foams made of polyurethane (PUR) were created using a one-stage process involving component A, the polyol premix, and component B – an isocyanate. The polyol premix was a mixture of a polyol or a mix of petrochemical and bio-based polyols, along with a catalyst, a surfactant, a flame retardant, and water. It was prepared in 500 ml polypropylene containers. Then, the appropriate amount of isocyanate was added to the premix container and immediately stirred for 7 seconds using a mechanical stirrer. The resulting mixture was used to create composites containing cork in proportions of 3%, 6%, 9%, and 12% relative to the polyol mass in the petrochemical polyol (PU) system. This blend was poured into prepared plastic moulds, expanded, and underwent cross-linking. Testing of the materials took place 24 hours after the synthesis. The reference materials were synthesized using two formulations: one based solely on petrochemical polyol (PU) and the other based on a mixture of petrochemical polyol and bio-polyol (BPU) in a 1:1 weight ratio. The isocyanate index of the synthesized materials was 1.1 [141]. The samples are visualized in Figure 17.

---

[6] The chapter was adapted from one of the co-authored publications, Cork porous biocomposites with polyurethane matrix modified with polyol based on used cooking oil. Materials. 2023, vol. 16, nr 8, art. 3032, s. 1-15, https://doi.org/10.3390/ma16083032 and Eco-Friendly Cork–Polyurethane Biocomposites for Enhanced Impact Performance: Experimental and Numerical Analysis. Polymers. 2024 vol.16, nr 7, art. 887, s. 1-18, https://doi.org/10.3390/polym16070887
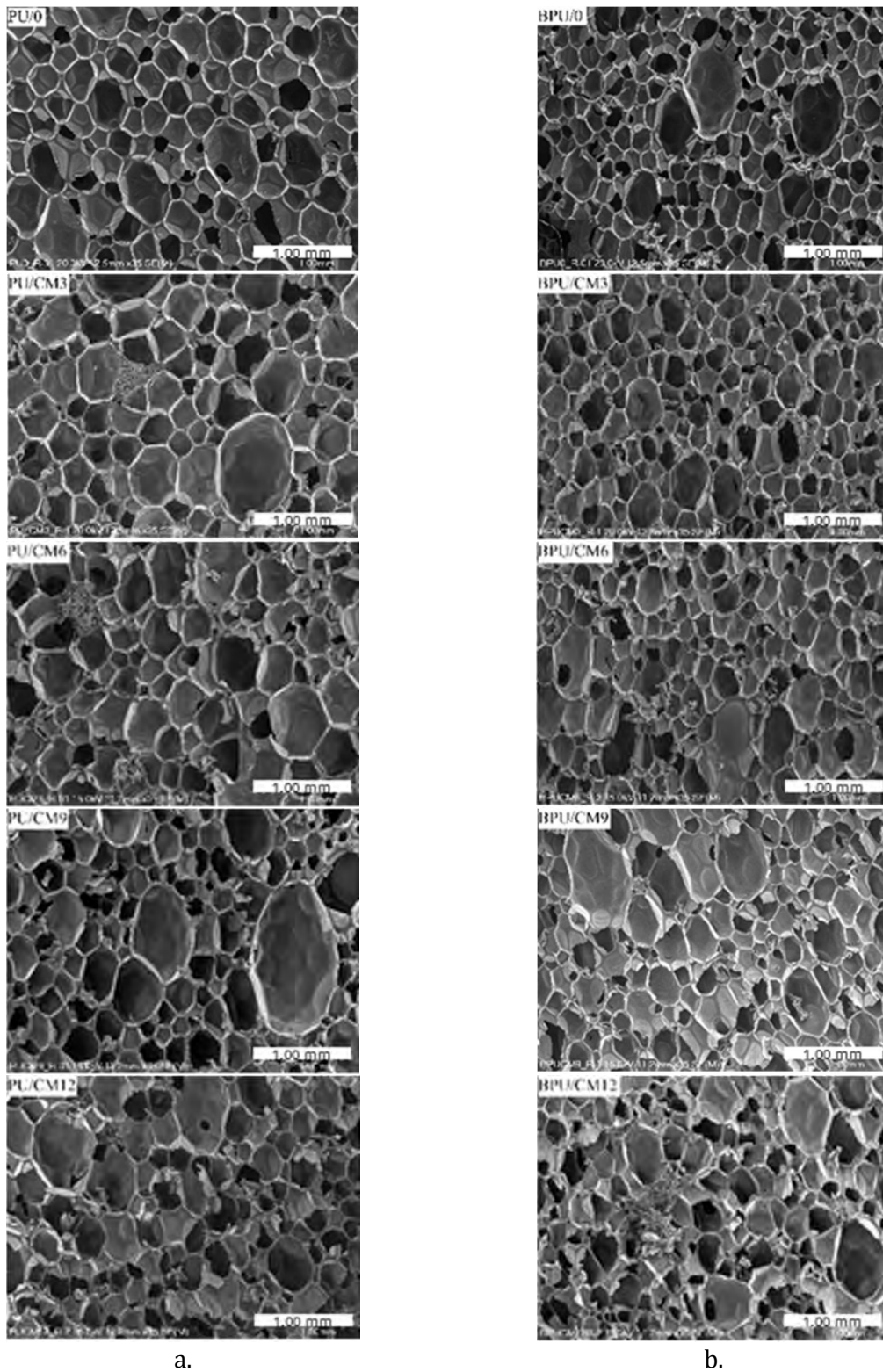
Figure 17. SEM images of the cellular structure of foams without a) and with b) the bio-polyol, adapted from [141].

6.2. Experimental and numerical dynamic testing

There were 24 submitted samples for mechanical testing. The materials are separated into the following groups:

1. One petrochemical polyol foam without cork (PU_0) and four petrochemical polyol with different amounts of modified cork (PU_CM_3, PU_CM_6, PU_CM_9, PU_CM_12);
2. Two foams of a petrochemical polyol with varying amounts of natural cork (PU_C_3, PU_C_6);
3. One petrochemical polyol and bio-polyol (mass ratio 1:1) foam without cork (BPU_0) and petrochemical polyol and bio-polyol (mass ratio 1:1) foams with varying amounts of modified cork (BPU_CM_3, BPU_CM_6, BPU_CM_9, BPU_CM_12).

Table 10 presents the description of the composition of the samples and the terminology used in this work. All samples are 50x50x60 mm in size (width x depth x height).

Table 10. Cork composite samples composition and the terminology used, adapted from [142].

Description	Cork content %	Nomenclature
Petrochemical polyol foam	-	PU_0
Petrochemical polyol foam	3% modified cork	PU_CM_3
Petrochemical polyol foam	6% modified cork	PU_CM_6
Petrochemical polyol foam	9% modified cork	PU_CM_9
Petrochemical polyol foam	12% modified cork	PU_CM_12
Petrochemical polyol foam	3% natural cork	PU_C_3
Petrochemical polyol foam	6% natural cork	PU_C_6
Petrochemical polyol and bio-polyol foam	-	BPU_0
Petrochemical polyol and bio-polyol foam	3% modified cork	BPU_CM_3
Petrochemical polyol and bio-polyol foam	6% modified cork	BPU_CM_6
Petrochemical polyol and bio-polyol foam	9% modified cork	BPU_CM_9
Petrochemical polyol and bio-polyol foam	12% modified cork	BPU_CM_12

Dynamic impact tests were conducted using the Instron Dynatup 9250HV, with an initial impact velocity of 4.8 m/s. All 12 cork composite samples underwent experimental testing. The impacts were delivered by an 8.515 kg cylindrical steel impactor featuring a flat surface, with an impact energy of 100 J. The impact energy was picked in order to obtain a solid reference to previously conducted studies on cork agglomeration in the literature [134], [135]. Each specimen was precisely positioned at the centre of the lower anvil. The impacts were recorded for visual analysis using an ultra-high-speed camera, the Phantom V12 (Figure 18). Employing bumpers in the machine setup allowed the impactor to descend a maximum of 50 mm from the initial contact point. Consequently, the maximum experimental strain observed reached 83%. The test setup enabled collecting essential impactor data such as displacement, velocity, and acceleration over time.

(1)	(2)	(3)
(4)	(5)	(6)
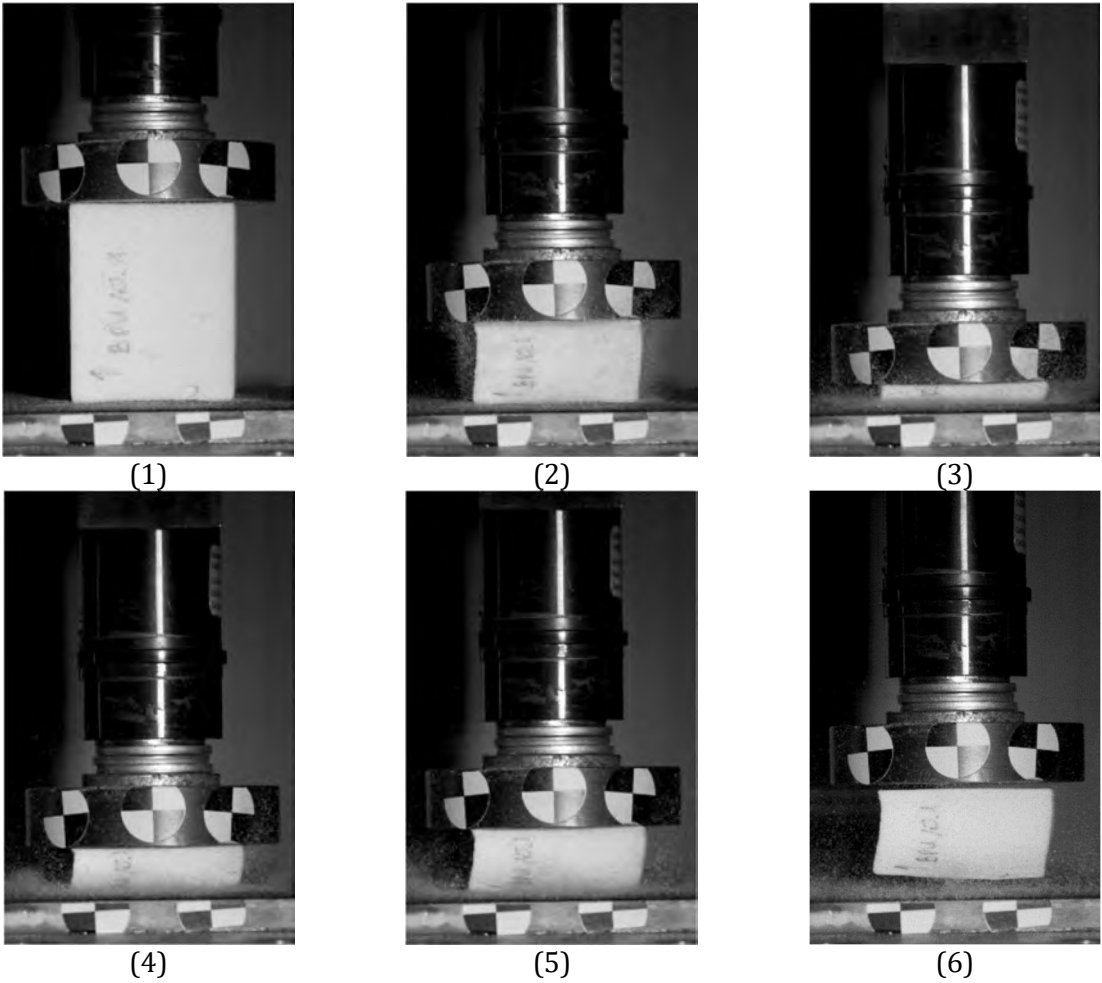
Figure 18. Experimental setup – cork sample BPU_0 at 5 ms time intervals, adapted from [142].

Replicating the experimental dynamic tests in Abaqus involved modelling two rigid analytical planes to simulate the steel anvil and impactor. The rigid impactor was designed with a single degree of freedom along the compression direction (vertical axis), mirroring the experimental setup. A predefined field represented the impact velocity of 4.8 m/s. The interaction between the samples and the rigid bodies was simulated using a surface-to-surface contact approach within the explicit dynamic solver. This employed a friction coefficient of 0.2 and a "hard" contact pressure-overclosure, as presented in the literature [130]. The bottom plate was entirely constrained to maintain its fixed position. The deformable body was discretized using selective reduced integrated 32 805 C3D8R (8-node linear brick, reduced integration with hourglass control) elements.

The samples were modelled as nonlinear elastic materials to mirror the observed minimal permanent deformation shortly after impact in the physical experiments. Consequently, the tested foams were represented as hyperelastic materials, utilizing a combination of the Hyperfoam and Mullins Effect material models found in the Abaqus computer-aided-engineering (CAE) nonlinear material library.

Table 11. Model of material for biocomposite samples.

ρ kg/m³	ν	N	r	m	β
90	0	3	1.1	0.5	0.1

Table 11 presents the parameters introduced into the Abaqus software to characterize all samples, where N (polynomial order) and ν (Poisson's ratio) were defined based on existing literature. Parameters: r, β and m are material coefficients (without direct physical interpretations). While the parameters r and β are dimensionless, the parameter m has the dimensions of energy. The parameter m controls whether the damage occurs at low strain levels; r and β control the amount of damage [142], [143]. Each sample was uniquely defined by its stress-strain curve derived from physical experiments.

6.3. Results

In order to clarify the different aspects undertaken in this chapter, the physical experiments are presented separately from the numerical results.

6.3.1. Experimental results

The BPU sample, obtained from a mixture of petrochemical polyol and bio-polyol, exhibits a 15% lower energy absorption capability compared to the PU sample generated from petrochemical polyol. Notably, at a 45 mm impactor displacement post-initial contact, the BPU absorbed 37.75 J, while the PU absorbed 44.35 J. This phenomenon is observed due to reduced compressive stress within the plateau region ($0.1 < \varepsilon < 0.35$), registering at σ_{BPU_0} = 0.283 MPa and σ_{PU_0} = 0.344 MPa [142].

The samples resulting from a blend of petrochemical polyol and bio-polyol (BPU_CM) display an energy absorption capacity of 9% to 25% lower (depending on the modified cork content) than samples composed solely of petrochemical polyol (PU_CM). No visible trend is observed between the cork content in the samples and their energy absorption levels. The most noticeable contrast is observed between samples containing 3% modified cork content (E_{avg}BPU_CM_3 / E_{avg}PU_CM_3 = 34.7 / 46.3 = 0.75), while the smallest distinction is observed in samples with 6% modified cork content (E_{avg}BPU_CM_6 / E_{avg}PU_CM_6 = 33.7 / 37.1 = 0.90) [142].

The overall worse energy absorption performance of BPU samples can be attributed to the lower hydroxyl content in the bio-polyol compared to the petrochemical polyol. This discrepancy requires maintaining an equivalent isocyanate index, resulting in reduced isocyanate incorporated into the PUR formulation when incorporating bio-polyol. Consequently, this generates rigid segments within the PUR chains, impacting their mechanical strength [141], [142].

Adding modified cork to samples restricts their ability to absorb impact energy. For petrochemical polyol samples containing up to 3% cork, there is minimal influence on energy absorption (Figure 19). However, as cork content increases, there is a noticeable decrease in impact energy absorption by around 19%, declining from 45.4 J (average value for PU_0 and PU_CM_3) to 36.9 J (average value for PU_CM_6, PU_CM_9, and PU_CM_12) [142].
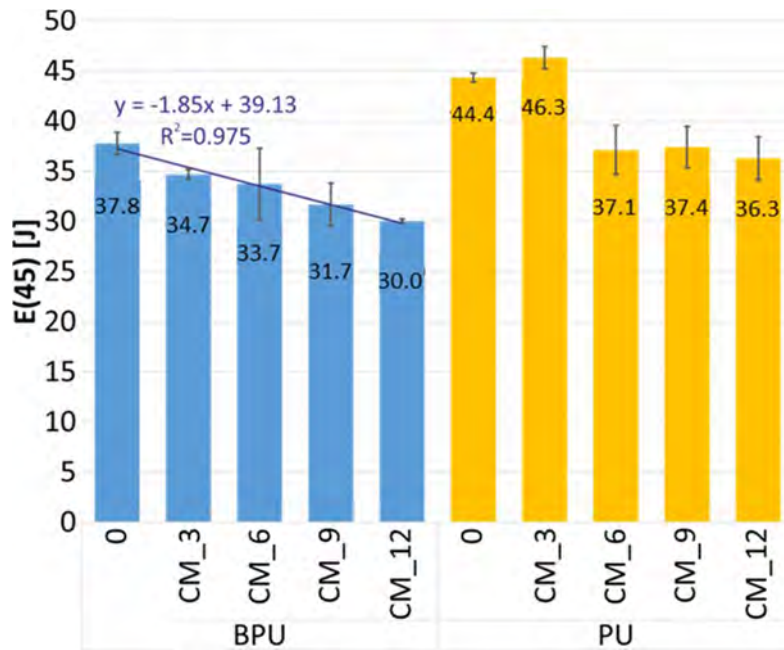
Figure 19. Influence of cork content on the energy absorption level at 45mm impactor displacement after the initial contact, adapted from [142].

In the case of petrochemical polyol with bio-polyol samples, the increase in cork content proportionally influences the decline in energy absorption. This trend can be described by the formula $E = -1.85 \cdot k + 39.13$ ($R^2 = 0.975$), where k represents the percentage content of modified cork (Figure 19). This equation suggests that for every 1% increase in cork content, the energy absorption capability decreases by an average of 1.85 J, approximately 4.89%, based on the base value of 37.8 J. Using linear approximation aims to optimize sample stiffness for specific purposes [142].

The cork's impact on limiting the composites' energy absorption capacity is closely linked to the system's structural integrity. Previous investigations, such as Kurańka's study [141], suggest that incorporating cork filler dilutes the reaction system, reducing reactivity measured through dielectric polarization. This reduced reactivity is also evident in lower core temperatures of the foams when cork is present. Additionally, introducing cork into the composite matrix expands cell dimensions and reduces apparent density in both BPU_CM and PU_CM samples. These alterations significantly affect structural integrity and subsequently impact the materials' mechanical properties [142].

The physical experiments resulted in calculating stress-strain curves for each sample. This data is used as an individual input in the FE analysis as well as a comparison for results. The curves are presented in Figure 20.

a)

b)

c)
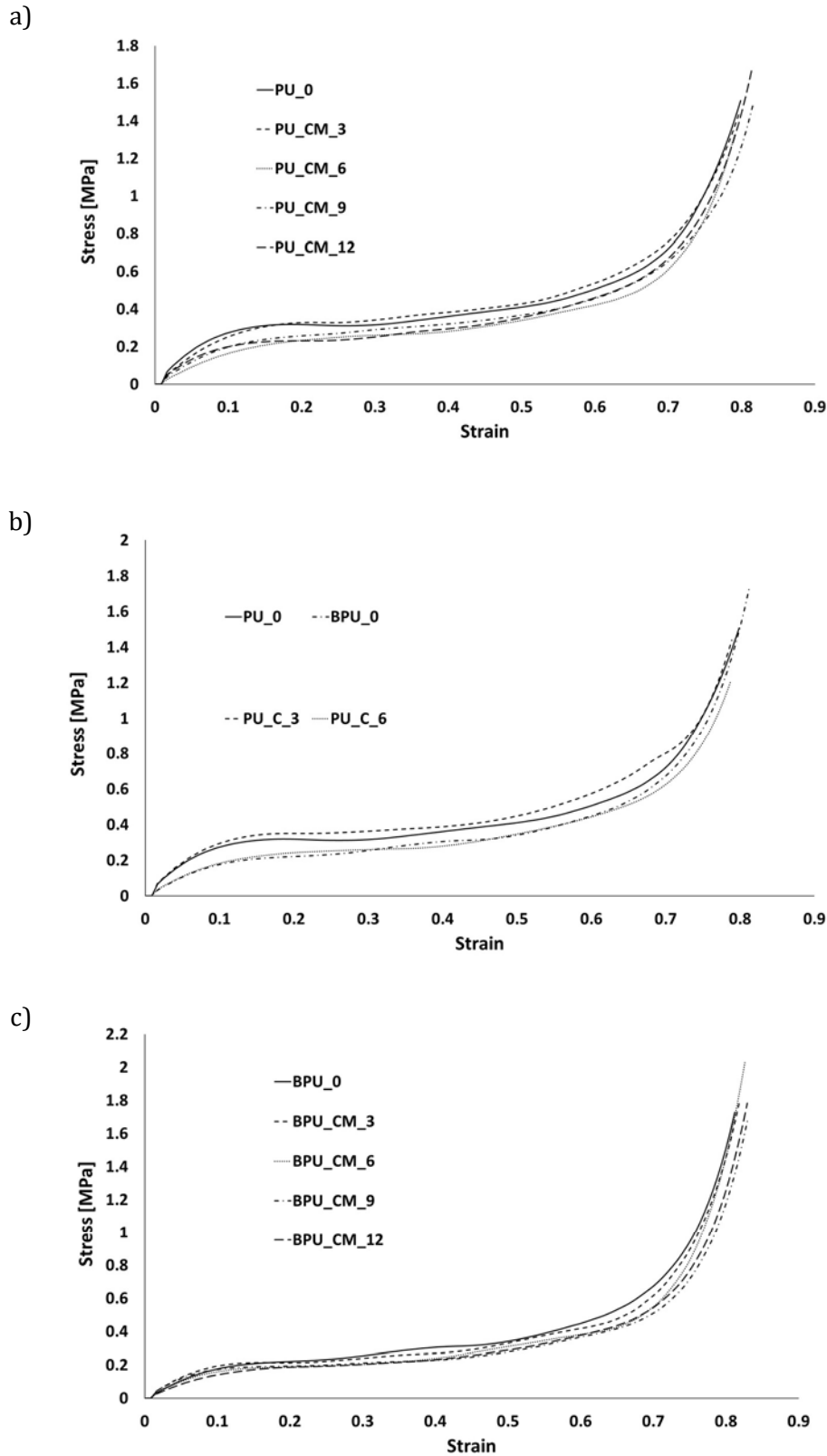
Figure 20. Uniaxial Stress vs Uniaxial Strain experimental curves: a) PU_0, PU_CM_3, PU_CM_6, PU_CM_9 and PU_CM_12; b) PU_0, BPU_0, PU_C_3 and PU_C_6; c)BPU_0, BPU_CM_3, BPU_CM_6, BPU_CM_9 and BPU_CM_12, adapted from [142].

6.3.2. Numerical results

Figure 21, Figure 22 and Figure 23 compare experimental and numerical stress-strain curves. Across various samples, deviations are mostly observed during the densification phase. While most experiments align with the simulations, a common discrepancy emerges at higher strains.

Combining the hyperfoam model with the Mullins effect offers a mechanism to include permanent energy dissipation and stress-softening effects in elastomeric foams. This numerical phenomenon is typically observed when evaluating material relaxation for validation or multi-impact testing. However, in this instance, it facilitated achieving a stable response, converging toward the desired behaviour of the experimental strain-strain curves. Nonetheless, it could induce premature and unrealistic stress softening during loading in certain cases. This hypothesis is put forward to explain the stress deviations observed at high strains [142].

a)

b)

c)
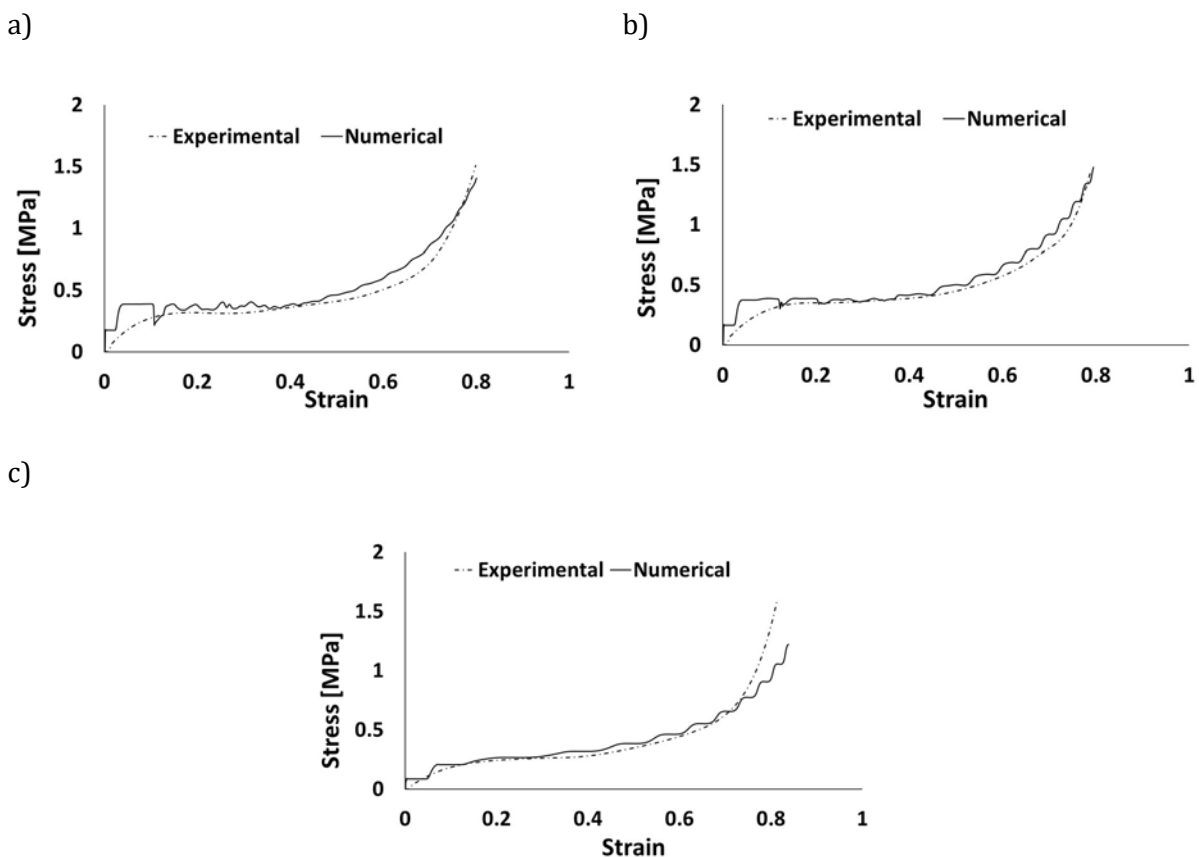
Figure 21. Experimental and numerical stress vs strain of PU samples with and without the addition of natural cork: PU_0 (a)), PU_C_3 (b)), PU_C_6 (c)) , adapted from [142].

Both in simulations and experiments, the composites' applicability is based on their mechanical behaviour and performance. They exhibit characteristic S-shaped stress-strain curves, signifying their suitability for applications requiring impact energy-absorbing materials or structures, particularly in crashworthiness scenarios. When aiming to maximize energy absorption, it is ideal for each material's mechanical response to feature an extended plateau phase with moderate stress levels, eventually leading to densification at higher strains [142].
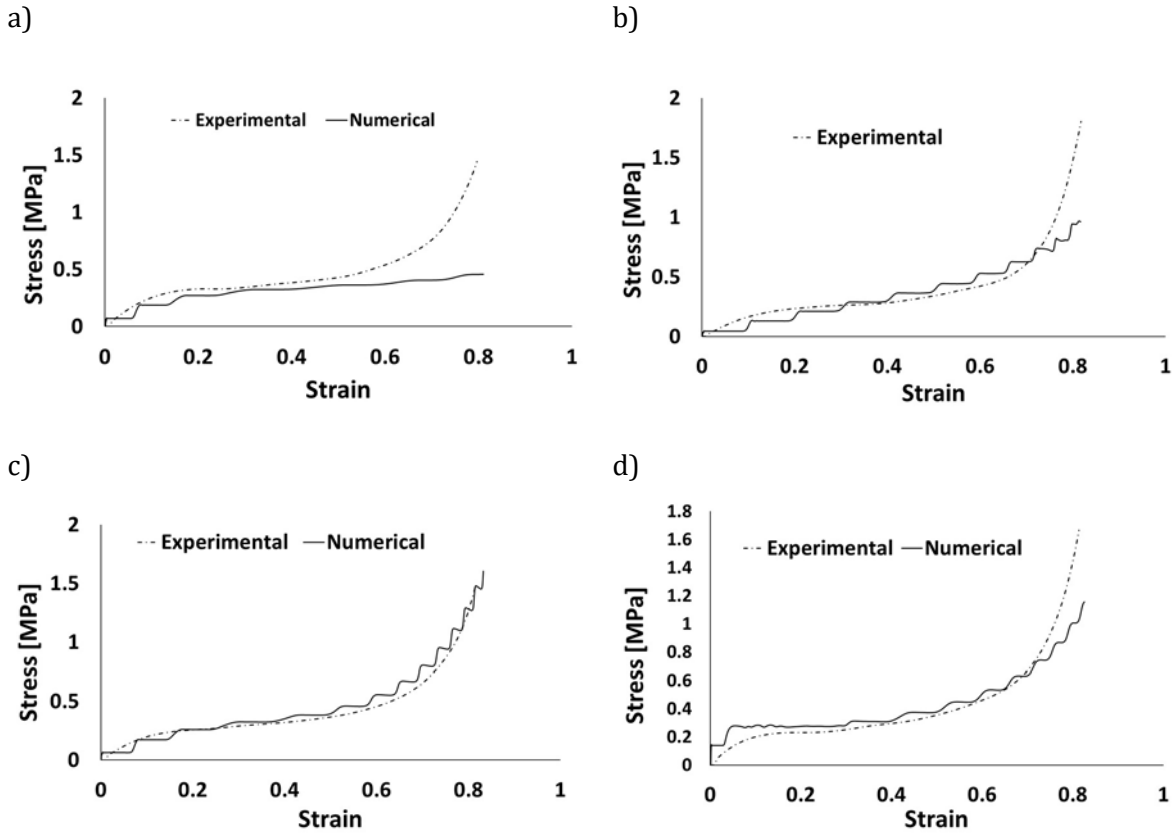
Figure 22. Experimental and numerical stress vs strain of PU samples with the addition of modified cork: PU_CM_3 (a)) PU_CM_6 (b)) PU_CM_9 (c)) and PU_CM_12 (d)) , adapted from [142].

The numerical curves representing the behaviour of pure PU samples and those incorporating natural cork (Figure 21) mirrored the experimental curves, with minor discrepancies primarily seen in the PU_C_6 sample during densification. A "staircase effect" in all numerical curves across simulations could be attributed to numerical instability arising from surface contact. Despite this irregular appearance, these curves effectively replicate the observed material behaviour in experimental tests, providing satisfactory results [142].

Examining the numerical curves for PU samples containing modified cork (Figure 22) reveals more significant deviation from experimental results, especially near the densification phase. Notably, the PU_CM_3 sample fails to accurately replicate this final stage of material behaviour. Nonetheless, it is crucial to emphasize that within the linear elastic and plateau regions, the performance of these PU-modified cork composites remains adequate, validating their suitability for energy-absorbing applications. These regions are pivotal in determining the material's effectiveness for such purposes [142].

Figure 23 highlights that BPU samples with modified cork exhibit a shorter linear elastic region and a lower plateau, indicating reduced impact resistance. Consequently, these simulations provide smoother curves, reflecting poorer performance in terms of energy absorption.

a)

b)

c)

d)

e)
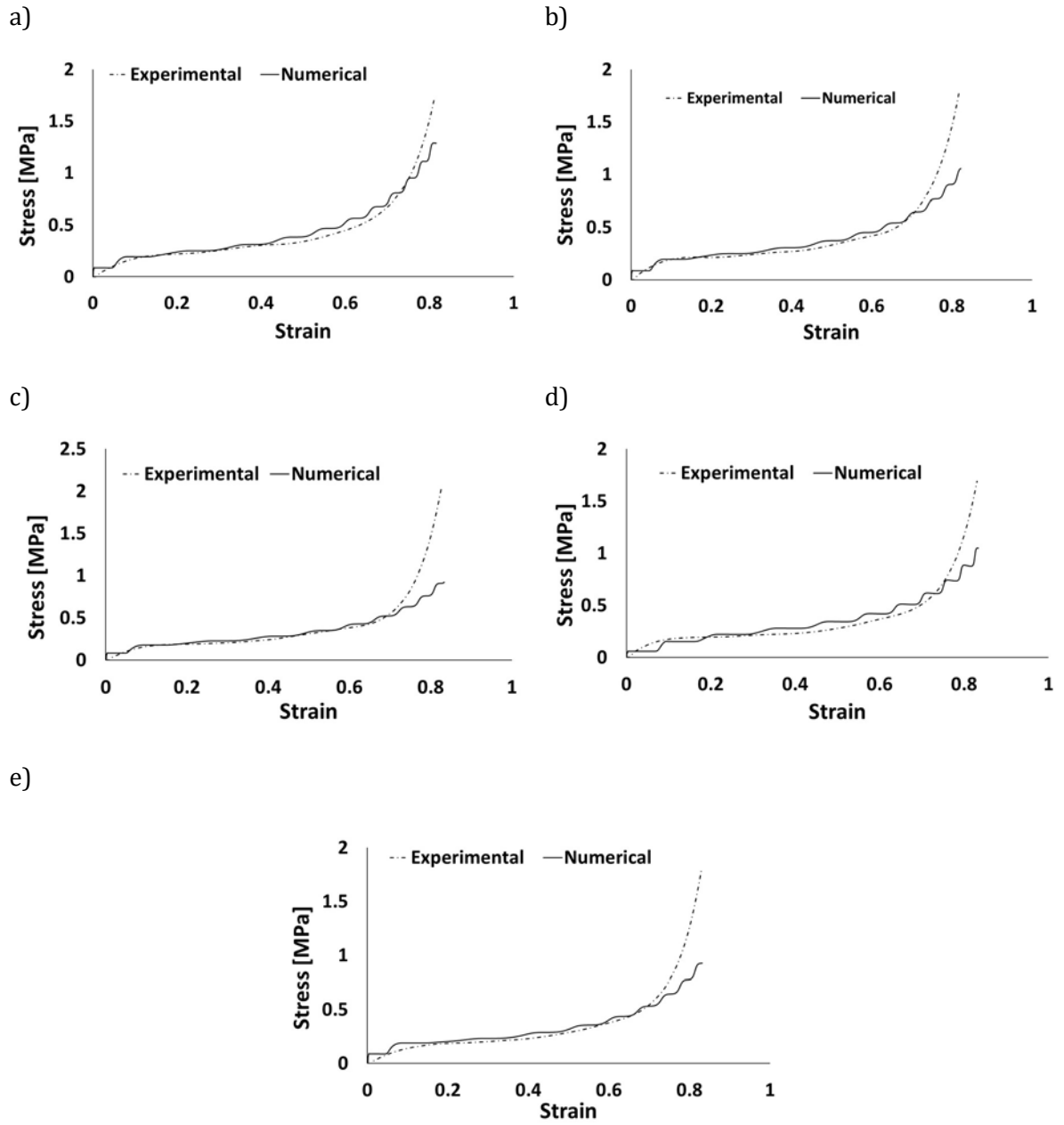
Figure 23. Experimental and numerical stress vs strain of BPU samples with and without the addition of modified cork: BPU_0 a), BPU_CM_3 b), BPU_CM_6 c) BPU_CM_9 d) and BPU_CM_12 e) , adapted from [142].

6.4. Chapter conclusions

Cork composites were developed by Kurańska's group and subjected to dynamic impact testing at Wrocław University of Science and Technology, revealing distinct differences between petrochemical polyol foams, petrochemical polyol with bio-polyol (mass ratio 1:1), with differences in modified or natural cork content. The comprehensive testing setup, combined with numerical simulations, allowed the acquisition of stress-strain data, specifically identifying energy absorption levels.

Interestingly, while no precise relationship between cork content and energy absorption levels was observed for PU samples, a notable correlation emerged between cork content and energy absorption for BPU samples. However, it is important to acknowledge the study's limitation of testing samples under a single loading condition. Recognizing the influence of strain rate on results, future investigations should explore sample behaviour under different loading conditions, thus defining the strain rate dependency [142].

Comparing the results from cork literature review, the best performance and durability under impacts was shown for the agglomerated cork with density equal to 216 kg/m³ (AC216)[132]. The sample absorbed 92 J under 100 J dynamic impact with 50% deformation [132]. In comparison, the most effective sample among biocomposites: PU_CM_3 absorbed 30 J for 50% deformation. Additionally, the biocomposite sample was destroyed after the impact and proved to be inefficient for multiple impacts. On the other hand, AC216 was tested under multiple dynamic impacts for 50 J and 100 J and proved to be durable [132]. For comparison, the specific energy and strain energy density values for AC216 are 22% and 67% higher, respectively.

The energy absorption levels exhibited by these composites are notably lower compared to cork agglomerates. While this implies challenges in integrating these composites into energy absorption structures such as helmets, their potential applications in packaging and various types of personal protective equipment remain promising. It was decided that, with the low energy absorption properties of biocomposites, compared to AC216, the next studies will be conducted with cork agglomerate.

7. Physical experiments with cork and helmets

This part of the research aims to assess the effectiveness of two proposed cork liners added to an American Football helmet. The testing procedure was divided into three stages: firstly, a set of linear impacts was conducted using a Riddell Revolution helmet as the reference. Secondly, the same helmet underwent modification by incorporating a 5 mm layer of cork between the outer shell and the inner padding, subjecting it to the same test conditions. Lastly, the reference helmet was modified by adding a 10 mm layer of cork on the outer shell. For the modified helmets, two distinct cork agglomerates were utilized – the smaller grain size (1 mm) for the inner layer and the larger grain size (4 mm) for the outer layer. The testing was carried out using a Hybrid-III dummy head and neck, maintaining a setup consistent with the National Football League's (NFL) helmet evaluation program [144]. The evaluation of all three helmets involved assessing the resulting head kinematics: HIC [145], DAMAGE [87], and Head Acceleration Response Metric (HARM) [144].

To summarize, the experiment had three parts to simulate impacts under two specified velocities (5.5 m/s and 9.3 m/s) for:

- A basic helmet;
- A modified helmet featuring a 5 mm thick cork layer between the shell and inner coating;
- A modified helmet with a 10 mm thick cork layer on the outer shell, resembling a guardian cap.

The impact locations were chosen based on 182 NFL game impacts involving helmet-to-helmet, helmet-to-ground, and helmet-to-shoulder pad collisions, along with laboratory reconstructions of 31 impacts. The linear impact tests covered four configurations on the shell sites labelled F, C, D, and R (Figure 24) [32], [34], [146]. It is worth noting that the NFL considers a impact velocity of 7.4 m/s as a threshold condition for concussion [31], [35], [146]. This study utilized one velocity below the threshold (5.5 m/s) and one above (9.3 m/s) based on prior literature studies [35], [144], [146].

a)   b)
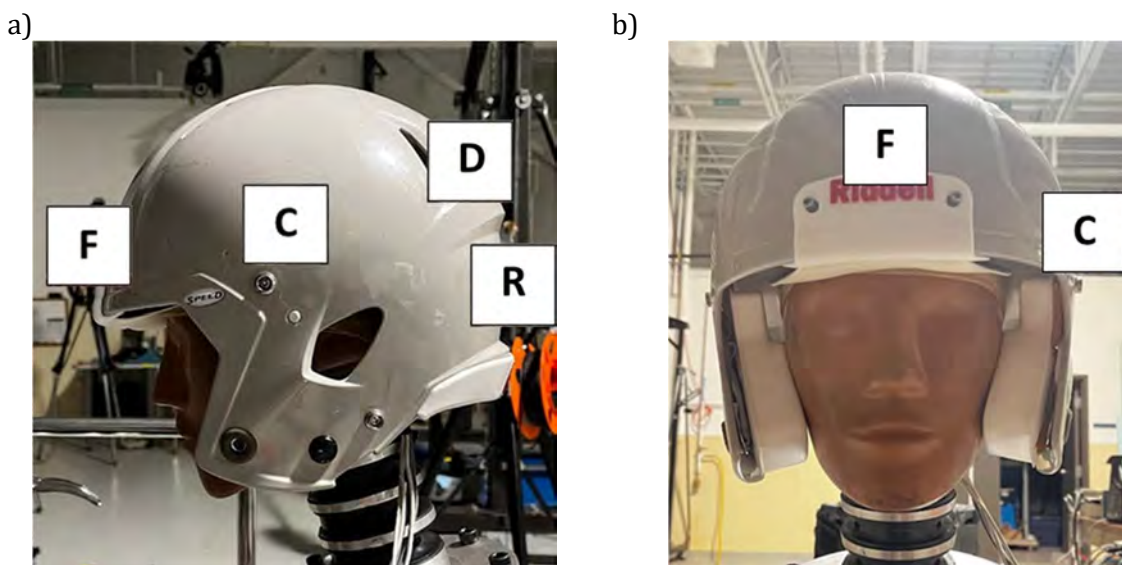
Figure 24. Locations for linear impacts to the shell (F, C, D and R), a) side view, b) front view; based on [38].

Each test involved the use of the Riddell Revolution helmet and the Hybrid III head and neck, following the Biocore helmet fitting procedure [147]–[149]. In compliance with the helmet fitting protocol, a nylon stocking was placed over the Hybrid III head [150]. Prior to each test, checks were conducted, and adjustments were made as necessary to ensure proper pad inflation, jawpad position, and overall fit. Notably, no face mask damage was reported during shell impacts. Selected tests were repeated to confirm impact boundary conditions and ensure result reliability.

The tests were evaluated based on the HARM criterion, including both HIC and DAMAGE [87], [144]. Accelerometer data was sampled at 10 kHz, with linear accelerations filtered using Channel Filter Class (CFC) 1000 and rotational accelerations by CFC 180 [151]. The cork agglomerate, with an average grain size of 1 mm, was placed in the front, rear, and sides of the helmet (excluding the crown). The total weight of the added cork was 300 grams. The inflation of pads was adjusted to ensure proper helmet fit. Further modification involved adding a 10 mm cork liner to the outside of the shell. Each cork layer, weighing 100 grams, was separately applied for each test. The cork agglomerate for the outer layer had an average grain size of 4 mm. A new layer was used for each test. In both modified setups, cork installation was performed using double-sided tape. The summarized setup details are presented in Table 12.
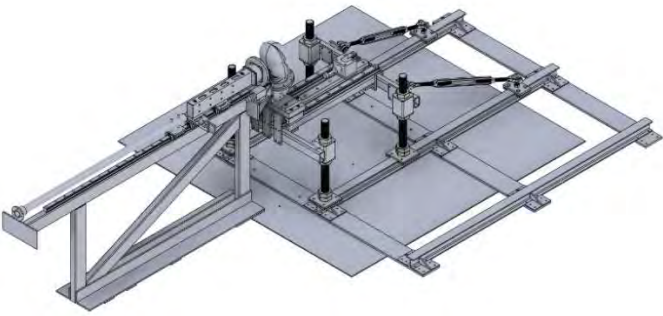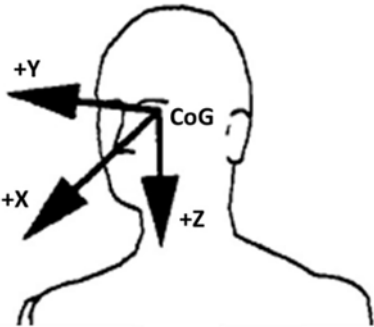
Table 12. Helmet modification with additional absorbing layer summary.

1. A layer of cork between the outer shell and the inner padding: 5 mm thick	2. A layer of cork on the outside of the shell, in the locations of impact: 10 mm thick
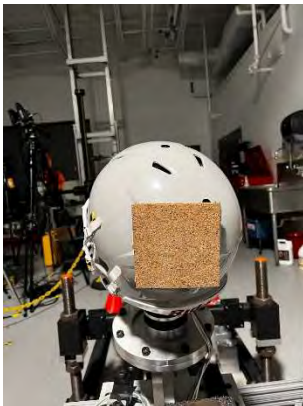
The test fixture and linear impactor system were specifically designed to replicate the conditions outlined in the NFL Helmet Testing Protocol [144]. This setup consists of a pneumatic impactor with a slider table, and carriage aligned parallel to the ram's impact direction. Attached to the carriage was a Hybrid III head and neck assembly, connected to a pivot that allowed rotation around a horizontal axis perpendicular to the ram's movement. Furthermore, the head and neck assembly could rotate along the long axis of the neck, providing a broad range of orientations relative to the impactor ram. The entire table was adjustable in terms of height, lateral movement, and positioning for precise alignment (Table 13). The impactor weighed 12.7 kg, while the total mass of the sliding table was 17.1 kg (excluding the dummy and helmet mass).

Table 13. The test stand used in the experiment and coordinate system adapted based on SAE J211/1.

Test stand – Computer-aided design (CAD) model	Coordinate system with respect to SAE J211/1

The impacting surface between the impactor ram and the test setup, known as the "end cap," was constructed using a cylindrical vinyl nitrile puck featuring a spherical nylon face. This end cap was fixed to the ram via Velcro. In the impactor tests, the ram acted as the simulated collision partner in a helmet-to-helmet impact scenario, while the test dummy, positioned on the sliding table, represented the player experiencing the impact. To establish the head reference position, the following steps are taken [150]:

1. The head is initially positioned with the neck vertical (β=0°) and the right side of the head (+Y-axis) facing the impactor (α = 90°);
2. The table position is then adjusted along the *Y* and *Z* axes until the centreline of the impactor ram passes through the COG marks on the dummy's skull;

Next, the head and neck are rotated 90 degrees (α = 0°) so that the head faces the impactor. This orientation defines the head reference position, and the displacements in Table 14 can be used to orient the dummy head for each of the six impact locations.

It is worth highlighting that COG of the dummy head, located anterior to the neck axis, rotating the dummy to face the impactor causes the COG of the head to move away from the centreline of the impactor. Additionally, the Hybrid III dummy head exhibits a tilt of approximately 4.75^0 backward (extension) when the neck is vertical, causing the head's z-axis to deviate from parallel alignment with the neck's long axis. Consequently, the angle α does not fall within the head's x-y plane [150]. Table 14 summarises the adjustments made to the table, head rotation, and impact visualization.

Table 14. Summary of table adjustments, head rotation and impact visualization based on [32].

Impact Side	Table adjustment		Neck angle	
	(mm)	Z (mm)	α (°)	β (°)
F	15.0	-75.0	0	15
C	27.0	-2.0	-95	11
D	27.0	-2.0	-157	11
R	15.0	6.0	180	-15

Side (C) Rear Upper (D) Front (F) Rear (R)
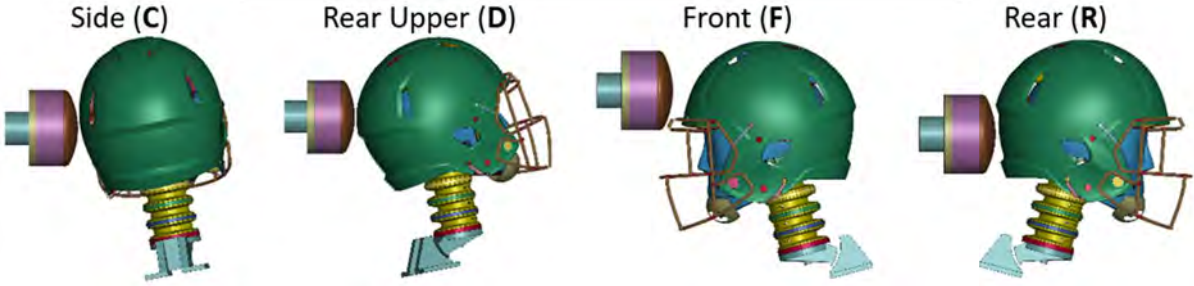
7.1. Results

Several researchers have proposed diverse concussion mechanisms and advocated considering both translational and rotational head movements to predict injuries [152], [153]. To evaluate impact severity with a unified parameter encompassing both linear and rotational aspects, the HARM criterion was employed (equation 10) [144]. For assessing rotational injury, HARM incorporates the DAMAGE [87]. This metric predicts brain strain based on angular head kinematics across three head coordinate directions, utilizing a simplified model as an alternative to finite element method (FEM). DAMAGE demonstrates close correlation with multiple FE brain model results [87], [154] and includes associated injury risk functions [155]. Given the approximate duration of the highest acceleration peak, roughly 20 ms for each impact, HIC15 was employed in this study.

$$HARM = C_1\,HIC + C_2\,DAMAGE \tag{10}$$

where $C1$=0.0148 and $C2$=15.6 are constants that were determined from fits to head kinematics measured in physical dummy reconstructions [144]. It should be noted that lower HARM value indicates a less severe impact and a better helmet performance. Additionally, the reduction factor is implemented. It is a ratio comparing the parameters from reference experiments to experiments with modified helmets. The exemplary formula for HARM reduction factor is displayed below (equation 11):

$$HARM\ reduction\ factor\ =$$

$$\frac{HARM\ for\ reference\ helme\ test - HAR\quad for\ modified\ helme\ test}{HARM\ for\ modified\ helmet\ test} \tag{11}$$

Table 15, the reduction factor is presented in percentage and:

- if the difference is within 5% and -5% (improvement or decrease) – grey,
- if the difference is positive and higher than 5% (improvement) – green,
- if the difference is negative and higher than -5% (decrease) – red.

The experiment resulted in two primary conclusions. Firstly, both cork-modified helmets showed improved performance for lower velocity impacts. Secondly, the modified helmets did not significantly improve HIC, DAMAGE, or HARM metrics during high-velocity impacts in configurations C and D (side and side-rear). In comparison, the average reduction in HARM for the inner layer modification (relative to the basic) stood at 8%. Specifically, a reduction of 12% was observed in the 5.5 m/s cases, while a 5% reduction was observed for the 9.3 m/s cases.

On the other hand, the average reduction in HARM for the outer layer design (relative to the basic) was almost 2%, with various outcomes based on test velocity. For low-speed impacts (5.5 m/s), there was a 10% reduction in HARM, whereas a 6% increase was observed with 9.3 m/s. The underlying mechanism behind these differences in results remained unclear due to the limited test data available. The future studies should explain this phenomenon and increase the number of tests. Additionally, the peak linear acceleration magnitude decreased across all configurations (except case C due to data noise), with an 11% decrease for 5.5 m/s impacts and a 3% decrease for 9.3 m/s impacts (Figure 25).

Table 15. Summary of calculated parameters and reduction factor with an indication if the value is higher (red) or lower (green) than for the reference test.

	Configuration	C		D		F		R	
		5.5 m/s	9.3 m/s	5.5 m/s	9.3 m/s	5.5 m/s	9.3 m/s	5.5 m/s	9.3 m/s
HARM		4.05	9.08	5.38	11.16	3.89	10.63	4.01	5.58
DAMAGE	Basic	0.16	0.26	0.25	0.42	0.19	0.38	0.17	0.19
HIC		101.67	329.94	93.98	308.27	65.70	316.74	85.52	176.98
HARM		3.78	8.94	6.24	12.82	3.48	9.22	2.17	4.44
DAMAGE	Inner Layer	0.18	0.31	0.30	0.49	0.17	0.27	0.18	0.46
HIC		59.88	274.64	105.47	293.26	77.66	335.99	17.19	107.40
HARM		3.71	10.13	4.81	11.68	3.29	9.71	3.82	6.44
DAMAGE	Outer Layer	0.16	0.29	0.23	0.42	0.19	0.33	0.17	0.24
HIC		76.32	381.02	98.54	312.83	59.17	306.62	77.65	178.58
Reduction factor [%]									
HARM		7	2	-14	-13	12	15	85	26
DAMAGE	Inner Layer	-11	-16	-17	-14	12	41	-6	-59
HIC		70	20	-11	5	-15	-6	397	65
HARM		9	-10	12	-4	18	9	5	-13
DAMAGE	Outer Layer	0	-10	9	0	0	15	0	-21
HIC		33	-13	-5	-1	11	3	10	-1
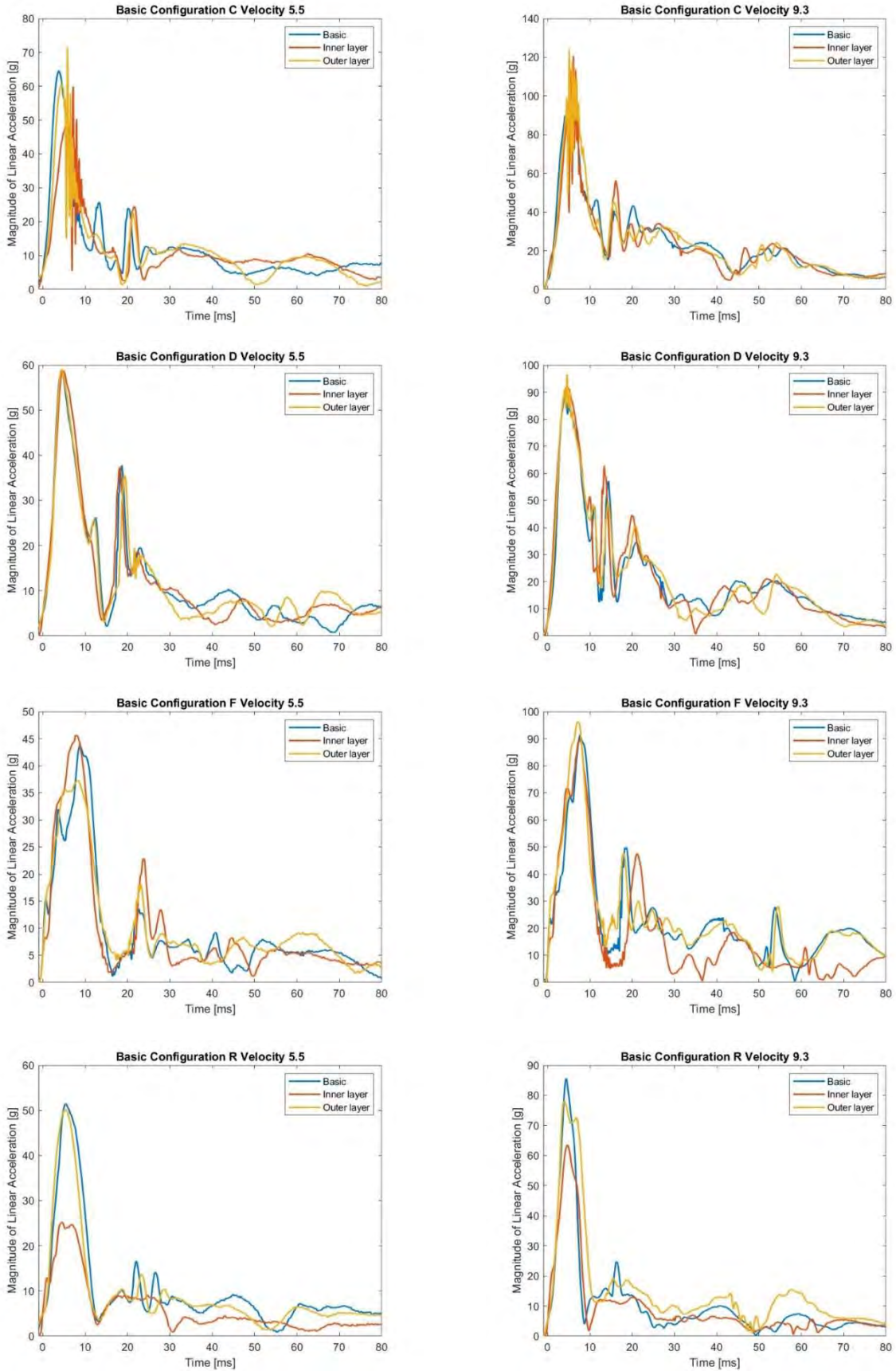
Figure 25. Linear acceleration graphs in the headform centre of gravity for the selected configuration and velocity in [m/s].

During the experiment, it was observed that both types of cork modifications did not consistently reduce HARM values across all test conditions. One reason for the increase in investigated parameters in the outer layer modification could be the imperfect geometry of the cork add-on's to the helmet's structure. Specific boundary conditions of the test were critical: the impactor is in form of a spherical cap with a 140 mm radius, sphere with a 203 mm diameter cap, and contact made along a longitudinal axis set by the impactor. Consequently, the contact area between the shell and impactor was intentionally minimal. A hypothesis could be formulated that the additional compressing layer might have transferred the force over a larger area due to cork deflection, potentially impacting the shell differently. Concerning the 5 mm thick inner cork layer, the design might have reduced the air volume in the inflated helmet pads. Given air's compressibility, reducing its volume could decrease the overall design's compressibility, potentially leading to an increase in investigated parameters.

The inner cork layer, weighing approximately 300 g, is 17% of the helmet mass, likely influencing the helmet's impact response. The outer layer configuration provided more flexibility in terms of thickness since there was no helmet geometry limit. Each configuration used a 10 mm thick cork sample, while each batch weighed 100 g. Overall, the cork shell's estimated mass was around 600 g, equivalent to approximately 34% of the helmet mass. By comparison, the Guardian Cap available on the market varies in weight from 369 to 603 g.

Additionally, significant noise remained in the head acceleration data despite filtering. This could potentially be related to the design of the Hybrid III neck, originally intended for flexion rather than lateral bending. The steel cable within the neck might act as a stiff resonating spring during certain side impacts, increasing accelerometer noise. Nevertheless, the head and neck were chosen due to their alignment with US Government standards for automotive crash testing, known repeatability, humanlike impact responses, and their prior use in professional football player helmet impact research.

7.2.   Chapter conclusions

In recent years, minimizing the probability of head injuries has become crucial in American Football games and practices, both in preseason and during the season. The study's experiments highlighted the potential success of using natural cork as an additional layer in existing protective equipment. Significantly improved performance was observed in cases of low-velocity impacts, showcasing a notable 10% reduction in the HARM parameter. However, in high-velocity impacts, the cork layer displayed only marginal improvement in reducing HARM, indicating the need for further refinement to improve the materials' performance in higher-impact scenarios. The tendency to perform well in low-velocity cases may be beneficial since the frequency of low-velocity impacts is much higher than the high-velocity impacts. However, some limitations have to be addressed. Even though each test was repeated, the sample size was limited. In the future, the experiment should be expanded with different thicknesses, especially in the outer design and maybe even with different cork agglomerates. Another limitation is that the experiments were conducted with only one helmet type. Since there were no visible damages to the integrity of structure the helmet was not replaced throughout the tests. There are three most frequently used helmets: Riddell Speedflex, Schut F7 and Vicis Elite and the expanded studies shall cover each of them. Regarding pilot studies, the cork samples proved that different designs and materials could enrich the market for Guardian Caps.

8. Injury criteria to head biomechanics[7]

This research employed the αHEAD finite element head and brain model, a validated numerical model developed by Ratajczak et al. [76]. The used model incorporates a system of bridging veins with differentiation of mechanical properties across different regions of the head [156]. In comparison to alternative head models such as Yet Another Head Model (YEAHM) or GHBMC, the αHEAD model offers the advantage of obtaining accurate data with optimization of computational efficiency [50], [75], [97], [157], [158].

The helmet model utilized in this study was developed and validated by Biocore [159], [160]. The research employed the LS-DYNA environment, and the 3D geometric model of the brain and skull was constructed from medical images obtained through medical scanners. The resulting 3D object was exported to the stereolithography format (STL), with further digital processing through computer-aided design programs [97]. The comparison of HIC values obtained from the HIII head-neck model and intracranial pressure using αHEAD is presented [50].

To address volume-locking issues, the ELFORM13 formulation in LS-DYNA was used. The volumetric locking is prevented by defining nodal volumes and assessing average nodal pressures in relation to these volumes [50]. The brain's geometry is segmented into four parts: the right/left brain hemispheres and the right/left cerebellum portions. The brain material model is defined with a Mooney-Rivlin formulation. The model incorporated anatomically accurate features such as dura mater, CSF, falx cerebri, cerebellar tentorium, superior sagittal sinus, and bridging veins. Geometrical parameters and distribution of the bridging veins were based on descriptions provided by Oka [161] and Kleiven's research [162]. In the numerical model, the bridging veins were differentiated among the frontal, parietal, and occipital regions. Mechanical properties employed in this study are summarized in Figure 26 and Table 16 [50], [97].
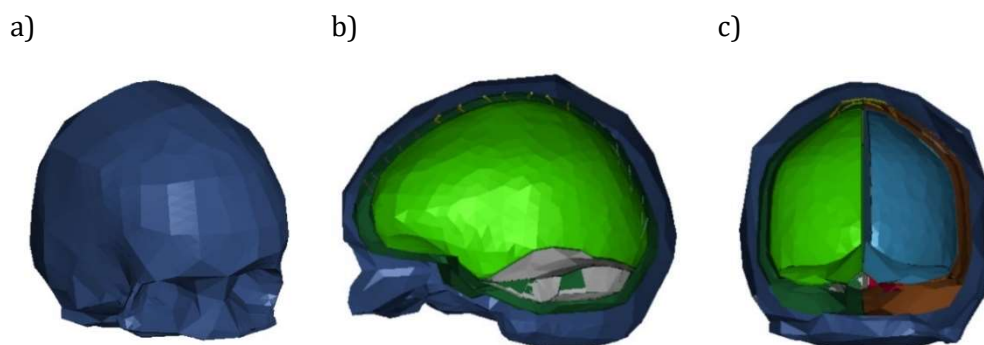
Figure 26. αHEAD model: a) isometric view, b) sagittal section view through the skull, c) coronal section view through the skull, adapted from [97].

---

[7] The chapter was adapted from one of the co-authored publications, Analysis of HIC and hydrostatic pressure in the human head during NOCSAE tests of American football helmets. Brain Sciences. 2021, vol. 11, nr 3, art. 287, s. 1-29, https://doi.org/10.3390/brainsci11030287

Table 16. Mechanical properties for each component of the head–presented in detail in [163].

Element	Young's (E) or Bulk Modulus (K) [MPa]	Density [kg/m³]	Poisson's Ratio
Skull	E = 15 000.0	2 000	0.22
Dura mater	E = 31.5	1 130	0.45
Cerebrospinal fluid	K = 2 200.0	1 000	0.49
Superior sagittal sinus	E = 28.2	1 040	0.45
Falx cerebri and cerebellar tentorium	E = 31.5	1 130	0.45
Brain tissue	K = 1 130.0	1 040	0.49

The simulations of the investigated approach were performed using the Hybrid III head-neck model. This model consists of a skull, head skin, neck, and neck mount. The centre of gravity of the head model is indicated in Figure 27, with a local head accelerometer also designated at this point, enabling local head acceleration data collection. The total mass of the model is 5.74 kg [159]. Table 17 presents the local coordinate system with its function and definition [97].
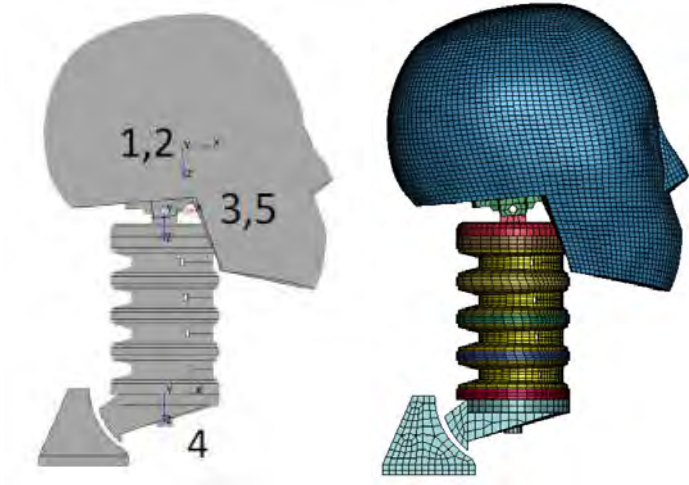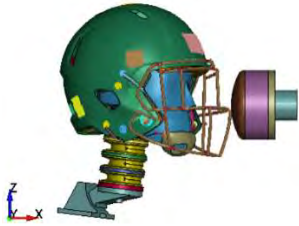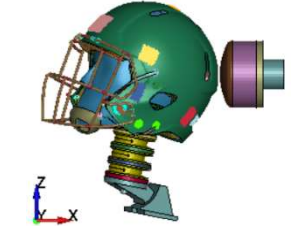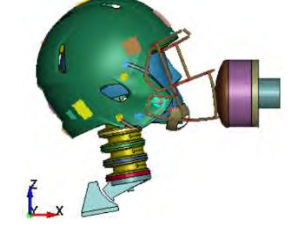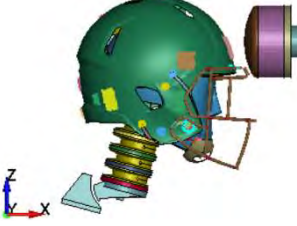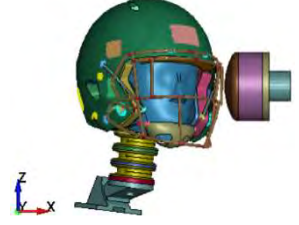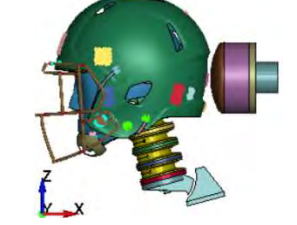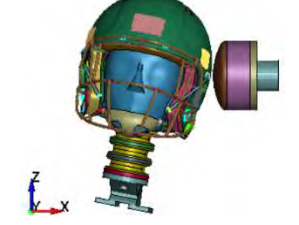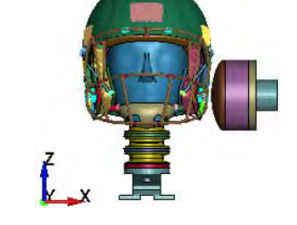
Figure 27. HIII head neck model with coordinate systems used in the study [159].

Table 17. Local coordinate systems definitions [159].

Number and name	Function
1. Skull (inertia)	Defines location and orientation of head's center of gravity. Application of head part inertia properties.
2. Head accelerometer (local)	Defines location and orientation of head accelerometer. Allows for output of local head accelerations.
3. Head Occipital Condyle (Local)	Defines location and orientation of nodding block discrete beam at the Occipital Condyle.
4. Neck: lower	Defines location and orientation of discrete beam joining neck to neck mount. Allows for output of lower neck forces.
5. Neck: upper	Defines location and orientation of upper neck mounting. Allows for output of relative head-neck motion and upper neck forces.

In the investigated approach, eight simulations were performed, each with a different point of contact. In each simulation, the moving part was the impactor [97]. The linear impact tests include four configurations on the shell sites labelled F, C, D, and R and four on the facemask labelled A, AP, B and UT (Table 18) [32], [34], [146]. This study uses velocity, which is higher (9.3 m/s) than provided as the injury threshold [31], [35], [146] and is based on the previously conducted studies in the literature [144]. The αHEAD model was evaluated based on intracranial pressure injury prediction introduced by Ward et al. [164], [165]. The threshold for serious and fatal injuries is approximately the same: 237 kPa. Most of these injuries are brain contusions or haemorrhages in the high stress regions.

Table 18. Investigated approach setup, adapted from [97].

Configuration	Visualisation	Configuration	Visualisation
A		D	
AP		F	
B		R	
C		UT	

In order to analyse the behaviour of the brain instances during the tests, it was necessary to appropriately combine a helmet model with the αHEAD model (Figure 28) [97]. The connection between the neck geometry and the skull remained the same as in the Hybrid HIII model, which is the nodding joint at the top of the neck connected to the adapter at the bottom of the head with a pin. The following changes were performed: the neurocranium was replaced with the αHEAD model. The movements at the occipital condyle were not modified. The connection between the neurocranium (αHEAD) and the facial skeleton (Hybrid HIII with the adapter) is rigid (LS-DYNA: Constrained-Rigid Bodies). The geometry of the αHEAD skull was tied to the layer representing the skin of Hybrid HIII. The remaining contacts between the helmet and the skin layer remained unchanged. To compare the results to actual validation tests, all configurations were simulated with the Hybrid HIII head-neck model and αHEAD [97].
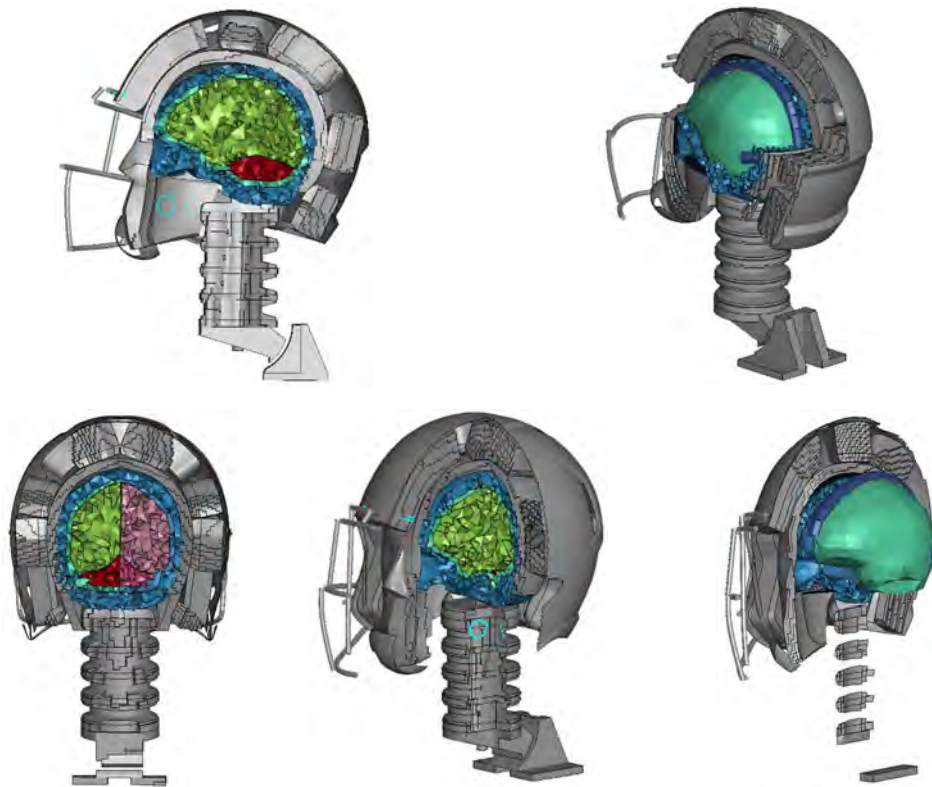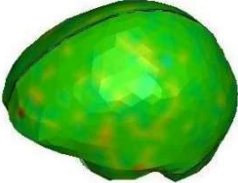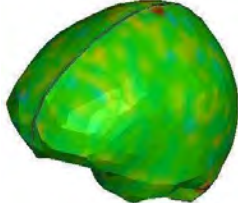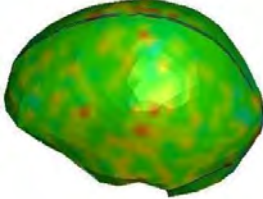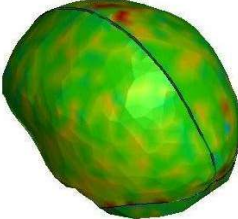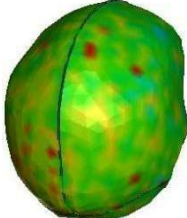
Figure 28. Selected views of the helmet model (grey) with the αHEAD model (colors), adapted from [97].

8.1. Results

The primary goal of this study was to examine the effect of impact location on HIC (measured with respect to head's centre of gravity) and intracranial pressure in football helmets. Impact locations were based on the previously conducted studies in the literature [144], maintaining fixed initial impactor velocity. While kinematic parameters like velocities, accelerations, and impact locations might be associated with brain strain, this study did not aim to explore these correlations in depth.

Table 19. Comparison of HIC score for Hybrid III dummy to the maximal value of hydrostatic pressure for αHEAD, adapted from [97].

Configu-ration	HIC Score (HIII Model)	Hydrostatic Pressure [kPa] at 6 ms after Impact [ms] (αHEAD Model)	Ratio of Finite Elements Exceeding Threshold Criterion (237 kPa)
A	536		29.18%
P	650		29.62%
B	449		24.20%
C	557		21.60%
D	594		20.64%

F	403		25.55%
R	731		25.42%
UT	304		25.66%

Pressure

500
450
400
350
300
250
200
150
100
50
0
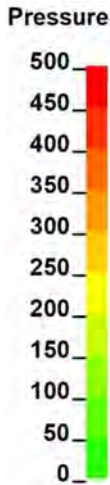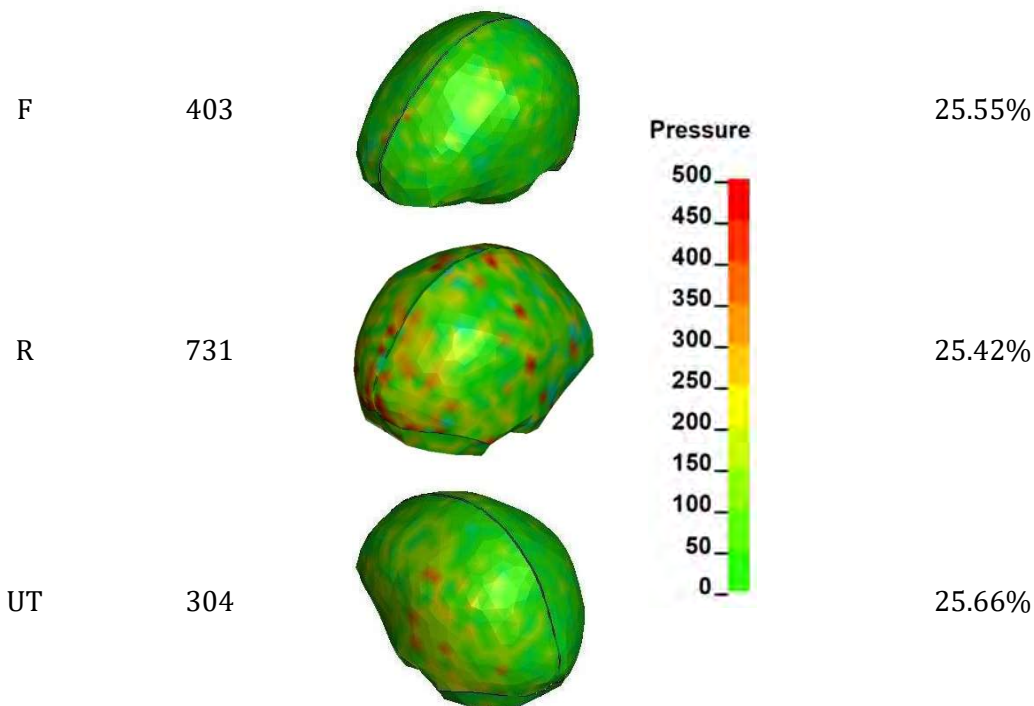
Notably, the highest HIC were recorded for frontal and rear impact locations (AP: 650 and R: 731), likely due to the HIC's sensitivity to longitudinal acceleration. On the other hand, the lowest HIC value was recorded for oblique impact (configuration UT: 304). The simulations showed, that the HIC, which is based on linear accelerations, is limited in his damage expression regarding different impact locations. In world scenarios only a small percentage of direct (translational) impacts takes place [97].

It is shown that HIC values fall within permissible limits (the HIC threshold value being 1000) but intracranial pressure surpasses threshold values (~237 kPa) across all configurations (Table 19) [28], [166]. The pressure values are averaged using LS-DYNA nodal averaging technique, due to the models' high-pressure values at the boundary nodes (αHEAD is based mainly on the tetrahedral mesh approach).

The course of simulation in Figure 29 presents the kinematics of the helmet after being hit with the impactor. Figure 30 depicts the resultant linear accelerations in time and presents the HIC value graphically. Figure 31 presents a cross-section in the sagittal plane during the simulation. Hydrostatic pressure (kPa) in the brain is highlighted. The remaining configurations (AP–UT) are presented in Appendix A [97].

Figure 29. Configuration A: course of simulation (0–20 ms, 5 ms interval), adapted from [97].
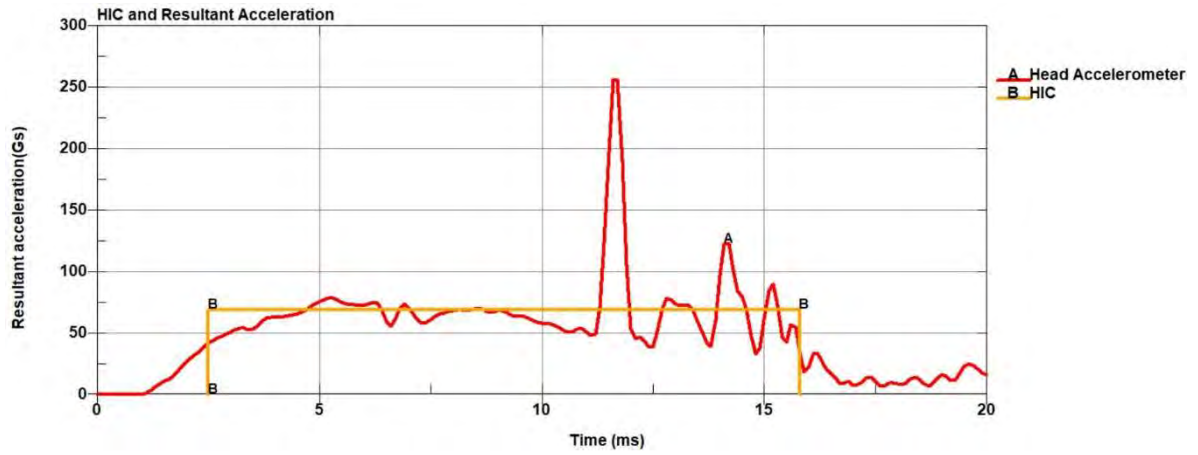
Figure 30. HIC and Resultant Acceleration (G) in time (ms) plot (HIC36 = 536), adapted from [97].
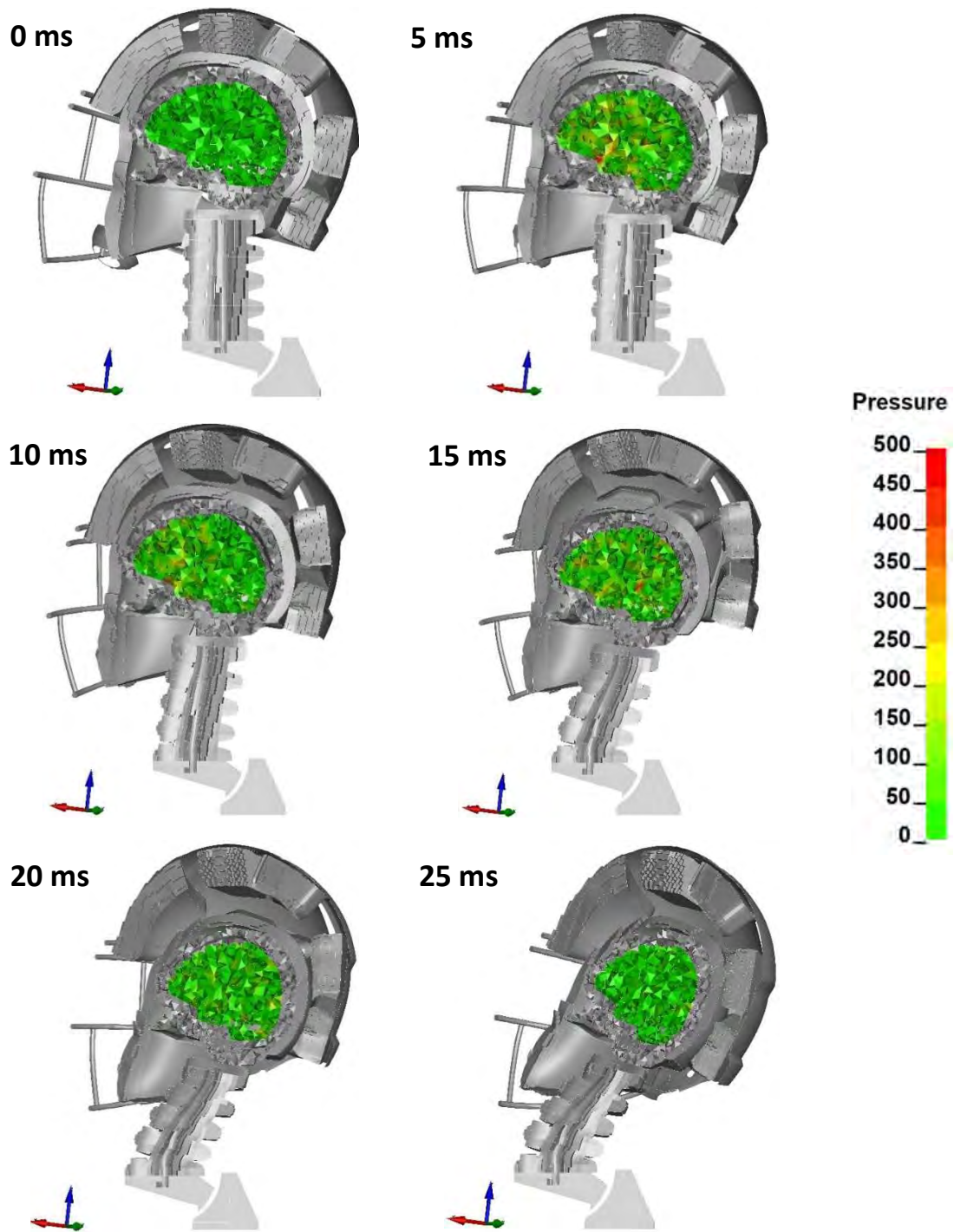
Figure 31. Head kinematics during the numerical test, configuration A, with the cross-section in the sagittal plane and showing the hydrostatic pressure (kPa) in the brain, adapted from [97].

8.2.   Chapter conclusions

The findings from this research carry significant implications for the design process, urging the continuation of broader, standardized testing. The study sheds light on the prevalence of the HIC, commonly employed across various head injury research areas, including TBI and concussion studies. While HIC was initially developed for automotive crashworthiness, its application transcends specific head impacts. It underscores the need for a deeper understanding of brain behaviour during impacts, especially in implementing new energy-absorbing materials and potential concussion diagnosis. Furthermore, as helmets are primarily designed to safeguard the head and brain, this research did not prioritize investigating neck injury criteria or normalized neck injury criteria [50], [97].

The results highlight the need for helmet validation tests to adjust to stricter and more rigorous standards. One suggestion would be the adoption of, for example, the THUMS dummy head, equipped with a simplified brain, instead of a basic dummy head model. Given today's technological advancements, investigations should progress to include a broader range of parameters. The findings underline the need for continued brain research and analysis in helmet testing to mitigate the risk of injury [50], [97]. It should be highlighted, that the employed αHEAD discrete model lacks the brain's complete vascular structure, which may influence tissue behaviour [76]. Nonetheless, this model proved to be sufficient to validate initial assumptions regarding intracranial pressure surpassing threshold values while HIC remaining within acceptable limits [97].

The study emphasizes the necessity to replace current headform models with more advanced ones, such as the THUMS dummy, equipped with a simplified brain structure. Additionally, it raises concerns about the applicability of HIC in predicting brain injuries resulting from direct head impacts in American Football. The research suggests diversifying certification tests across various helmet types, exploring brain displacement, principal strain and stress, as well as analysing neck forces and their interpretation in Neck Injury Criteria or Normalized Neck Injury Criteria [97].

Given the complexity of brain injury and its neuropathological changes that may lead to mental impairment, neurological changes remain a diagnostic challenge that lacks comprehensive understanding, resulting in diverse findings across the literature. Numerical brain models offer insights into biomechanical tissue responses and aid in determining a football helmet's safety across different impact configurations. However, the study highlights disadvantages of HIC, emphasizing its limitation in understanding tissue angular responses. The research demonstrates the lack of correlation between ICP and HIC values, cautioning against relying only on acceleration-based injury criteria [97].

Continued investigations into brain injury mechanisms during helmet tests remain necessary to minimise injury probabilities. Validated discrete head models serve as tools in evaluating brain behaviour during collisions. Finite element methods enable the simulation and validation of various safety systems. Advancements in modelling human body structures offer opportunities to simulate injuries and develop protective gear with enhanced efficiency. The pursuit of an accurate brain model will enable a detailed examination of brain responses under diverse loading inputs, providing valuable insights into parameters such as intracranial pressure and brain strain [97].

9. Material model validation for the brain tissue[8]

The previous chapter lead to a conclusion, that the studies regarding brain tissue should be continued. Since there literature tests with brain tissue focus on tension or compression, it was decided to verify the tissue behaviour under dynamic loading.

Porcupine brain samples underwent testing using an in-house developed shaking machine (specimen shaker). Fresh porcine brains were obtained from a commercial slaughterhouse, and their use did not necessitate consent from any ethical or regulatory bodies. The tests were performed under stable temperature conditions to minimize the impact of external factors on the experiment. The shaking machine was specifically constructed to reduce the influence of gravity on measurements (a horizontal orientation). The inductor, an MTS Systems Model 2100E11, was linked to the base frame and rail to generate vibrations. The vibration examination test bench was designed as a guide rail and carriage, featuring an attached sample holder (Figure 32). Vibrations were induced by the inductor connected to the frame, and the resulting vibrations were transmitted via a rod to the test bench and sample holder [167].
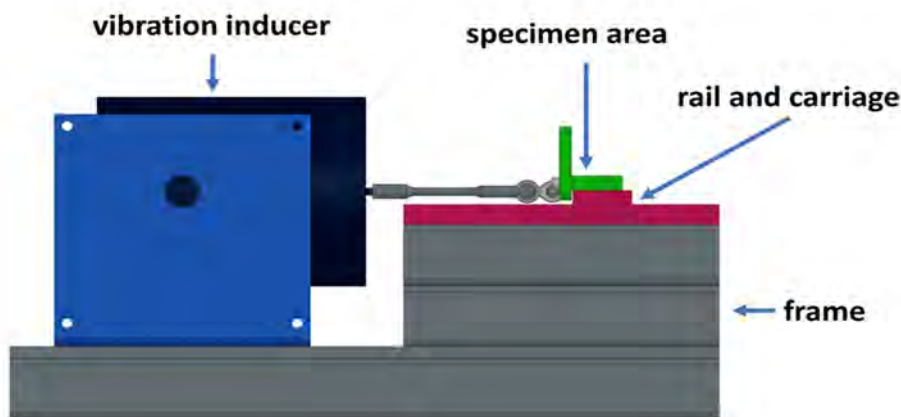
Figure 32. Designed specimen shaker for the material tests, adapted from [167].

The imposing signal was an audio file sent to a QSC RMX2450 amplifier directly connected to the shaker. A written Python script imposed signal generation, which created a .wav file with variable frequency and sinusoidal amplitude. The script allowed the instrument to impose a sine sweep test of constant acceleration, which was used to find the system's resonance frequency. The generated waveform was created according to the following formula (equations 8 and 9):

- Logarithmic frequency change with respect to time:

$$f(t) = f_0 \cdot \beta^t$$

$$\beta = \left(\frac{f_1}{f_0}\right)^{\frac{1}{t}} \tag{8}$$

---

[8]The chapter was adapted from one of the co-authored publications, Experimental and computational approach to human brain modelling – aHEAD. Archives of Civil and Mechanical Engineering. 2023, vol. 23, nr 3, art. 218, s. 1-18, https://doi.org/10.1007/s43452-023-00758-9

- Imposed amplitude proportional to velocity (inducer controlled by voltage):

$$v = \frac{a}{2 \cdot \pi \cdot f} \tag{9}$$

Where: where f is frequency, t is time, f_0 is starting frequency, f_1 is the frequency at the end of the test, t is the time of the test, v is the velocity, and a is the requested acceleration [167].

All experiments were conducted within 12 hours of the animal's death, and the brain tissue was refrigerated at 4°C leading up to the tests. Shortly before experimentation, the tissue was sliced into small samples, approximately 20x30 mm, and allowed to equilibrate to room temperature. It was crucial to identify the specific brain region from which each sample was extracted. During the experiment, samples were prepared from four distinct parts of the brain: the medulla, cerebellum, cerebral hemisphere, and brain nuclei. Each brain sample was placed on a scale to measure its mass. Later, it was important to perform the experiment as quickly as possible to prevent the sample from drying. After the mechanical testing, the volume of each sample was measured. A comprehensive summary of all tested samples is presented below in Table 20 [167].

Table 20. A summary of all tested samples, adapted from [167].

Sample number		Weight [g]	Volume [ml]	Frequency 1st [Hz]	Frequency 2nd [Hz]
Sample 1	Medulla	2.1	2	35-45	-
Sample 2	Medulla	2.4	2.25	35-45	-
Sample 3	Cerebellum	3.5	3.5	35-45	60-100
Sample 4	Hemisphere	2.1	2	35-45	60-100
Sample 5	Hemisphere	1.9	1.5	35-45	60-100
Sample 6	Cerebellum	1.5	1.5	35-45	200-1000
Sample 7	Medulla	1	1	60-100	-
Sample 8	Medulla	1.1	1	35-45	60-100
Sample 9	Brain Nuclei	2.2	2	35-45	-
Sample 10	Hemisphere	6.5	6.5	35-45	-
Sample 11	Hemisphere	7.1	7	60-100	-

A single high-speed Phantom camera setup, operating at 1 000 frames per second, was used with a 45° mirror, enabling to capture two perpendicular sides of a specimen in a single image. This innovative setup proved successful. Due to the vibrational movement induced by the excitation, a high-speed camera was set to record multiple frames of the test bench with specimens at the midpoint of the cycle — between the two extreme positions [167].
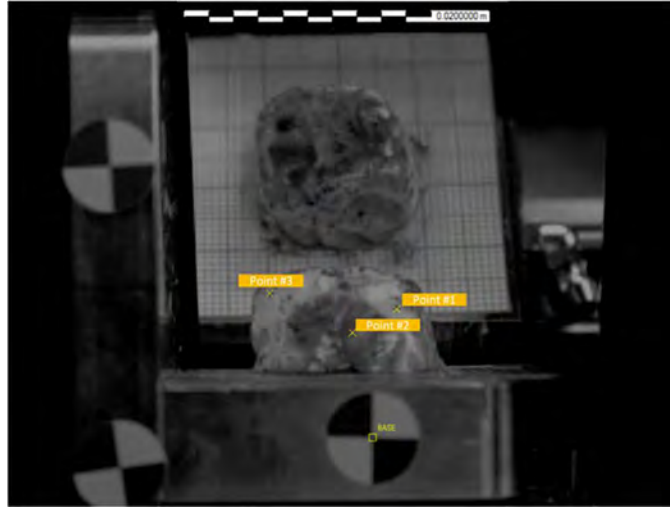
Figure 33. A sample on the shaker with marked tracking points and a reference base point, adapted from [167].

The results obtained from the experiment include the relative-to-base displacements of characteristic points on the specimen (Figure 33). Point 1 is located in the right-upper corner, point 2 is in the middle of the sample, and point 3 is in the left-upper corner [167].

The second phase of this experiment involved validating the numerical material model based on the observed behaviour of the samples under induced vibration. The samples using CAD software were replicated to achieve this, and simulations using LS-DYNA software were prepared [168]. The simulation aimed to simulate the brain specimen's actual support and mounting conditions. The nodes on the bottom surface were fixed in 5 degrees of freedom except Y translation (Figure 34 – left). For these nodes, the extension in the Y direction was determined by the displacement amplitude, which was derived from the physical experiment (Figure 34 – right). The amplitude was set to match the amplitude of the base point, which was tracked during the experiment using high-speed camera tracking software, TEMA. The highlighted sets of nodes correspond to the tracked points in Figure 33. The displacement plotted in the corresponding result section represents a node-averaged value for each point. Four different material models were tested [167].
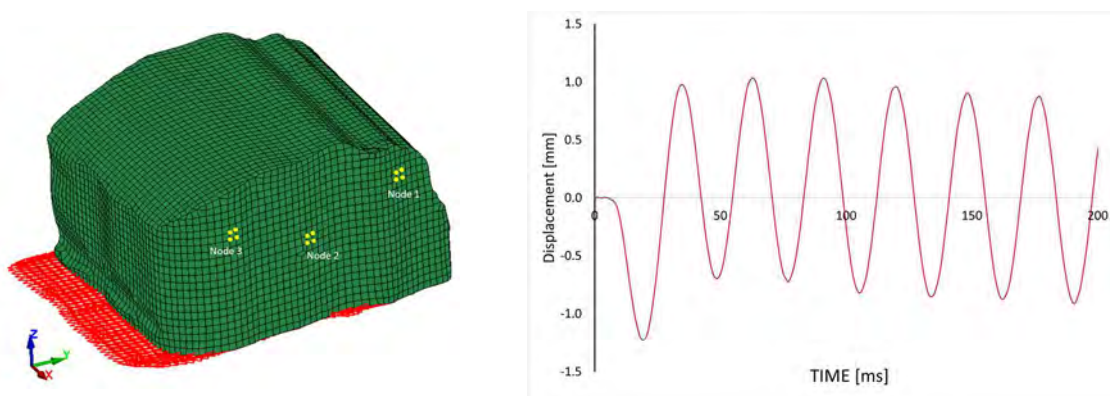
Figure 34. Boundary conditions and tracked nodes on the discrete brain sample (left), the amplitude of the base applied as the boundary condition along the Y axis (right); adapted from [167].

The validation procedure was based on the displacement response to the induced vibrations. The tested material configurations used in THUMS, GHBMC or Mooney-Rivlin and Ogden were verified. The material model parameters are summarized in Table 21 [167].

Table 21 Material model parameters used in the study in LS-DYNA [167].

Material Model	Parameters				
THUMS white matter (Viscoelastic Maxwell model)	$\rho = 1000\ \text{kg/m}^3$	$K = 2160\ \text{MPa}$	$G_1 = 6\ 125\ \text{Pa}$	$\beta = 0.06$	$G_o = 12\ 500\ \text{Pa}$
GHBMC white matter (Viscoelastic Kelvin model)	$\rho = 1000\ \text{kg/m}^3$	$K = 2190\ \text{MPa}$	$G_1 = 1\ 500\ \text{Pa}$	$\tau = 12.5$	$G_o = 7\ 500\ \text{Pa}$
Mooney-Rivlin (Hyperelastic)	$\rho = 1000\ \text{kg/m}^3$	$\upsilon = 0.49$	$A = 6.205 \cdot 10^{-04}$		$B = 6.894 \cdot 10^{-04}$
Ogden (Hyperelastic)	$\rho = 1000\ \text{kg/m}^3$	$\upsilon = 0.49$	$\mu = 0.0012$		$\propto\ = 5.0500698$

Where:

THUMS white matter (Viscoelastic Maxwell model)	ρ – Density, K – Bulk modulus, G_1 – Long-time (infinite) shear modulus, G_o – Short-time shear modulus, β – Maxwell decay constant,
GHBMC white matter (Viscoelastic Kelvin model)	ρ – Density, K – Bulk modulus, G_1 – Long-time (infinite) shear modulus, G_o – Short-time shear modulus, τ – Kelvin relaxation constant,
Mooney-Rivlin (Hyperelastic)	ρ – Density, υ – Poisson's ratio, A, B, C and D – Constants: $W = A(I - 3) + B(II - 3) + C(III^{-2} - 1) + D(III - 1)^2,$ $C = 0.5A + B,$ $D = \frac{A(5\upsilon - 2) + B(11\upsilon - 5)}{2(1 - 2\upsilon)},$ W – Strain Energy density, $2(A + B)$ = Shear modulus of linear elasticity, I, II, III = Invariants of right Cauchy-Green Tensor C,
Ogden (Hyperelastic)	ρ – Density, υ – Poisson's ratio, μ – Shear modulus, α – Material constant $W = \sum_{i=1}^{3} \sum_{j=1}^{n} \frac{\mu_j}{\alpha_j} (\alpha^{*\alpha_j} - 1) + K(J - 1 - \ln J),$ W – Strain Energy density, J – Hydrostatic work, K – Bulk modulus, The asterisk (*) indicates that the volumetric effects have been eliminated from the principal stretches λ_j^*.

9.1. Results

The most suitable material model used for the experiment – among the many tested – turned out to be the Viscoelastic Maxwell material model presented in THUMS for white matter (Figure 35) [169], [170].
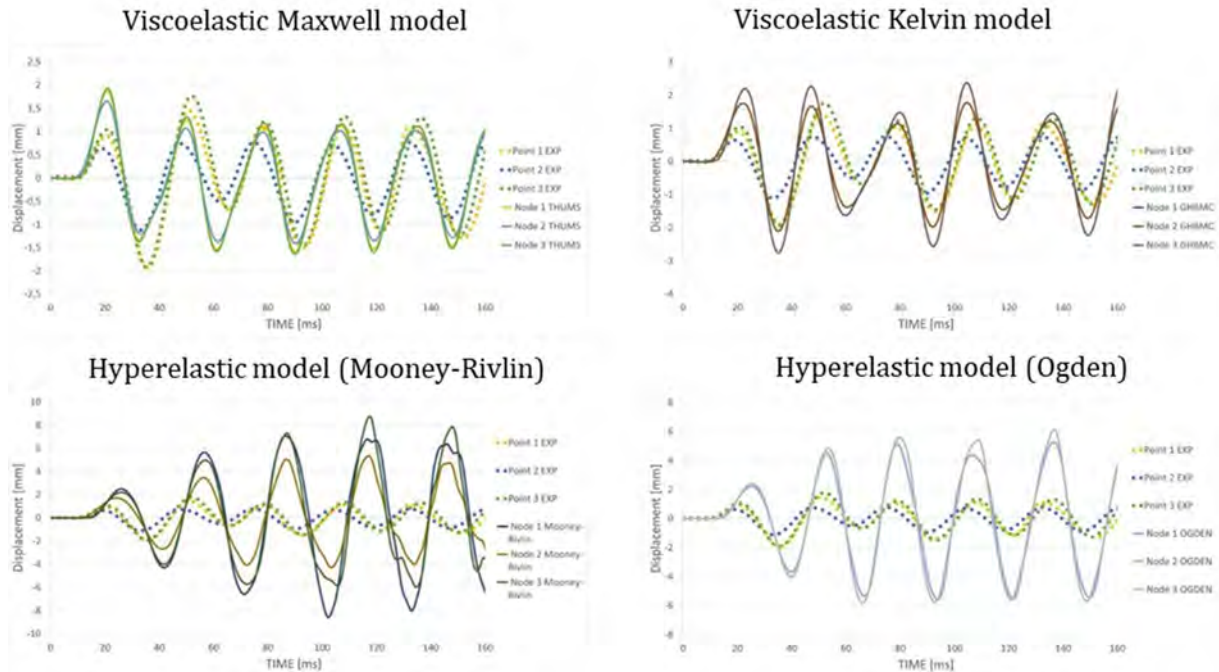
Figure 35. Displacement with respect to time for experimental recordings and a numerical simulation for each material model with the track points/nodes, adapted from [167].

A strong correlation of displacement peak values was achieved, specifically in terms of amplitude and wave period alignment matching the experimental sample. Especially visible after the physical specimen stabilized post: 80 ms. It was observed that the amplitude of points and corresponding nodes (#1 and #3), tracked farther from the base, exceeded those closer to the base (point #2). In simpler terms, locations closer to the base exhibited more excitation-like displacement concerning time. This observation can be explained by considering the brain's viscoelastic properties incorporated into the material model for the FE simulation. The material exhibited a combination of viscous and elastic characteristics during deformation. Interestingly, for certain commonly used material models found in the literature [76], [171]–[174], a behaviour close to rigid-body dynamics was observed (all nodes displaying very similar displacement in time). However, this did not authentically replicate the true nature of brain tissues [167], [175], [176].

9.2. Chapter conclusions

The mechanical testing of brain tissue remains an open-ended challenge in the scientific field. Material models and properties remain diverse, lacking universally acknowledged standards or guidelines within the scientific community. While quasi-static compression and tension have dominated material testing approaches, this study shows that viscoelastic material should reveal its properties during cycling load conditions, aspects often overlooked by static material tests [167].

The presented research can be treated as pilot study for the new numerical head model development. Since the models presented in the literature have simplified geometry, the focus could be moved to represent fine geometric accuracy that would verify the differences in stress concentrations or strain between sulci and gyri. Additionally, there are no numerical head models with a detailed cardiovascular structure. The super sagittal sinus, transverse sinus, Labbe and Trolard veins, and bridging veins could be successfully modelled with 2D FE elements. This approach would allow to investigate the veins damage for specific loading conditions. With the development of computational methods, the CSF could be represented not as a solid FE elements but with a smooth particle hydrodynamics (SPH), Incompressible Computational Fluid Dynamics or arbitrary Lagrangian–Eulerian (ALE) Finite Elements.

10.   Final conclusions

The experiments prepared and executed throughout the dissertation aimed to identify the mechanical properties of prepared cork biocomposites and compare the energy absorption capabilities with agglomerated cork based on literature. Then, the pilot studies were organised in cooperation with the University of Virginia and two designs were proposed. Significantly improved performance was observed in cases of low-velocity impacts, showcasing a notable 10% reduction in the HARM parameter. However, in high-velocity impacts, the cork layer displayed only marginal improvement and even deterioration in HARM, indicating the need for further refinement to improve the materials' performance in higher-impact scenarios. The tendency to perform well in low-velocity cases may be beneficial since the frequency of low-velocity impacts is much higher than the high-velocity impacts. It is observed that retired players that suffered numerous low-velocity impacts in games suffer from chronic encephalopathy that affects their health.

The next step of the studies was to identify the correlation between the acceleration of dummy's centre of gravity and the brain injury criteria in the simplified numerical head model. The presented study and state of the art showed that various numerical head models are available on the market. However, most models have a simplified geometry of the cortex and very little or even no representation of cardiovascular structures.

To conclude, the research aimed to answer whether the current homologation and regulation procedures of American Football helmets are a sufficient predictor considering brain trauma. The steps included the athlete's measurements and an attempt to determine the safest body placement to tackle the ball carrier. Moreover, the proposed design of an additional liner that would absorb energy during impact is proposed. The studies showed promising results regarding collected HIC, HARM and DAMAGE parameters. Finally, it was verified that the currently used homologation parameters do not pair with more advanced injury criteria such as intracranial pressure.

The hypothesis is proven, the *open-field* tackle is safer in terms of head injury in American Football. The HIC values were 26% lower than for the *sideline* tackling technique. Considering the additional targets, the presented biocomposites proved not to have enough energy-absorbing capabilities to withstand the 100 J impacts. The chosen AC216 decreased the acceleration based injury criteria for lower velocity impacts, and increased for higher velocity impacts. This conclusion matches the literature review about guardian caps available on the market. The additional layer may have changed the way the outer shell is managing impact energy and provide ambiguous results. It has to be kept in mind, that the helmets manufacturers maximise the helmet under specific, set by the standard, conditions and any additional equipment may limit the performance. Nevertheless, the proposed design could be used for youth helmets as the players do not have as high accelerations and impacts as the professionals. The study emphasizes the necessity to replace current headform models with more advanced ones, such as the THUMS dummy, equipped with a simplified brain structure. Additionally, it raises concerns about the applicability of HIC in predicting brain injuries resulting from direct head impacts in American Football. The research suggests diversifying certification tests across various helmet types, exploring brain displacement, principal strain and stress, as well as analysing neck forces and their interpretation in Neck Injury Criteria or Normalized Neck Injury Criteria. Finally, the studies have shown that the viscoelastic material model with Maxwell formulation outperforms others under dynamic loading for brain tissue.

11. Future studies

The studies presented in the dissertation do not close the related topics. The nature of science is that the steps taken to solve a problem usually raise multiple new questions. My career as a PhD student also followed this path. I hope the presented results will motivate others to continue the research on biomechanics, brain injury mechanisms, and helmet design in the same way it motivates me.

The proposed studies in the second methodology subchapter showed that although there is a significant limitation and limited time window in the attempt, it could be improved. Having collected the data with higher frequencies for each limb, it could be possible to introduce the limb behaviour instead of general velocity. Ideally, the tackle could be measured with Vicon sensors that individually measure the limbs' position. Another improvement that could be used is the active MADYMO multibody models. However, the insight is very limited. An interesting approach could be undertaken to verify the neck forces acting on the athletes during the collision.

The actions in subchapter four proved the energy-absorbing capabilities of agglomerated cork fitted to the American Football helmet. There could be another set of testing to broaden the studies but with a broader set of cork agglomerates and different thicknesses. It must be kept in mind that the overall mass cannot exceed too much so as not to cause discomfort or additional muscle failure in the neck. Firstly, tests under specific dynamic loading in a helmet-to-helmet collision should be performed for a set of energy-absorbing materials from the literature. Then, based on the results, a few full design concepts should be developed and subjected to testing for different helmets. Finally, a justified conclusion could be written after such testing, and the tests could proceed to in-vivo testing in preseason camps.

An additional idea not covered in the dissertation is the measurements of mechanical loads during helmet-to-helmet or helmet-to-ground collisions with a developed in-house mouthguard. A teeth-protective device with implemented accelerometers and gyroscopes could provide crucial information on the accelerations acting on the head and, with further analysis, could be successfully used as an injury predictor. Compiling the measurements with numerical head models could introduce new injury criteria and most importantly, provide information on injury mechanisms.

The models presented in the literature have simplified geometry, the focus could be moved to represent fine geometric accuracy that would verify the differences in stress concentrations or strain between sulci and gyri. Additionally, there are no numerical head models with a detailed cardiovascular structure. The super sagittal sinus, transverse sinus, Labbe and Trolard veins, and bridging veins could be successfully modelled with 2D FE elements. This approach would allow to investigate the veins damage for specific loading conditions. With the development of computational methods, the CSF could be represented not as solid FE elements but with a smooth particle hydrodynamics (SPH), Incompressible Computational Fluid Dynamics or ALE Finite Elements. The numerical model should have its kinematics verified by experiments or data from literature. One of the test could be, for example, cadaver tests prepared by the Panzer's group (UVA, CAB, USA).

12. Bibliography

[1] W. P. Meehan, *Kids, sports, and concussion : a guide for coaches and parents, 2nd Edition*. 2018.

[2] R. H. Kraft, P. J. Mckee, A. M. Dagro, and S. T. Grafton, "Combining the Finite Element Method with Structural Connectome-based Analysis for Modeling Neurotrauma: Connectome Neurotrauma Mechanics," *PLoS Comput. Biol.*, vol. 8, no. 8, p. e1002619, Aug. 2012, doi: 10.1371/journal.pcbi.1002619.

[3] J. A. Saal, "Common American Football Injuries," *Sport. Med.*, 1991, doi: 10.2165/00007256-199112020-00005.

[4] E. O'Keeffe *et al.*, "Dynamic Blood–Brain Barrier Regulation in Mild Traumatic Brain Injury," *J. Neurotrauma*, vol. 37, no. 2, pp. 347–356, Jan. 2020, doi: 10.1089/neu.2019.6483.

[5] J. G. Beckwith, R. M. Greenwald, and J. J. Chu, "Measuring Head Kinematics in Football: Correlation Between the Head Impact Telemetry System and Hybrid III Headform," *Ann. Biomed. Eng.*, vol. 40, no. 1, pp. 237–248, Jan. 2012, doi: 10.1007/s10439-011-0422-2.

[6] S. Ji, W. Zhao, Z. Li, and T. W. McAllister, "Head impact accelerations for brain strain-related responses in contact sports: a model-based investigation," *Biomech. Model. Mechanobiol.*, vol. 13, no. 5, pp. 1121–1136, Oct. 2014, doi: 10.1007/s10237-014-0562-z.

[7] M. Dymek, M. Ptak, and F. A. O. Fernandes, "Design and Virtual Testing of American Football Helmets–A Review," *Archives of Computational Methods in Engineering*. 2021, doi: 10.1007/s11831-021-09621-7.

[8] A. E. Lincoln, S. V. Caswell, J. L. Almquist, R. E. Dunn, J. B. Norris, and R. Y. Hinton, "Trends in Concussion Incidence in High School Sports," *Am. J. Sports Med.*, vol. 39, no. 5, pp. 958–963, May 2011, doi: 10.1177/0363546510392326.

[9] G. J. Tierney and C. Simms, "Predictive Capacity of the MADYMO Multibody Human Body Model Applied to Head Kinematics During Rugby Union Tackles," *Appl. Sci.*, vol. 9, no. 4, p. 726, Feb. 2019, doi: 10.3390/app9040726.

[10] Y. HASEGAWA *et al.*, "Changes of the Cervical Spine in Response to Head-first Impact in Rugby: A Finite Element Analysis," *Juntendo Med. J.*, 2020, doi: 10.14789/jmj.2020.66.JMJ20-OA04.

[11] L. Cogoluenhes, M. Evin, A. Forodighasemabadi, W. Wei, L. Thollon, and M. Llari, "A modelisation of quantification of head and neck risks associated with tackles in rugby union," *Comput. Methods Biomech. Biomed. Engin.*, vol. 22, no. sup1, pp. S273–S275, Oct. 2019, doi: 10.1080/10255842.2020.1714910.

[12] K. L. Kucera *et al.*, "Traumatic Brain and Spinal Cord Fatalities Among High School and College Football Players — United States, 2005–2014," *MMWR. Morb. Mortal. Wkly. Rep.*, vol. 65, no. 52, pp. 1465–1469, Jan. 2017, doi: 10.15585/mmwr.mm6552a2.

[13] S. Rowson, R. W. Daniel, and S. M. Duma, "Biomechanical performance of leather and modern football helmets," *J. Neurosurg.*, vol. 119, no. 3, pp. 805–809, Sep. 2013, doi: 10.3171/2013.3.JNS121735.

[14] J. J. Crisco *et al.*, "Frequency and Location of Head Impact Exposures in Individual Collegiate Football Players," *J. Athl. Train.*, vol. 45, no. 6, pp. 549–559, Nov. 2010, doi: 10.4085/1062-6050-45.6.549.

[15] S. M. Duma *et al.*, "Analysis of Real-time Head Accelerations in Collegiate Football Players,"

Clin. J. Sport Med., vol. 15, no. 1, pp. 3–8, Jan. 2005, doi: 10.1097/00042752-200501000-00002.

[16]   S. Rowson *et al.*, "Rotational Head Kinematics in Football Impacts: An Injury Risk Function for Concussion," *Ann. Biomed. Eng.*, vol. 40, no. 1, pp. 1–13, Jan. 2012, doi: 10.1007/s10439-011-0392-4.

[17]   E. J. Pellman *et al.*, "Concussion in Professional Football: Location and Direction of Helmet Impacts - Part 2," *Neurosurgery*, vol. 53, no. 6, pp. 1328–1341, 2003, doi: 10.1227/01.NEU.0000093499.20604.21.

[18]   P. G. Brolinson, S. Manoogian, D. McNeely, M. Goforth, R. Greenwald, and S. Duma, "Analysis of Linear Head Accelerations from Collegiate Football Impacts," *Curr. Sports Med. Rep.*, vol. 5, no. 1, pp. 23–28, Feb. 2006, doi: 10.1097/01.CSMR.0000306515.87053.fa.

[19]   G. B. Choi *et al.*, "Head Impact Exposure in Youth and Collegiate American Football," *Ann. Biomed. Eng.*, vol. 50, no. 11, pp. 1488–1497, Nov. 2022, doi: 10.1007/s10439-022-02974-5.

[20]   S. Rowson *et al.*, "Can helmet design reduce the risk of concussion in football? Technical note," *J. Neurosurg.*, vol. 120, no. 4, pp. 919–922, 2014, doi: 10.3171/2014.1.JNS13916.

[21]   I. R. Casson, D. C. Viano, J. W. Powell, and E. J. Pellman, "Twelve Years of National Football League Concussion Data," *Sport. Heal. A Multidiscip. Approach*, vol. 2, no. 6, pp. 471–483, Nov. 2010, doi: 10.1177/1941738110383963.

[22]   B. P. Boden, R. L. Tacchetti, R. C. Cantu, S. B. Knowles, and F. O. Mueller, "Catastrophic head injuries in high school and college football players," *Am. J. Sports Med.*, 2007, doi: 10.1177/0363546507299239.

[23]   L. M. Gessel, S. K. Fields, C. L. Collins, R. W. Dick, and R. D. Comstock, "Concussions among United States high school and collegiate athletes.," *J. Athl. Train.*, vol. 42, no. 4, pp. 495–503, [Online]. Available: http://www.ncbi.nlm.nih.gov/pubmed/18174937.

[24]   Y. Liu *et al.*, "Validation and Comparison of Instrumented Mouthguards for Measuring Head Kinematics and Assessing Brain Deformation in Football Impacts," *Ann. Biomed. Eng.*, vol. 48, no. 11, pp. 2580–2598, Nov. 2020, doi: 10.1007/s10439-020-02629-3.

[25]   A. Arnason, S. B. Sigurdsson, A. Gudmundsson, I. Holme, L. Engebretsen, and R. Bahr, "Risk Factors for Injuries in Football," *Am. J. Sports Med.*, vol. 32, no. 1_suppl, pp. 5–16, Mar. 2004, doi: 10.1177/0363546503258912.

[26]   A. S. McIntosh and P. McCrory, "Preventing head and neck injury," *British Journal of Sports Medicine*, vol. 39, no. 6. pp. 314–318, Jun. 2005, doi: 10.1136/bjsm.2005.018200.

[27]   Jimmy Stamp, "Leatherhead to Radio-head: The Evolution of the Football Helmet," *Smithsonian magazine*, 2012. https://www.smithsonianmag.com/arts-culture/leatherhead-to-radio-head-the-evolution-of-the-football-helmet-56585562/ (accessed Apr. 19, 2021).

[28]   National Operating Committee on Standards for Athletic Equipment, "Standart Performance Specification for Newly Manufactured Football Helmets," 2019.

[29]   S. Rowson and S. M. Duma, "Development of the STAR Evaluation System for Football Helmets: Integrating Player Head Impact Exposure and Risk of Concussion," *Ann. Biomed. Eng.*, vol. 39, no. 8, pp. 2130–2140, Aug. 2011, doi: 10.1007/s10439-011-0322-5.

[30]   B. Rowson, S. Rowson, and S. M. Duma, "Hockey STAR: A Methodology for Assessing the Biomechanical Performance of Hockey Helmets," *Ann. Biomed. Eng.*, vol. 43, no. 10, pp.

2429–2443, Oct. 2015, doi: 10.1007/s10439-015-1278-7.

[31]   E. J. Pellman, D. C. Viano, C. Withnall, N. Shewchenko, C. A. Bir, and P. D. Halstead, "Concussion in Professional Football: Helmet Testing to Assess Impact Performance—Part 11," *Neurosurgery*, vol. 58, no. 1, pp. 78–95, Jan. 2006, doi: 10.1227/01.NEU.0000196265.35238.7C.

[32]   D. C. Viano, C. Withnall, and D. Halstead, "Impact Performance of Modern Football Helmets," *Ann. Biomed. Eng.*, vol. 40, no. 1, pp. 160–174, Jan. 2012, doi: 10.1007/s10439-011-0384-4.

[33]   E. J. Pellman, D. C. Viano, C. Withnall, N. Shewchenko, C. A. Bir, and P. D. Halstead, "Concussion in Professional Football: Helmet Testing to Assess Impact Performance—Part 11," *Neurosurgery*, vol. 58, no. 1, pp. 78–95, Jan. 2006, doi: 10.1227/01.NEU.0000196265.35238.7C.

[34]   D. C. Viano, E. J. Pellman, C. Withnall, and N. Shewchenko, "Concussion in Professional Football," *Neurosurgery*, vol. 59, no. 3, pp. 591–606, Sep. 2006, doi: 10.1227/01.NEU.0000231851.97287.C2.

[35]   E. J. Pellman, D. C. Viano, A. M. Tucker, I. R. Casson, and J. F. Waeckerle, "Concussion in Professional Football: Reconstruction of Game Impacts and Injuries," *Neurosurgery*, vol. 53, no. 4, pp. 799–814, Oct. 2003, doi: 10.1093/neurosurgery/53.3.799.

[36]   D. J. Lessley *et al.*, "Video Analysis of Reported Concussion Events in the National Football League During the 2015-2016 and 2016-2017 Seasons," *Am. J. Sports Med.*, vol. 46, no. 14, pp. 3502–3510, Dec. 2018, doi: 10.1177/0363546518804498.

[37]   D. J. Lessley *et al.*, "Position-Specific Circumstances of Concussions in the NFL: Toward the Development of Position-Specific Helmets," *Ann. Biomed. Eng.*, vol. 48, no. 11, pp. 2542–2554, Nov. 2020, doi: 10.1007/s10439-020-02657-z.

[38]   A. M. Bailey, J. R. Funk, J. R. Crandall, B. S. Myers, and K. B. Arbogast, "Laboratory Evaluation of Shell Add-On Products for American Football Helmets for Professional Linemen," *Ann. Biomed. Eng.*, vol. 49, no. 10, pp. 2747–2759, Oct. 2021, doi: 10.1007/s10439-021-02842-8.

[39]   N. J. Cecchi *et al.*, "Padded Helmet Shell Covers in American Football: A Comprehensive Laboratory Evaluation with Preliminary On-Field Findings," *Ann. Biomed. Eng.*, Mar. 2023, doi: 10.1007/s10439-023-03169-2.

[40]   National Football League, "NFL and NFLPA Release 2021 Helmet Testing Performance Results." 2021. https://operations.nfl.com/updates/football-ops/nfl-and-nflpa-release-2021-helmet-testing-performance-results/.

[41]   K. M. Breedlove, E. Breedlove, E. Nauman, T. G. Bowman, and M. R. Lininger, "The Ability of an Aftermarket Helmet Add-On Device to Reduce Impact-Force Accelerations During Drop Tests," *J. Athl. Train.*, vol. 52, no. 9, pp. 802–808, Sep. 2017, doi: 10.4085/1062-6050-52.6.01.

[42]   M. Matsumae *et al.*, "Age-related changes in intracranial compartment volumes in normal adults assessed by magnetic resonance imaging," *J. Neurosurg.*, vol. 84, no. 6, pp. 982–991, Jun. 1996, doi: 10.3171/jns.1996.84.6.0982.

[43]   D. Purves *et al.*, *Neuroglial Cells*, 2nd Ed. Neuroscience, 2001.

[44]   C. Rowe, *Neurosciences.*, vol. 52, no. 10. 2011.

[45]   A. N. Bashkatov, E. A. Genina, Y. P. Sinichkin, V. I. Kochubey, N. A. Lakodina, and V. V. Tuchin, "Glucose and Mannitol Diffusion in Human Dura Mater," *Biophys. J.*, vol. 85, no. 5, pp. 3310–

3318, Nov. 2003, doi: 10.1016/S0006-3495(03)74750-X.

[46] M. A. Reina, O. D. L. Casasola, M. C. Villanueva, A. L??pez, F. Mach??s, and J. A. De Andr??s, "Ultrastructural Findings in Human Spinal Pia Mater in Relation to Subarachnoid Anesthesia," *Anesth. Analg.*, pp. 1479–1485, May 2004, doi: 10.1213/01.ANE.0000113240.09354.E9.

[47] M. A. Reina, A. Prats-Galino, R. G. Sola, A. Puigdellívol-Sánchez, R. Arriazu Navarro, and J. A. De Andrés, "Morfología de la lámina aracnoidea espinal humana. Barrera que limita la permeabilidad del saco dural," *Rev. Esp. Anestesiol. Reanim.*, vol. 57, no. 8, pp. 486–492, Jan. 2010, doi: 10.1016/S0034-9356(10)70709-X.

[48] M. A. Reina, A. Prats-Galino, R. G. Sola, A. Puigdellívol-Sánchez, R. Arriazu Navarro, and J. A. De Andrés, "Morfología de la lámina aracnoidea espinal humana. Barrera que limita la permeabilidad del saco dural," *Rev. Esp. Anestesiol. Reanim.*, vol. 57, no. 8, pp. 486–492, Jan. 2010, doi: 10.1016/S0034-9356(10)70709-X.

[49] M. A. Reina, O. D. L. Casasola, M. C. Villanueva, A. L??pez, F. Mach??s, and J. A. De Andr??s, "Ultrastructural Findings in Human Spinal Pia Mater in Relation to Subarachnoid Anesthesia," *Anesth. Analg.*, pp. 1479–1485, May 2004, doi: 10.1213/01.ANE.0000113240.09354.E9.

[50] M. Dymek, "Numerical analysis of a professional American football helmet using a human head model," Wroclaw University of Science and Technology, 2020.

[51] W. W. D. Larysz, "Inżynieria biomedyczna, podstawy i zastosowania: Biomechanika i inżynieria rehabilitacyjna.," 2015.

[52] C. Simms, D. Wood, "Pedestrian and cyclist impact.," *2019*.

[53] A. I. K. L. Zhang, K.H. Yang, "Comparison of brain responses between frontal and lateral impacts by finite element modeling," pp. 21–30, 2001.

[54] M. Matsumae *et al.*, "Age-related changes in intracranial compartment volumes in normal adults assessed by magnetic resonance imaging," *J. Neurosurg.*, vol. 84, no. 6, pp. 982–991, Jun. 1996, doi: 10.3171/jns.1996.84.6.0982.

[55] M. H. Carstens, "The Meninges," in *The Embryologic Basis of Craniofacial Structure*, Cham: Springer International Publishing, 2023, pp. 1037–1085.

[56] M. Claessens, "Finite Element Modeling of the Human Head under Impact Conditions," 1997.

[57] Mayfield Clinic, "Traumatic brain injury," 2018. http://www.mayfieldclinic.com/pe-tbi.htm (accessed Mar. 25, 2021).

[58] M. Ratajczak *et al.*, "Symmetry of the Human Head—Are Symmetrical Models More Applicable in Numerical Analysis?," *Symmetry (Basel).*, vol. 13, no. 7, p. 1252, Jul. 2021, doi: 10.3390/sym13071252.

[59] R. J. H. Cloots, H. M. T. Gervaise, J. A. W. Van Dommelen, and M. G. D. Geers, "Biomechanics of traumatic brain injury: Influences of the morphologic heterogeneities of the cerebral cortex," *Ann. Biomed. Eng.*, vol. 36, no. 7, pp. 1203–1215, Jul. 2008, doi: 10.1007/s10439-008-9510-3.

[60] M. Ratajczak *et al.*, "Symmetry of the human head—are symmetrical models more applicable in numerical analysis?," *Symmetry (Basel).*, vol. 13, no. 7, 2021, doi: 10.3390/sym13071252.

[61] L. Zhang *et al.*, "Recent advances in brain injury research: a new human head model

development and validation.," *Stapp Car Crash J.*, vol. 45, pp. 369–94, Nov. 2001.

[62] L. Zhang *et al.*, "Computational study of the contribution of the vasculature on the dynamic response of the brain.," *Stapp Car Crash J.*, vol. 46, pp. 145–64, Nov. 2002.

[63] S. Kleiven and W. N. Hardy, "Correlation of an FE Model of the Human Head with Local Brain Motion--Consequences for Injury Prediction.," *Stapp Car Crash J.*, vol. 46, pp. 123–44, Nov. 2002.

[64] T. J. Horgan and M. D. Gilchrist, "The creation of three-dimensional finite element models for simulating head impact biomechanics," *Int. J. Crashworthiness*, vol. 8, no. 4, pp. 353–366, Jan. 2003, doi: 10.1533/ijcr.2003.0243.

[65] G. Belingardi, G. Chiandussi, and I. Gaviglio, "Development and Validation of a New Finite Element Model of Human Head," *Proc. 19th Int. Tech. Conf. Enhanc. Saf. Veh.*, 2005.

[66] Z. Zong, H. P. Lee, and C. Lu, "A three-dimensional human head finite element model and power flow in a human head subject to impact loading," *J. Biomech.*, vol. 39, no. 2, pp. 284–292, Jan. 2006, doi: 10.1016/j.jbiomech.2004.11.015.

[67] S. Kleiven, "Predictors for traumatic brain injuries evaluated through accident reconstructions.," *Stapp Car Crash J.*, vol. 51, pp. 81–114, Oct. 2007.

[68] E. G. Takhounts *et al.*, "Investigation of traumatic brain injuries using the next generation of simulated injury monitor (SIMon) finite element head model.," *Stapp Car Crash J.*, vol. 52, pp. 1–31, Nov. 2008.

[69] K. H. Yang, H. Mao, C. Wagner, F. Zhu, C. C. Chou, and A. I. King, "Modeling of the Brain for Injury Prevention," 2011, pp. 69–120.

[70] W. Zhao, S. Ruan, H. Li, S. Cui, L. He, and J. Li, "Development and validation of a 5th percentile human head finite element model based on the Chinese population," *Int. J. Veh. Saf.*, vol. 6, no. 2, p. 91, 2012, doi: 10.1504/IJVS.2012.049024.

[71] H. Mao *et al.*, "Development of a Finite Element Human Head Model Partially Validated With Thirty Five Experimental Cases," *J. Biomech. Eng.*, vol. 135, no. 11, Nov. 2013, doi: 10.1115/1.4025101.

[72] D. Sahoo, C. Deck, and R. Willinger, "Development and validation of an advanced anisotropic visco-hyperelastic human brain FE model," *J. Mech. Behav. Biomed. Mater.*, vol. 33, pp. 24–42, May 2014, doi: 10.1016/j.jmbbm.2013.08.022.

[73] N. Atsumi, Y. Nakahira, and M. Iwamoto, "Development and validation of a head/brain FE model and investigation of influential factor on the brain response during head impact," *Int. J. Veh. Saf.*, vol. 9, no. 1, p. 1, 2016, doi: 10.1504/IJVS.2016.077145.

[74] M. Ghajari, P. J. Hellyer, and D. J. Sharp, "Computational modelling of traumatic brain injury predicts the location of chronic traumatic encephalopathy pathology," *Brain*, vol. 140, no. 2, pp. 333–343, Feb. 2017, doi: 10.1093/brain/aww317.

[75] F. A. O. Fernandes, D. Tchepel, R. J. Alves de Sousa, and M. Ptak, "Development and validation of a new finite element human head model: Yet another head model (YEAHM)," *Eng. Comput. (Swansea, Wales)*, vol. 35, no. 1, pp. 477–496, 2018, doi: 10.1108/EC-09-2016-0321.

[76] M. Ratajczak, M. Ptak, L. Chybowski, K. Gawdzińska, and R. Będziński, "Material and Structural Modeling Aspects of Brain Tissue Deformation under Dynamic Loads," *Materials (Basel).*, vol. 12, no. 2, p. 271, Jan. 2019, doi: 10.3390/ma12020271.

[77] X. Li, Z. Zhou, and S. Kleiven, "An anatomically detailed and personalizable head injury

model: Significance of brain and white matter tract morphological variability on strain," *Biomech. Model. Mechanobiol.*, vol. 20, no. 2, pp. 403–431, Apr. 2021, doi: 10.1007/s10237-020-01391-8.

[78]   M. Ptak *et al.*, "Experimental and computational approach to human brain modelling – aHEAD," *Arch. Civ. Mech. Eng.*, vol. 23, no. 3, p. 218, Aug. 2023, doi: 10.1007/s43452-023-00758-9.

[79]   F. Hernandez *et al.*, "Lateral impacts correlate with falx cerebri displacement and corpus callosum trauma in sports-related concussions," *Biomech. Model. Mechanobiol.*, vol. 18, no. 3, pp. 631–649, Jun. 2019, doi: 10.1007/s10237-018-01106-0.

[80]   R. M. Wright and K. T. Ramesh, "An axonal strain injury criterion for traumatic brain injury," *Biomech. Model. Mechanobiol.*, vol. 11, no. 1–2, pp. 245–260, Jan. 2012, doi: 10.1007/s10237-011-0307-1.

[81]   J. W. F. Paulsen, *Sobotta Atlas anatomi człowieka Głowa, szyja i układ nerwowy*, 23rd ed. 2010.

[82]   R. Podemski, *Kompedium Neurologii*, 3rd ed. via Medica, 2014.

[83]   M. Aare, S. Kleiven, and P. Halldin, "Injury criteria for oblique helmet impacts," *Div. Neuronic Eng. CTV-Centre Technol. Heal. Care, R. Inst. Technol. Karolinska Institute, Stock. SwedenTitle, Monogr. IRCOBI Conf.*, no. September, 2003.

[84]   P. Prasad, H. Mertz, "The position of the United States delegation to the ISO Working Group 6 on the use of HIC in the automotive environment," 1985.

[85]   D. Marjoux, D. Baumgartner, C. Deck, and R. Willinger, "Head injury prediction capability of the HIC, HIP, SIMon and ULP criteria," *Accid. Anal. Prev.*, vol. 40, no. 3, pp. 1135–1148, May 2008, doi: 10.1016/j.aap.2007.12.006.

[86]   E. G. Takhounts, M. J. Craig, K. Moorhouse, J. McFadden, and V. Hasija, "Development of brain injury criteria (BrIC).," *Stapp Car Crash J.*, 2013.

[87]   L. F. Gabler, J. R. Crandall, and M. B. Panzer, "Development of a Second-Order System for Rapid Estimation of Maximum Brain Strain," *Ann. Biomed. Eng.*, vol. 47, no. 9, pp. 1971–1981, Sep. 2019, doi: 10.1007/s10439-018-02179-9.

[88]   T. Darling, J. Muthuswamy, and S. D. Rajan, "Finite element modeling of human brain response to football helmet impacts," *Comput. Methods Biomech. Biomed. Engin.*, vol. 19, no. 13, pp. 1432–1442, Oct. 2016, doi: 10.1080/10255842.2016.1149574.

[89]   P. J. Roache, *Verification and Validation in Computational Science and Engineering*. 1998.

[90]   S. Bansal, B. Mobasher, S. D. Rajan, and I. Vintilescu, "Development of Fabric Constitutive Behavior for Use in Modeling Engine Fan Blade-Out Events," *J. Aerosp. Eng.*, vol. 22, no. 3, pp. 249–259, Jul. 2009, doi: 10.1061/(ASCE)0893-1321(2009)22:3(249).

[91]   Z. Stahlecker, B. Mobasher, S. D. Rajan, and J. M. Pereira, "Development of reliable modeling methodologies for engine fan blade out containment analysis. Part II: Finite element analysis," *Int. J. Impact Eng.*, vol. 36, no. 3, pp. 447–459, Mar. 2009, doi: 10.1016/j.ijimpeng.2008.08.004.

[92]   A. Deivanayagam, A. Vaidya, and S. D. Rajan, "Enhancements to Modeling Dry Fabrics for Impact Analysis," *J. Aerosp. Eng.*, vol. 27, no. 3, pp. 484–490, May 2014, doi: 10.1061/(ASCE)AS.1943-5525.0000350.

[93]   D. A. Bruneau and D. S. Cronin, "Brain response of a computational head model for prescribed skull kinematics and simulated football helmet impact boundary conditions," *J.*

Mech. Behav. Biomed. Mater., vol. 115, p. 104299, Mar. 2021, doi: 10.1016/j.jmbbm.2020.104299.

[94]   A. Post, A. Oeur, E. Walsh, B. Hoshizaki, and M. D. Gilchrist, "A centric/non-centric impact protocol and finite element model methodology for the evaluation of American football helmets to evaluate risk of concussion," *Comput. Methods Biomech. Biomed. Engin.*, vol. 17, no. 16, pp. 1785–1800, Dec. 2014, doi: 10.1080/10255842.2013.766724.

[95]   C. Kuo, L. Wu, W. Zhao, M. Fanton, S. Ji, and D. B. Camarillo, "Propagation of errors from skull kinematic measurements to finite element tissue responses," *Biomech. Model. Mechanobiol.*, vol. 17, no. 1, pp. 235–247, Feb. 2018, doi: 10.1007/s10237-017-0957-8.

[96]   H. V. Alizadeh, M. G. Fanton, A. G. Domel, G. Grant, and D. B. Camarillo, "Prevention of Traumatic Brain Injury with Liquid Shock Absorption," Oct. 2019, [Online]. Available: http://arxiv.org/abs/1910.07722.

[97]   M. Dymek, M. Ptak, M. Ratajczak, F. A. O. Fernandes, A. Kwiatkowski, and J. Wilhelm, "Analysis of HIC and Hydrostatic Pressure in the Human Head during NOCSAE Tests of American Football Helmets," *Brain Sci.*, vol. 11, no. 3, p. 287, Feb. 2021, doi: 10.3390/brainsci11030287.

[98]   P. Honarmandi, A. M. Sadegh, and P. V. Cavallaro, "Modelling and impact analysis of football player head with helmet toward mitigating brain concussion," *Int. J. Exp. Comput. Biomech.*, vol. 3, no. 4, p. 267, 2015, doi: 10.1504/IJECB.2015.074732.

[99]   K. A. Zimmerman *et al.*, "Player position in American football influences the magnitude of mechanical strains produced in the location of chronic traumatic encephalopathy pathology: A computational modelling study," *J. Biomech.*, vol. 118, p. 110256, Mar. 2021, doi: 10.1016/j.jbiomech.2021.110256.

[100] D. B. Camarillo, P. B. Shull, J. Mattson, R. Shultz, and D. Garza, "An Instrumented Mouthguard for Measuring Linear and Angular Head Impact Kinematics in American Football," *Ann. Biomed. Eng.*, vol. 41, no. 9, pp. 1939–1949, Sep. 2013, doi: 10.1007/s10439-013-0801-y.

[101] G. P. Siegmund, K. M. Guskiewicz, S. W. Marshall, A. L. DeMarco, and S. J. Bonin, "A Headform for Testing Helmet and Mouthguard Sensors that Measure Head Impact Severity in Football Players," *Ann. Biomed. Eng.*, vol. 42, no. 9, pp. 1834–1845, Sep. 2014, doi: 10.1007/s10439-014-1052-2.

[102] K. R. Campbell *et al.*, "Laboratory Evaluation of the gForce Tracker™, a Head Impact Kinematic Measuring Device for Use in Football Helmets," *Ann. Biomed. Eng.*, vol. 44, no. 4, pp. 1246–1256, Apr. 2016, doi: 10.1007/s10439-015-1391-7.

[103] L. C. Wu *et al.*, "In Vivo Evaluation of Wearable Head Impact Sensors," *Ann. Biomed. Eng.*, vol. 44, no. 4, pp. 1234–1245, Apr. 2016, doi: 10.1007/s10439-015-1423-3.

[104] L. Zhang, K. H. Yang, and A. I. King, "A Proposed Injury Threshold for Mild Traumatic Brain Injury," *J. Biomech. Eng.*, vol. 126, no. 2, pp. 226–236, Apr. 2004, doi: 10.1115/1.1691446.

[105] R. Willinger and D. Baumgartner, "Numerical and physical modelling of the human head under impact - towards new injury criteria," *Int. J. Veh. Des.*, vol. 32, no. 1/2, p. 94, 2003, doi: 10.1504/IJVD.2003.003239.

[106] B. J. Pfister, T. P. Weihs, M. Betenbaugh, and G. Bao, "An In Vitro Uniaxial Stretch Model for Axonal Injury," *Ann. Biomed. Eng.*, vol. 31, no. 5, pp. 589–598, May 2003, doi: 10.1114/1.1566445.

[107] G. L. Farley, "Energy Absorption of Composite Materials," *J. Compos. Mater.*, vol. 17, no. 3, pp. 267–279, May 1983, doi: 10.1177/002199838301700307.

[108] S. Shan *et al.*, "Multistable Architected Materials for Trapping Elastic Strain Energy," *Adv. Mater.*, vol. 27, no. 29, pp. 4296–4301, Aug. 2015, doi: 10.1002/adma.201501708.

[109] T. M. Pham, W. Chen, A. M. Khan, H. Hao, M. Elchalakani, and T. M. Tran, "Dynamic compressive properties of lightweight rubberized concrete," *Constr. Build. Mater.*, vol. 238, p. 117705, Mar. 2020, doi: 10.1016/j.conbuildmat.2019.117705.

[110] X. Mei, Z. Cui, Q. Sheng, J. Zhou, and C. Li, "Application of the Improved POA-RF Model in Predicting the Strength and Energy Absorption Property of a Novel Aseismic Rubber-Concrete Material," *Materials (Basel).*, vol. 16, no. 3, p. 1286, Feb. 2023, doi: 10.3390/ma16031286.

[111] V. Oliveira, M. E. Rosa, and H. Pereira, "Variability of the compression properties of cork," *Wood Sci. Technol.*, vol. 48, no. 5, pp. 937–948, Sep. 2014, doi: 10.1007/s00226-014-0651-2.

[112] H. Pereira, "Variability of the Chemical Composition of Cork," *BioResources*, vol. 8, no. 2, pp. 2246–2256, Mar. 2013, doi: 10.15376/biores.8.2.2246-2256.

[113] F. A. O. Fernandes, "Análise Biomecânica de impactos com capacetes: novos materiais e geometrias, Biomechanical analysis of helmeted head impacts: novel materials and geometries," Universidade de Aveiro: Aveiro, Portugal, 2017.

[114] J. Sousa-Martins, D. Kakogiannis, F. Coghe, B. Reymen, and F. Teixeira-Dias, "Response of cork compounds subjected to impulsive blast loads," *Eur. Phys. J. Spec. Top.*, vol. 206, no. 1, pp. 61–70, May 2012, doi: 10.1140/epjst/e2012-01587-1.

[115] O. Anjos, C. Rodrigues, J. Morais, and H. Pereira, "Effect of density on the compression behaviour of cork," *Mater. Des.*, vol. 53, pp. 1089–1096, Jan. 2014, doi: 10.1016/j.matdes.2013.07.038.

[116] M. Urbaniak, R. Gołuch-Goreczna, A. K. Bledzki, and S. Gajdzinski, "Natural cork. Part I. Cork oak tree culture, macro- and micromorphology of cork," *Polimery*, vol. 62, no. 05, pp. 388–393, May 2017, doi: 10.14314/polimery.2017.388.

[117] H. Pereira, *Cork: Biology, Production and Uses*. 2007.

[118] I. M. Aroso, E. M. Fernandes, R. A. Pires, J. F. Mano, and R. L. Reis, "Cork extractives exhibit thermo-oxidative protection properties in polypropylene–cork composites and as direct additives for polypropylene," *Polym. Degrad. Stab.*, vol. 116, pp. 45–52, Jun. 2015, doi: 10.1016/J.POLYMDEGRADSTAB.2015.03.006.

[119] P. C. R. O. Pinto *et al.*, "Quercus suber and Betula pendula outer barks as renewable sources of oleochemicals: A comparative study," *Ind. Crops Prod.*, vol. 29, no. 1, pp. 126–132, Jan. 2009, doi: 10.1016/j.indcrop.2008.04.015.

[120] S. P. Silva, M. A. Sabino, E. M. Fernandes, V. M. Correlo, L. F. Boesel, and R. L. Reis, "Cork: properties, capabilities and applications," *Int. Mater. Rev.*, vol. 50, no. 6, pp. 345–365, Dec. 2005, doi: 10.1179/174328005X41168.

[121] H. Pereira, "Chemical composition and variability of cork from Quercus suber L.," *Wood Sci. Technol.*, vol. 22, no. 3, pp. 211–218, 1988, doi: 10.1007/BF00386015.

[122] M. Urbaniak, R. Goluch-Goreczna, A. K. Bledzki, and S. Gajdzinski, "Natural cork. Part II. Properties and applications," *Polimery*, vol. 62, no. 06, 2017, doi: 10.14314/polimery.2017.472.

[123] R. Miralbes Buil, D. Ranz Angulo, and J. Ivens, "Analysis of the capability of cork and cork agglomerates to absorb multiple compressive quasi-static loading cycles," *Eur. J. Wood*

Wood Prod., vol. 79, no. 5, pp. 1195–1208, Sep. 2021, doi: 10.1007/s00107-021-01658-6.

[124] R. T. Jardin, F. A. O. Fernandes, A. B. Pereira, and R. J. Alves de Sousa, "Static and dynamic mechanical response of different cork agglomerates," *Mater. Des.*, vol. 68, pp. 121–126, Mar. 2015, doi: 10.1016/j.matdes.2014.12.016.

[125] S. Sanchez-Saez, E. Barbero, S. K. Garcia-Castillo, I. Ivañez, and J. Cirne, "Experimental response of agglomerated cork under multi-impact loads," *Mater. Lett.*, vol. 160, pp. 327–330, Dec. 2015, doi: 10.1016/j.matlet.2015.08.012.

[126] R. Kottner, R. Hynek, T. Mandys, and J. Bartošek, "Material property determination of the lining layers of a versatile helmet," *MATEC Web Conf.*, vol. 157, p. 06005, Mar. 2018, doi: 10.1051/matecconf/201815706005.

[127] R. M. Coelho, R. J. Alves de Sousa, F. A. O. Fernandes, and F. Teixeira-Dias, "New composite liners for energy absorption purposes," *Mater. Des.*, vol. 43, pp. 384–392, Jan. 2013, doi: 10.1016/j.matdes.2012.07.020.

[128] C. P. Gameiro, J. Cirne, and G. Gary, "Experimental study of the quasi-static and dynamic behaviour of cork under compressive loading," *J. Mater. Sci.*, vol. 42, no. 12, pp. 4316–4324, Jun. 2007, doi: 10.1007/s10853-006-0675-6.

[129] S. Sanchez-Saez, E. Barbero, and J. Cirne, "Experimental study of agglomerated-cork-cored structures subjected to ballistic impacts," *Mater. Lett.*, vol. 65, no. 14, pp. 2152–2154, Jul. 2011, doi: 10.1016/j.matlet.2011.04.083.

[130] F. A. O. Fernandes, R. J. S. Pascoal, and R. J. Alves de Sousa, "Modelling impact response of agglomerated cork," *Mater. Des.*, vol. 58, pp. 499–507, Jun. 2014, doi: 10.1016/j.matdes.2014.02.011.

[131] S. Sanchez-Saez, S. K. García-Castillo, E. Barbero, and J. Cirne, "Dynamic crushing behaviour of agglomerated cork," *Mater. Des.*, vol. 65, pp. 743–748, Jan. 2015, doi: 10.1016/j.matdes.2014.09.054.

[132] F. A. O. Fernandes, R. T. Jardin, A. B. Pereira, and R. J. Alves de Sousa, "Comparing the mechanical performance of synthetic and natural cellular materials," *Mater. Des.*, vol. 82, 2015, doi: 10.1016/j.matdes.2015.06.004.

[133] P. T. Santos, S. Pinto, P. A. A. P. Marques, A. B. Pereira, and R. J. Alves de Sousa, "Agglomerated cork: A way to tailor its mechanical properties," *Compos. Struct.*, vol. 178, 2017, doi: 10.1016/j.compstruct.2017.07.035.

[134] M. Ptak, P. Kaczynski, F. A. O. Fernandes, and R. J. A. de Sousa, "Assessing impact velocity and temperature effects on crashworthiness properties of cork material," *Int. J. Impact Eng.*, vol. 106, 2017, doi: 10.1016/j.ijimpeng.2017.04.014.

[135] P. Kaczynski, M. Ptak, J. Wilhelm, F. A. O. Fernandes, and R. J. A. de Sousa, "High-energy impact testing of agglomerated cork at extremely low and high temperatures," *Int. J. Impact Eng.*, vol. 126, 2019, doi: 10.1016/j.ijimpeng.2018.12.001.

[136] NBCS, "NFL says positions wearing Guardian Caps saw 52% decrease in concussions," 2023. https://www.nbcsports.com/nfl/profootballtalk/rumor-mill/news/nfl-says-positions-wearing-guardian-caps-saw-52-decrease-in-concussions.

[137] A. McKinlay, A. Bishop, and T. McLellan, "Public knowledge of 'concussion' and the different terminology used to communicate about mild traumatic brain injury (MTBI)," *Brain Inj.*, vol. 25, no. 7–8, pp. 761–766, Jul. 2011, doi: 10.3109/02699052.2011.579935.

[138] National Football League, "NFL ANNOUNCES PLAY SMART. PLAY SAFE., A NEW

COMMITMENT TO IMPROVE PLAYER HEALTH AND SAFETY," 2016. https://operations.nfl.com/updates/football-ops/nfl-announces-play-smart-play-safe-a-new-commitment-to-improve-player-health-and-safety/.

[139] J. S. Giudice *et al.*, "Finite Element Model of a Deformable American Football Helmet Under Impact," *Ann. Biomed. Eng.*, vol. 48, no. 5, pp. 1524–1539, 2020, doi: 10.1007/s10439-020-02472-6.

[140] Biocore, "Biocore Finite element models." .

[141] M. Kurańska *et al.*, "Cork Porous Biocomposites with Polyurethane Matrix Modified with Polyol Based on Used Cooking Oil," *Materials (Basel).*, vol. 16, no. 8, p. 3032, Apr. 2023, doi: 10.3390/ma16083032.

[142] M. Dymek *et al.*, "Eco-Friendly Cork–Polyurethane Biocomposites for Enhanced Impact Performance: Experimental and Numerical Analysis," *Polymers (Basel).*, vol. 16, no. 7, p. 887, Mar. 2024, doi: 10.3390/polym16070887.

[143] F. Fernandes, R. Alves de Sousa, M. Ptak, and G. Migueis, "Helmet Design Based on the Optimization of Biocomposite Energy-Absorbing Liners under Multi-Impact Loading," *Appl. Sci.*, vol. 9, no. 4, p. 735, Feb. 2019, doi: 10.3390/app9040735.

[144] A. M. Bailey *et al.*, "Development and Evaluation of a Test Method for Assessing the Performance of American Football Helmets," *Ann. Biomed. Eng.*, 2020, doi: 10.1007/s10439-020-02626-6.

[145] J. Versace, "A review of the severity index," in *Proceedings of Stapp Car Crash Conference*, 1971, pp. 771–96.

[146] E. J. Pellman, D. C. Viano, A. M. Tucker, and I. R. Casson, "Concussion in Professional Football: Location and Direction of Helmet Impacts—Part 2," *Neurosurgery*, vol. 53, no. 6, pp. 1328–1341, Dec. 2003, doi: 10.1227/01.NEU.0000093499.20604.21.

[147] NOCSAE, "001-04m05, Standard Drop Test Method and Equipment Used in Evaluating the Performance Characteristics of Protective Headgear," 2004.

[148] NOCSAE, "002-98m03, Standard Performance Specification for Newly Manufactured Football Helmets," 1998, [Online]. Available: www.nocsae.org.

[149] NOCSAE, "021-98m05, Standard Projectile Impact Testing Method and Equipment Used in Evaluating the Performance Characteristics of Protective Headgear, Faceguards or Projectiles," 1998.

[150] L. Biomechanics Consulting and Research, "Helmet test protocol," 2019. [Online]. Available: www.biocorellc.com/resources.

[151] Society of Automotive Engineers, "J211-1 instrumentation for impact test—Part 1—electronic instrumentation," SAE Int. 211/1201403, 2014.

[152] L. F. Gabler, J. R. Crandall, and M. B. Panzer, "Assessment of Kinematic Brain Injury Metrics for Predicting Strain Responses in Diverse Automotive Impact Conditions," *Ann. Biomed. Eng.*, vol. 44, no. 12, pp. 3705–3718, Dec. 2016, doi: 10.1007/s10439-016-1697-0.

[153] S. Rowson and S. M. Duma, "Brain injury prediction: Assessing the combined probability of concussion using linear and rotational head acceleration," *Ann. Biomed. Eng.*, vol. 41, no. 5, pp. 873–882, May 2013, doi: 10.1007/s10439-012-0731-0.

[154] M. Fahlstedt *et al.*, "Ranking and Rating Bicycle Helmet Safety Performance in Oblique Impacts Using Eight Different Brain Injury Models," *Ann. Biomed. Eng.*, vol. 49, no. 3, pp. 1097–1109, Mar. 2021, doi: 10.1007/s10439-020-02703-w.

[155] T. Wu *et al.*, "Integrating Human and Nonhuman Primate Data to Estimate Human Tolerances for Traumatic Brain Injury," *J. Biomech. Eng.*, vol. 144, no. 7, Jul. 2022, doi: 10.1115/1.4053209.

[156] J. M. C. Costa, F. A. O. Fernandes, and R. J. Alves de Sousa, "Prediction of subdural haematoma based on a detailed numerical model of the cerebral bridging veins," *J. Mech. Behav. Biomed. Mater.*, vol. 111, p. 103976, Nov. 2020, doi: 10.1016/j.jmbbm.2020.103976.

[157] J. Wilhelm *et al.*, "Injury Biomechanics of a Child's Head: Problems, Challenges and Possibilities with a New aHEAD Finite Element Model," *Appl. Sci.*, vol. 10, no. 13, p. 4467, Jun. 2020, doi: 10.3390/app10134467.

[158] E. G. Takhounts, M. J. Craig, K. Moorhouse, J. McFadden, and V. Hasija, "Development of brain injury criteria (BrIC)," *Stapp Car Crash J.*, vol. 57, no. November, p. 243, 2013.

[159] M. B. P. Giudice, J. Sebastian, K. Kong, A.Caudillo, S. Mukherjee, "Finite Element Models of Helmet Assessment Tools," 2018.

[160] J. S. Giudice, G. Park, K. Kong, A. Bailey, R. Kent, and M. B. Panzer, "Development of Open-Source Dummy and Impactor Models for the Assessment of American Football Helmet Finite Element Models," *Ann. Biomed. Eng.*, vol. 47, no. 2, pp. 464–474, Feb. 2019, doi: 10.1007/s10439-018-02155-3.

[161] K. Oka, A. L. Rhoton, M. Barry, and R. Rodriguez, "Microsurgical anatomy of the superficial veins of the cerebrum," *Neurosurgery*, vol. 17, no. 5, 1985, doi: 10.1227/00006123-198511000-00003.

[162] S. Kleiven and H. Von Holst, "Consequences of head size following trauma to the human head," *J. Biomech.*, vol. 35, no. 2, 2002, doi: 10.1016/S0021-9290(01)00202-0.

[163] S. Kleiven, "Finite Element Modeling of the Human Head," Royal Institute of Technology, Stockholm, Sweden, 2002.

[164] A. M. Nahum, R. Smith, and C. C. Ward, "Intracranial Pressure Dynamics During Head Impact," Feb. 1977, doi: 10.4271/770922.

[165] C. Ward, M. Chan, and A. Nahum, "Intracranial Pressure–A Brain Injury Criterion," Sep. 1980, doi: 10.4271/801304.

[166] M. Ptak, "Method to Assess and Enhance Vulnerable Road User Safety during Impact Loading," *Appl. Sci.*, vol. 9, no. 5, p. 1000, Mar. 2019, doi: 10.3390/app9051000.

[167] M. Ptak *et al.*, "Experimental and computational approach to human brain modelling – aHEAD," *Arch. Civ. Mech. Eng.*, vol. 23, no. 3, p. 218, Aug. 2023, doi: 10.1007/s43452-023-00758-9.

[168] Livermore Software Technology Corporation (LSTC), "LS-DYNA keyword user's manual vol. 1," Livermore, 2007.

[169] Dyna More, "Human Model - Total HUman Model for Safety THUMS v 4.0," 2012. .

[170] C. Yu, F. Wang, B. Wang, G. Li, and F. Li, "A Computational Biomechanics Human Body Model Coupling Finite Element and Multibody Segments for Assessment of Head/Brain Injuries in Car-To-Pedestrian Collisions," *Int. J. Environ. Res. Public Health*, vol. 17, no. 2, p. 492, Jan. 2020, doi: 10.3390/ijerph17020492.

[171] D. C. Viano, I. R. Casson, E. J. Pellman, L. Zhang, A. I. King, and K. H. Yang, "Concussion in professional football: Brain responses by finite element analysis: Part 9," *Neurosurgery*, vol. 57, no. 5, pp. 891–915, Nov. 2005, doi: 10.1227/01.NEU.0000186950.54075.3B.

[172] K. K. Mendis, R. L. Stalnaker, and S. H. Advani, "A constitutive relationship for large deformation finite element modeling of brain tissue.," *J. Biomech. Eng.*, vol. 117, no. 3, pp. 279–85, Aug. 1995.

[173] K. Miller and K. Chinzei, "Constitutive modelling of brain tissue: Experiment and theory," *J. Biomech.*, vol. 30, no. 11–12, pp. 1115–1121, Nov. 1997, doi: 10.1016/S0021-9290(97)00092-4.

[174] D. A. Patton, A. S. McIntosh, and S. Kleiven, "The biomechanical determinants of concussion: finite element simulations to investigate brain tissue deformations during sporting impacts to the unprotected head.," *J. Appl. Biomech.*, vol. 29, no. 6, pp. 721–30, Dec. 2013.

[175] Y. Wan, A. L. Fawzi, and H. Kesari, "Determining rigid body motion from accelerometer data through the square-root of a negative semi-definite tensor, with applications in mild traumatic brain injury," *Comput. Methods Appl. Mech. Eng.*, vol. 390, p. 114271, Feb. 2022, doi: 10.1016/j.cma.2021.114271.

[176] H. Mao *et al.*, "Development of a finite element human head model partially validated with thirty five experimental cases," *J. Biomech. Eng.*, vol. 135, no. 11, 2013, doi: 10.1115/1.4025101.

Appendix A

The Appendix is adapted from the one of the co-authored publications, Analysis of HIC and hydrostatic pressure in the human head during NOCSAE tests of American football helmets. Brain Sciences. 2021, vol. 11, nr 3, art. 287, s. 1-29, https://doi.org/10.3390/brainsci11030287.
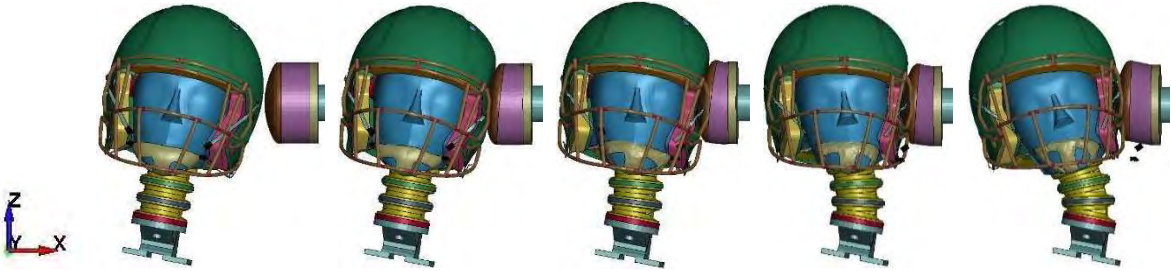
Appendix A.1. Configuration AP
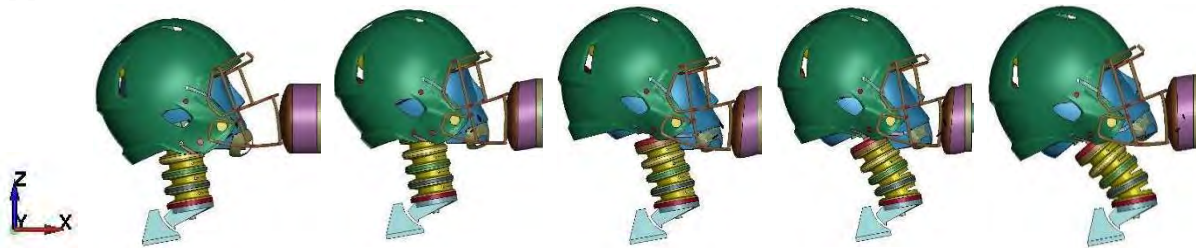
Figure A1. Configuration AP: course of simulation (0–20 ms, 5 ms interval).
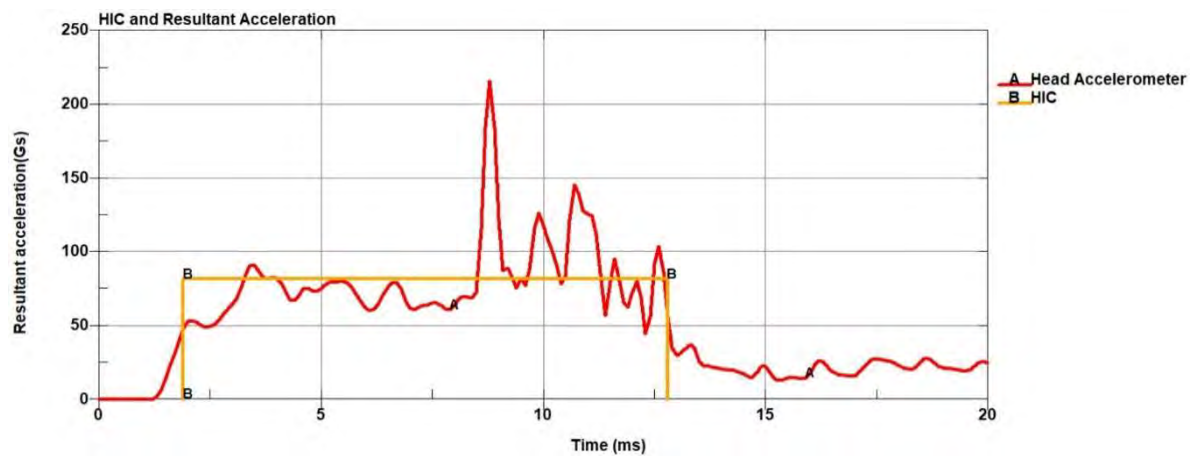
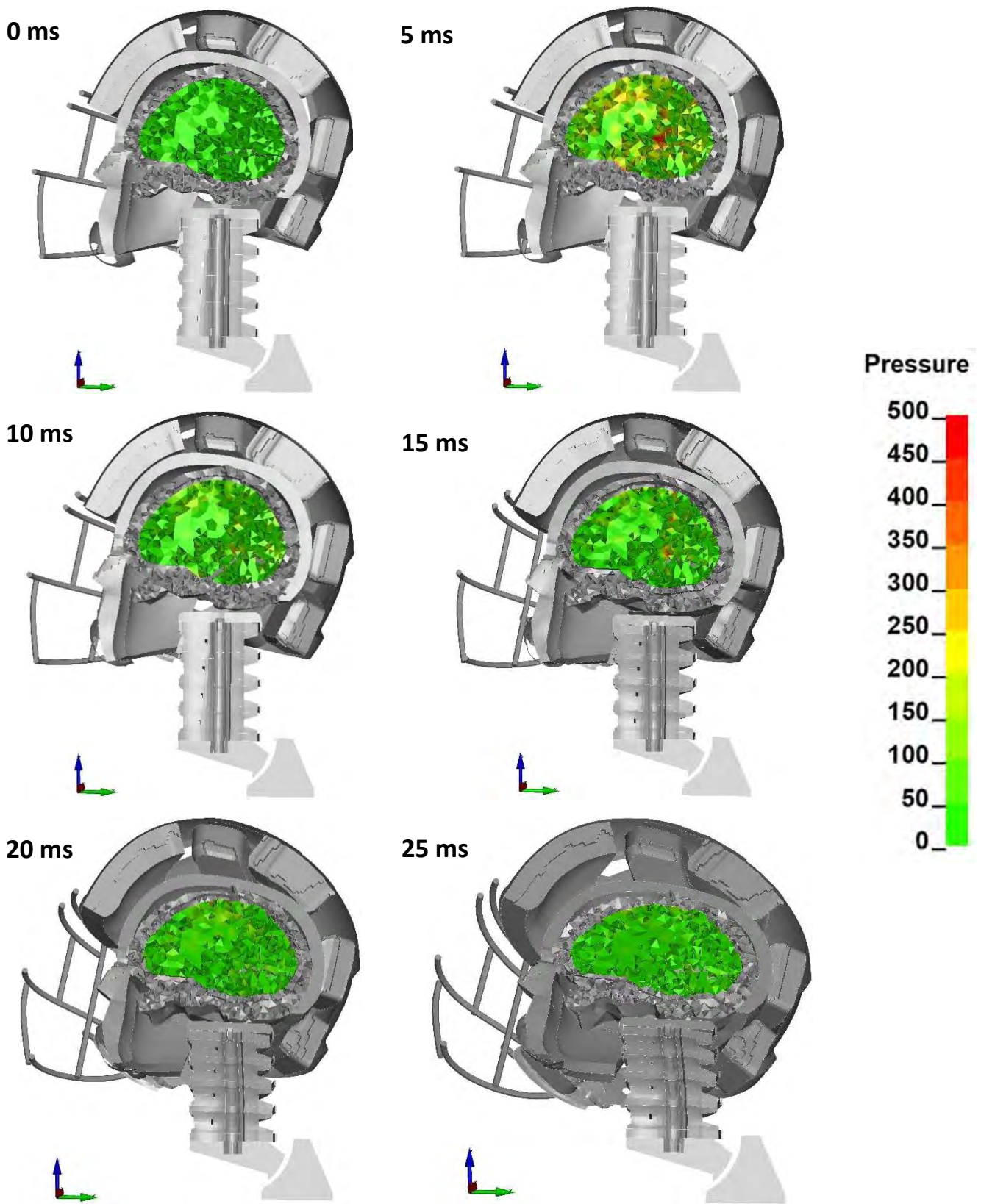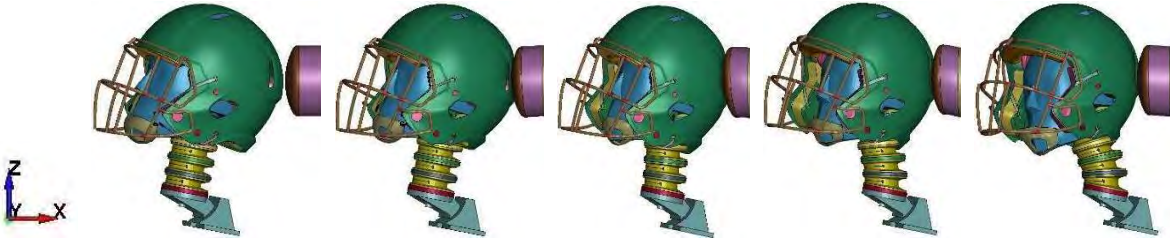**Figure A2.** HIC and Resultant Acceleration (g) in time (ms) plot (HIC36 = 650).
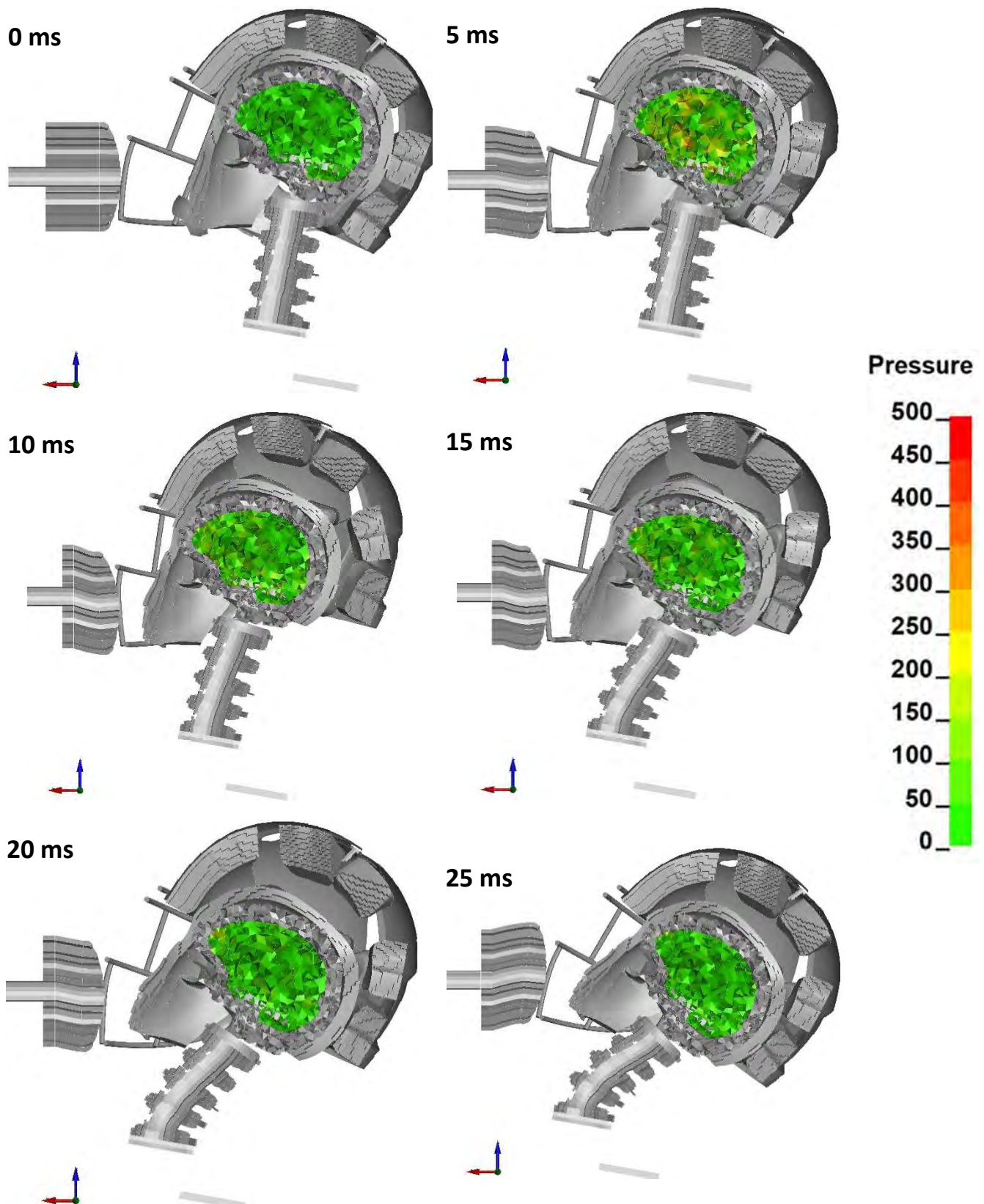
14.

Figure A3. Head kinematics during the numerical test, configuration AP, with the cross-section in the sagittal plane and showing the hydrostatic pressure (kPa) in the brain.

Appendix A.2. Configuration B
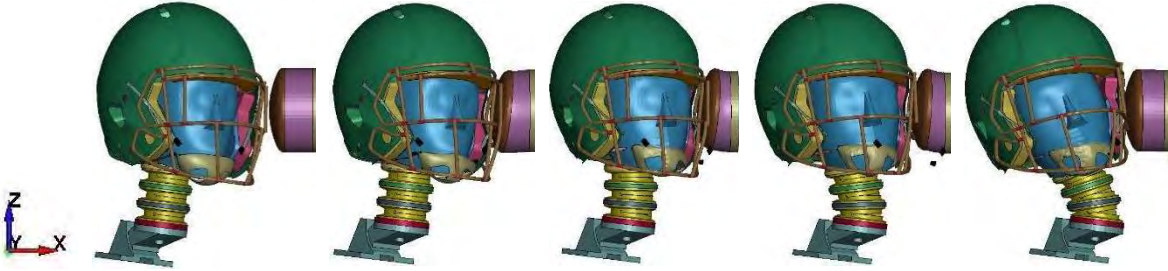
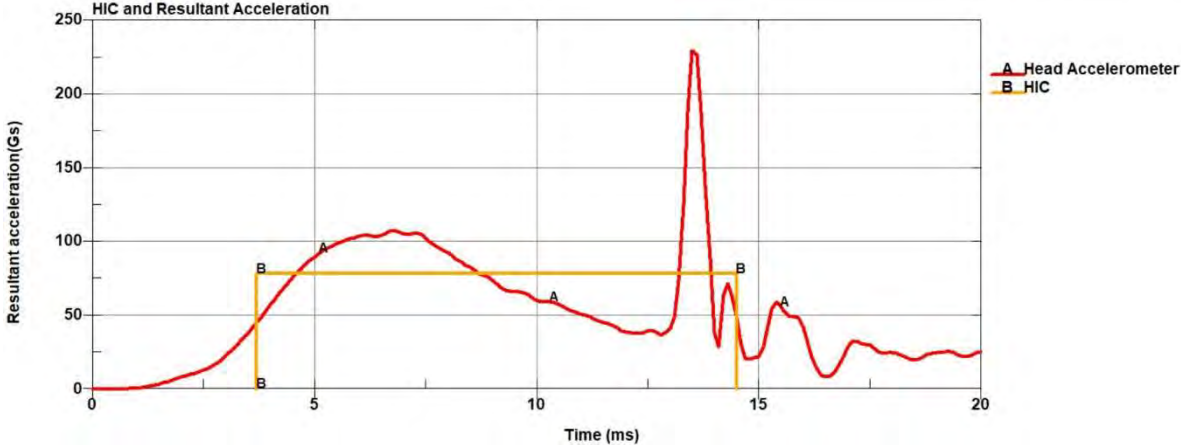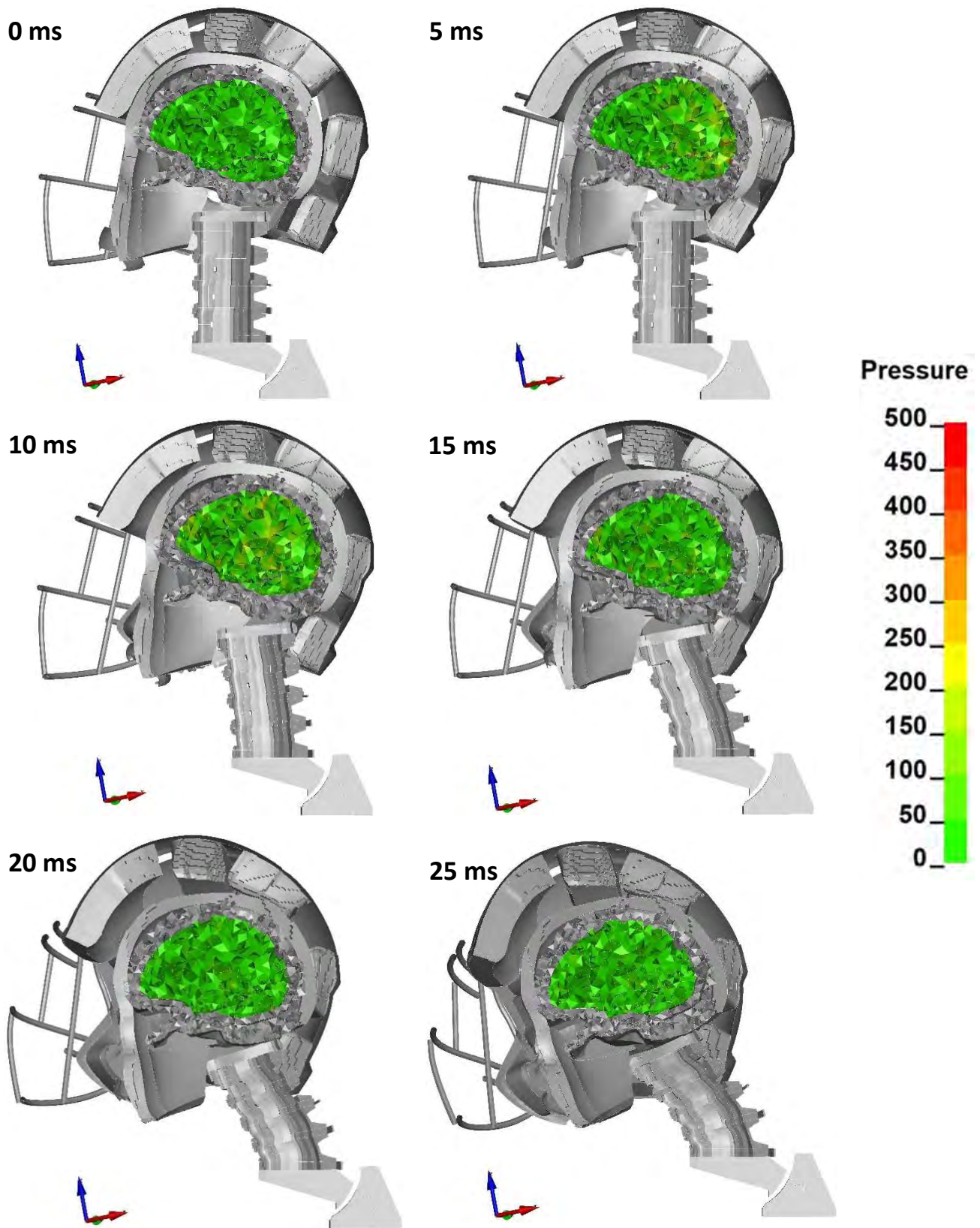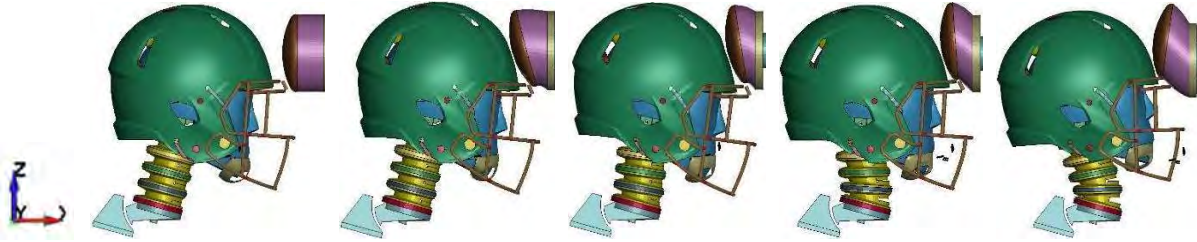**Figure A4.** Configuration B: course of simulation (0–20 ms, 5 ms interval).
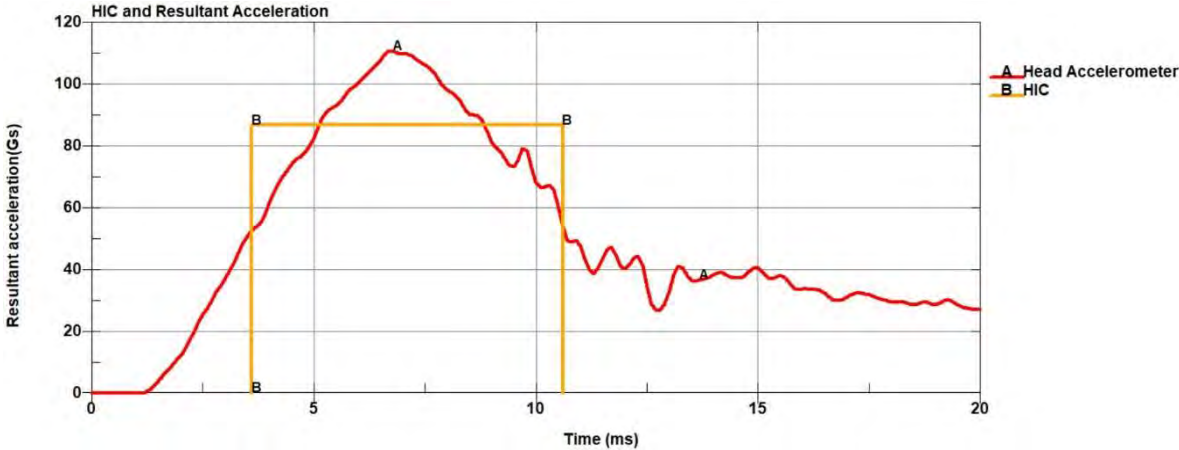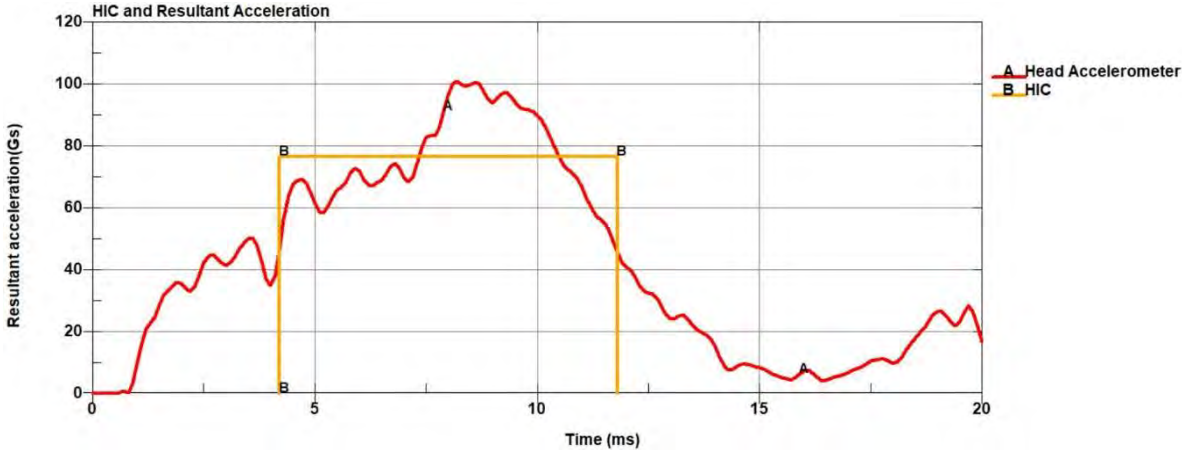

Figure A5. HIC and Resultant Acceleration (g) in time (ms) plot (HIC36 = 499).
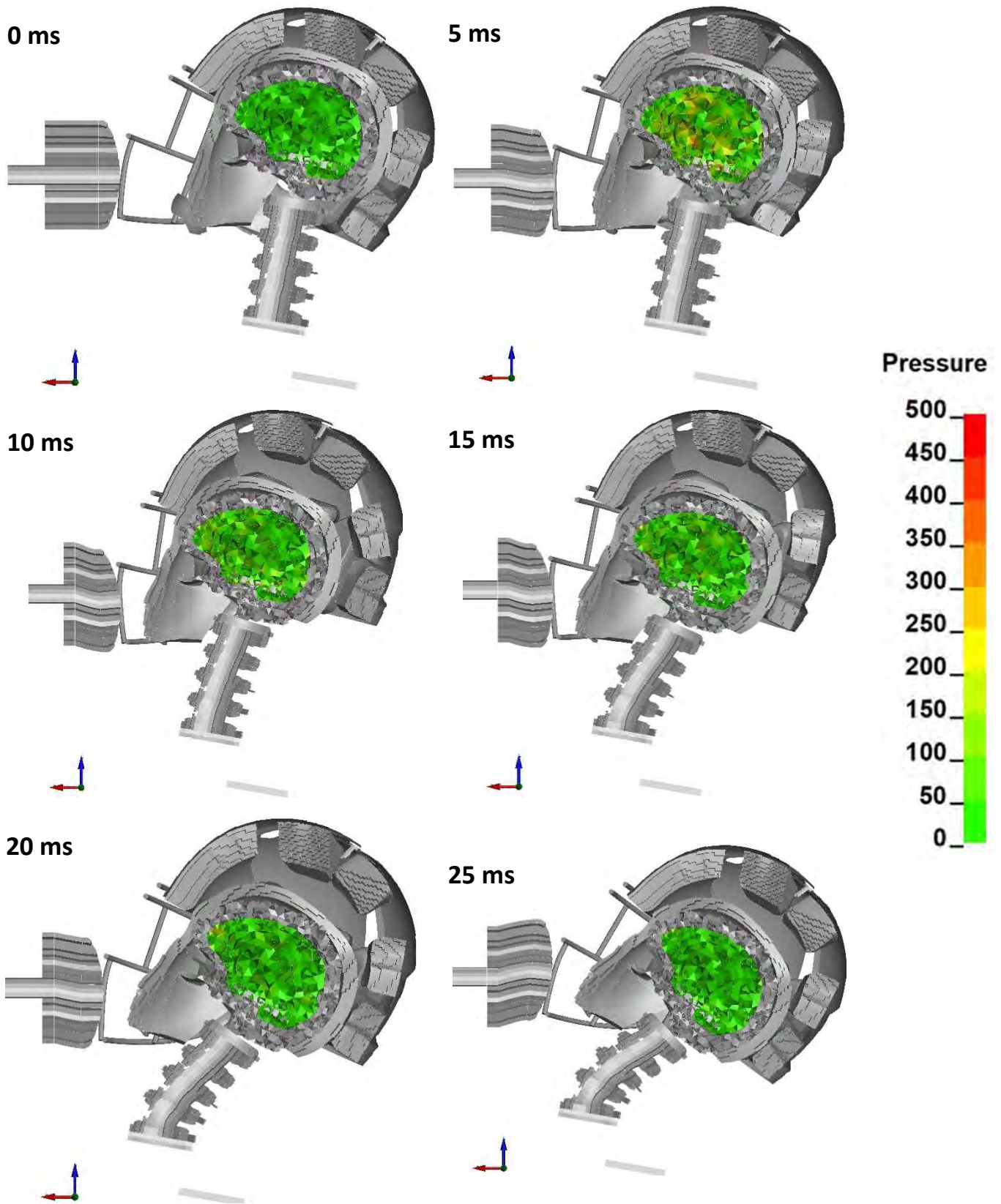
Figure A6. Head kinematics during the numerical test, configuration B, with the cross-section in the median plane and showing the hydrostatic pressure (kPa) in the brain.

Appendix A.3. Configuration C

Figure A7. Configuration C: course of simulation (0–20 ms, 5 ms interval)..
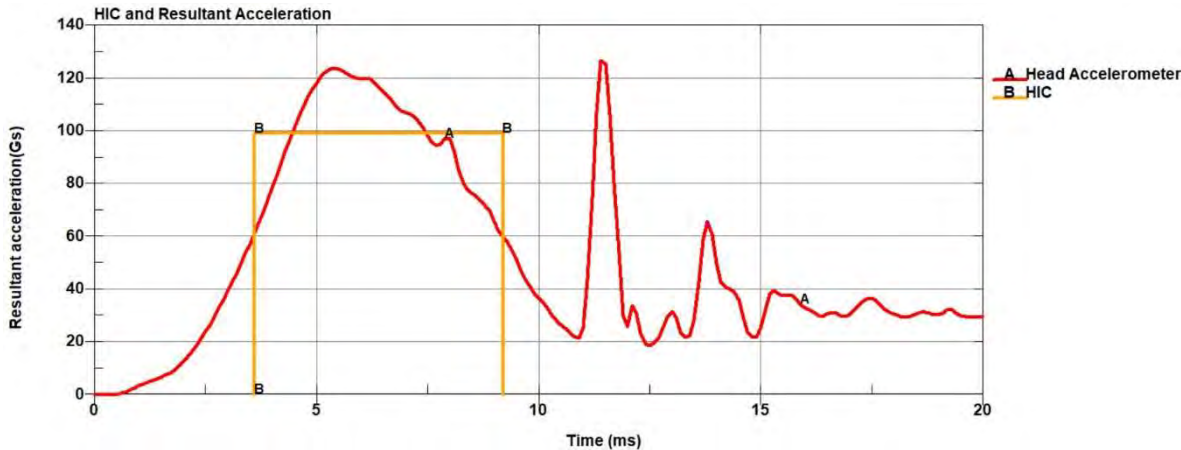
Figure A8. HIC and Resultant Acceleration (g) in time (ms) plot (HIC36 = 557).
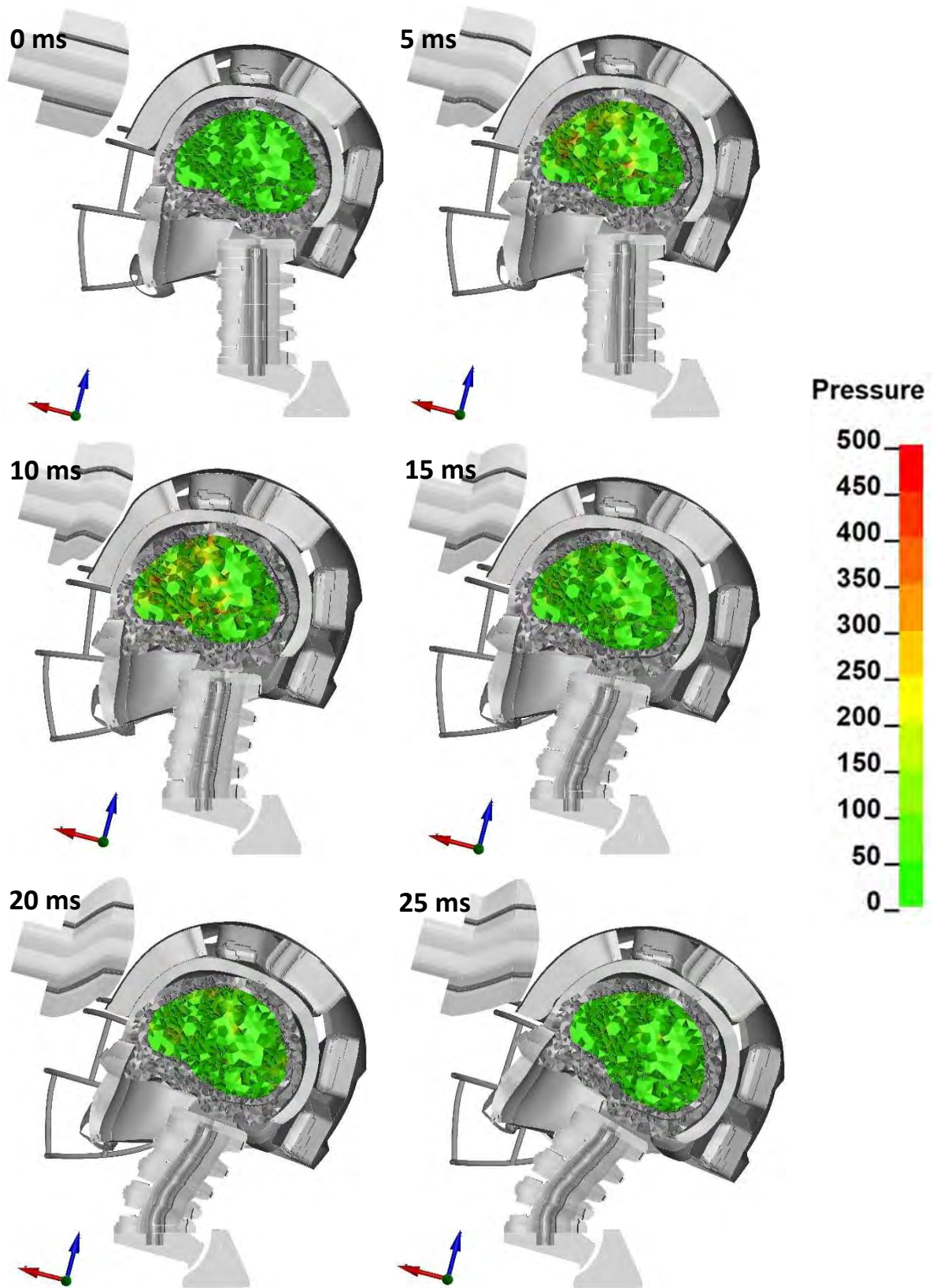
Figure A9. Head kinematics during the numerical test, configuration C, with the cross-section in the median plane and showing the hydrostatic pressure (kPa) in the cerebrum.
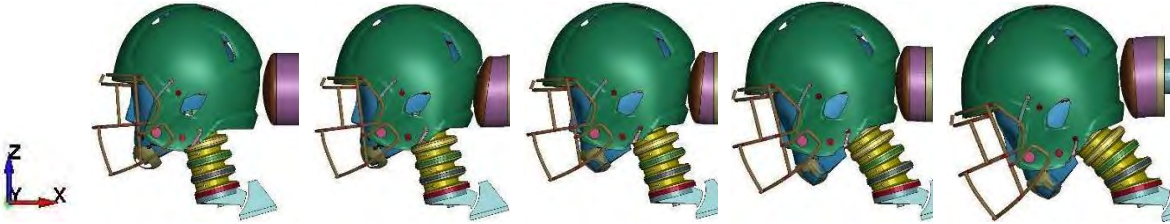
Appendix A.4. Configuration D

Figure A10. Configuration D: course of simulation (0–20 ms, 5 ms interval).

Figure A11. HIC and Resultant Acceleration (g) in time (ms) plot (HIC36 = 594).

Figure A12. Head kinematics during the numerical test, configuration D, with the cross-section in the median plane and showing the hydrostatic pressure (kPa) in the cerebrum.

Appendix A.5. Configuration F

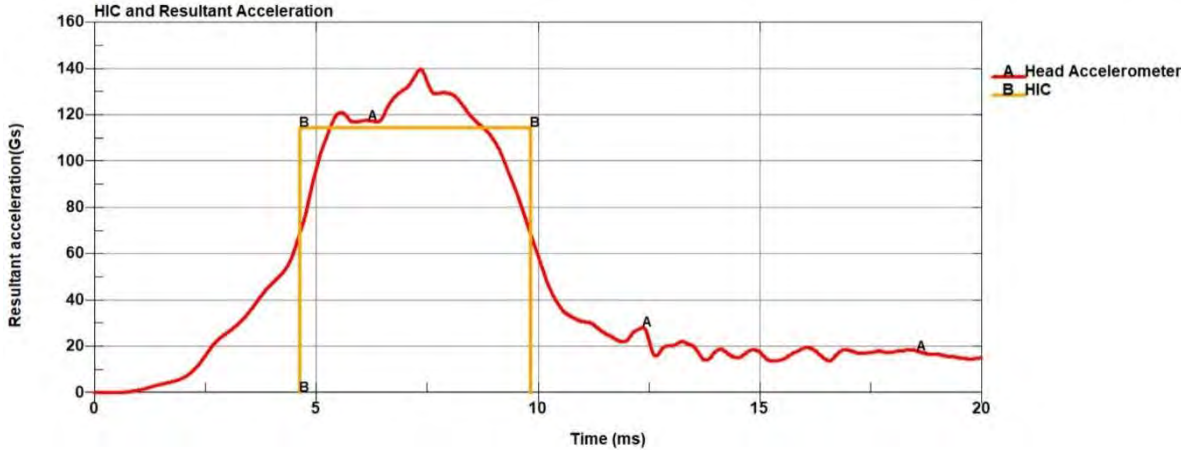**Figure A13.** Configuration F: course of simulation (0–20 ms, 5 ms interval).

Figure A14. HIC and Resultant Acceleration (g) in time (ms) plot (HIC36 = 403).
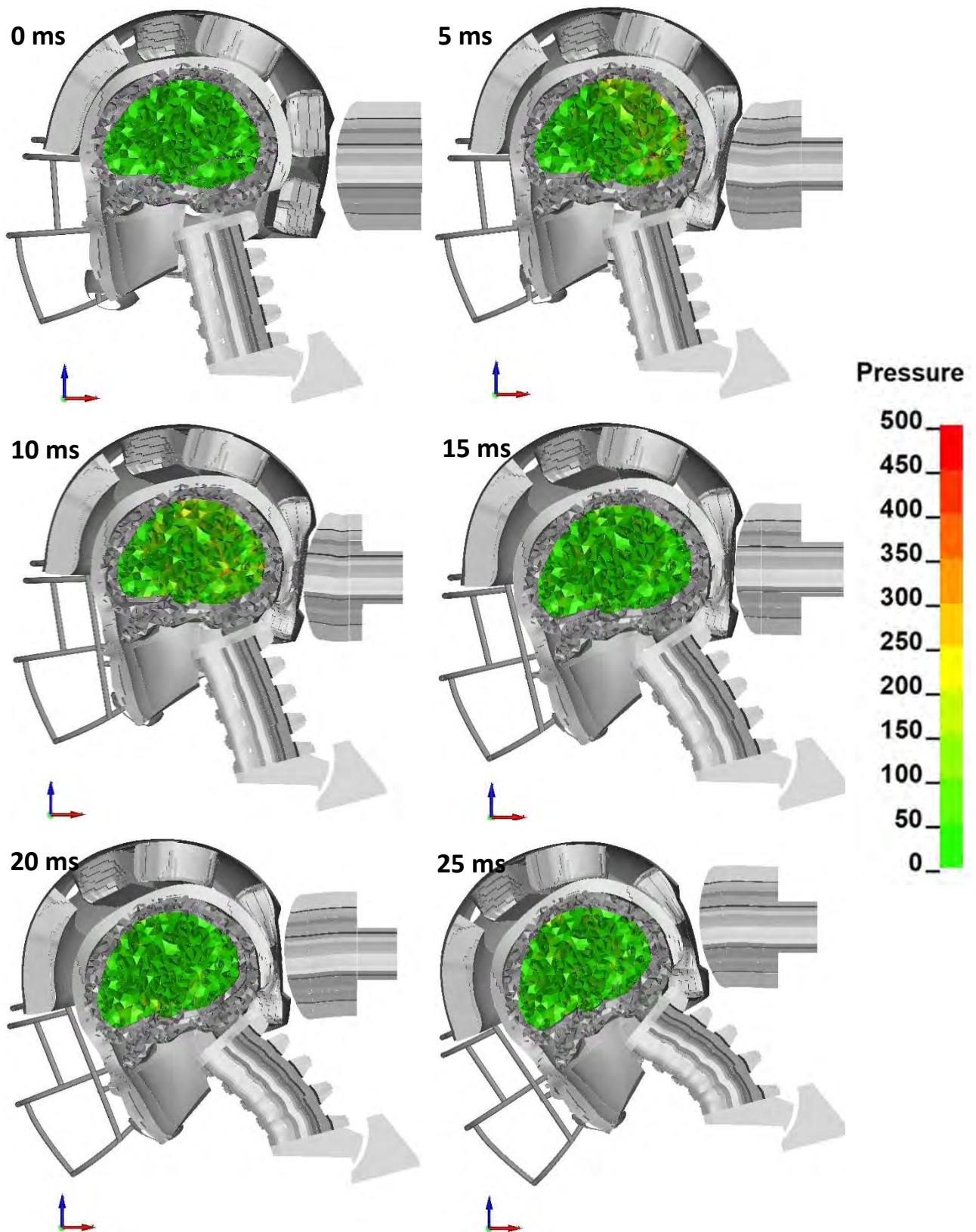
Figure A15. Head kinematics during the numerical test, configuration F, with the cross-section in the median plane and showing the hydrostatic pressure (kPa) in the cerebrum.
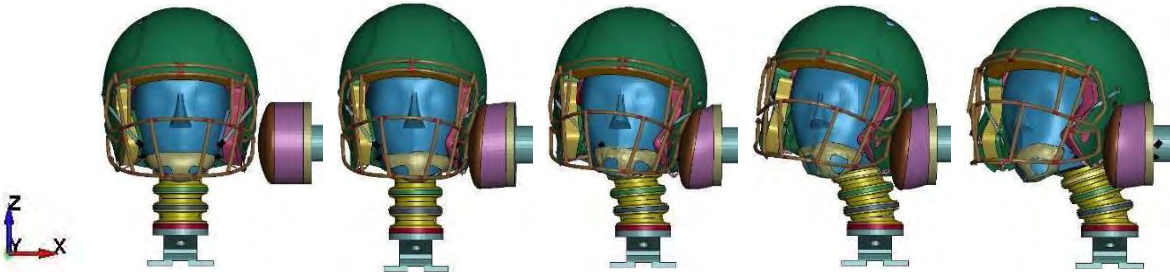
Appendix A.6. Configuration R

Figure A16. Configuration R: course of simulation (0–20 ms, 5 ms interval).

Figure A17. HIC and Resultant Acceleration (g) in time (ms) plot (HIC36 = 731).

Figure A18. Head kinematics during the numerical test, configuration R, with the cross-section in the median plane and showing the hydrostatic pressure (kPa) in the cerebrum.

Appendix A.7. Configuration UT

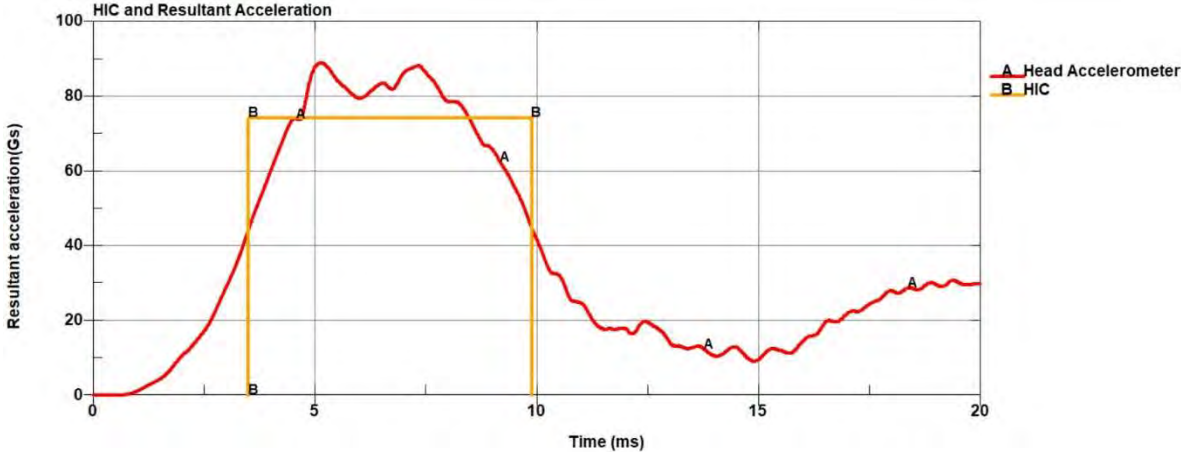**Figure A19.** Configuration UT: course of simulation (0–20 ms, 5 ms interval).

Figure A20. HIC and Resultant Acceleration (g) in time (ms) plot (HIC36 = 304).
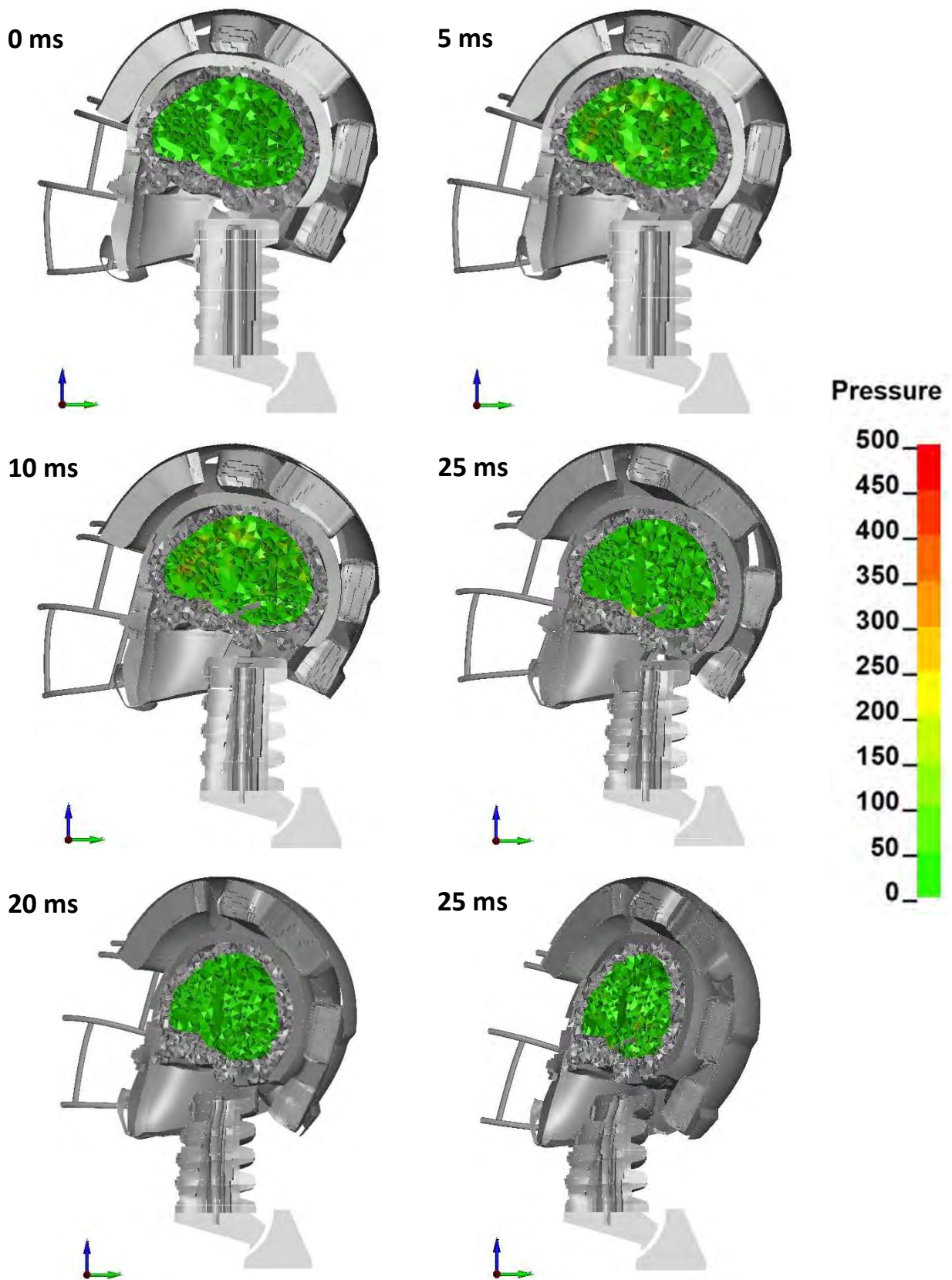
Figure A21. Head kinematics during the numerical test, configuration UT, with the cross-section in the median plane and showing the hydrostatic pressure (kPa) in the cerebrum.